SPREAD SPECTRUM FIBER LANs

by

Farideh Khaleghi, B.A.Sc.

A thesis submitted to the
School of Graduate Studies and Research
in partial fulfillment of the requirements for the degree of

Master of Applied Science

Ottawa-Carleton Institute for Electrical Engineering

Department of Electrical Engineering
Faculty of Engineering
University of Ottawa

ISBN 0-315-85782-X

Canada

UNIVERSITÉ D'OTTAWA
UNIVERSITY OF OTTAWA

Abstract

In this thesis, a hybrid scheme is proposed for the purpose of suppressing the effect of external modulation and/or laser nonlinearities in Subcarrier Multiplexing (SCM) fiber optic communications systems. Hybrid CDMA/FDMA combines two schemes in such a way that the resulting hybrid network is robust against interference and is much more spectrally efficient than a CDMA system. Several possible architectures for the hybrid CDMA/FDMA subcarrier fiber optic Local Area Network (LAN) are introduced. These networks utilize CDMA and SCM, an asynchronous multiple access scheme with no waiting time.

Direct Sequence Spread Spectrum Multiple Access (DS/SSMA), the most common form of CDMA in which each user is assigned a particular code sequence which modulates the carrier along with digital data, is employed. It is shown that by using the code sequence sets for which the shift-and-add property holds, the Intermodulation Products (IMPs) and harmonics have a similar interference-like effect as the non-matching sequences. Owing to the fact that shift-and-add property holds for conventional spreading sequences, i.e., Gold, Kasami and maximal-length sequences, the suppression of nonlinearity distortion is evaluated.

An average error probability performance evalution of the selected configuration for a transceiver pair is presented. In analysis of the system, we assume the interference term arising from other users is gaussian distributed. The results are compared to that obtained from exact evaluation of interference distribution using the Gauss Quadrature Rule integration (GQR) method.

We compare the performance of this scheme for two different code sequence sets (N=127 Gold and N=255 Kasami codes) and determine that there is a significant advantage in deploying the N=255 Kasami codes.

We also present some preliminary experimental results on the proposed LAN implementation as well as the transmission performance. The results show great promise.

Acknowledgements

I would like to express my sincere gratitude to my thesis supervisor, Dr. Mohsen Kavehrad who has been very supportive of this work. His guidance, encouragement and kindness are greatly appreciated. Also, thanks to Dr. Galko for his guidance on use of various software tools.

I would like to also thank Dr. Kavehrad and Mr. George Bodeep of ATT Bell Labs. for their help in realizing the experimental part of the work.

This work was supported partly by the Telecommunication Research Institute of Ontario (TRIO), Photonic Network Architectures project and partly by the National Science and Engineering Research Council of Canada (NSERC). I am grateful to both of these organizations.

Also, many thanks to my colleagues at Lightwave Communications Research Laboratory of University of Ottawa for many usefull discussions I had with them during the course of this work.

Abbreviations

AlGaAs	Aluminium Gallium Arsenide
AO/LSE	Auto-Optimal with Least Sidelobe Energy
APD	Avalanche Photodiode
AWGN	Additive White Gaussian Noise
BPSK	Binary Phase Shift Keying
CDMA	Code Division Multiple Access
CDMA/FDMA	Code Division Multiple Access/Frequency Division Multiple Access
CTB	Composite Triple Beat
DPSK	Differential Phase Shift Keying
DS	Direct Sequence
DS/SSMA	Direct Sequence/Spread Spectrum Multiple Access
FDMA	Frequency Division Multiple Access
FSK	Frequency Shift Keying
GaAsP	Gallium Arsenide Phosphide
GQR	Gauss Quadrature Rule
IC	Integrated Circuit
ILD	Injection Laser Diode
IMD	Intermodulation Distortion
IMP	Intermodulation Product
LAN	Local Area Network
LED	Light Emitting Diode
LO	Local Oscillator
pdf	probability density function
PIN diode	Positive-Intrinsic-Negative diode
PN	Pseudonoise

SAW	Surface Acoustic Wave
SAW-MF	SAW-Matched Filter
SCM	Subcarrier Multiplexing
SF	Single Frequency
TDM	Time-Division Multiplexing
WDMA	Wavelength Division Multiple Access

Table of Contents

List of Figures

Chapter 1
Introduction

1.1 Motives

Extremely low propagation loss and large bandwidth of fiber are two main reasons that lighwave technology has revolutionized telecommunications. However, at the present state of technology, Local Area Network (LAN) applications are limited mainly by expensive optical components and lossy optical couplers.

Wavelength Division Multiple Access (WDMA) is a technique which allows easily tapping the entire bandwidth of fiber. In optical communications literature, this technique is often called Frequency Division Multiple Access (FDMA) when the channel spacing is relatively close; i.e. comparable to the bit rate. A successful realization of such a system requires precise carrier frequency control to ensure a high signal-to-interference ratio at all times. For achieving high signal-to-interference ratios, a laser with a sharply peaked output spectrum or a so called Single Frequency (SF) laser is required. Conventional semiconductor lasers tend to oscillate simultaneously over a broad range of wavelengths, so they are not well suitable for high-density WDMA. However, SF lasers, based on the distributed feedback or distributed Bragg reflector structures are becoming available. These devices incorporate special resonators that suppress all modes of oscillation but one, resulting in an essentially single-frequency output. An additional feature of these lasers is their adaptability for direct frequency modulation. A change in the bias current through the device causes a small but easily detectable shift in the optical frequency of oscillation. This effect can be used to transmit data via Frequency Shift Keying (FSK) at speeds in excess of 1 Gb/S. Although we have alleviated phase noise caused by wide laser linewidth; the sensitivity of the laser light frequency to changes in bias current causes unstability in the laser oscillation. Hence, adjacent channels drift in frequency toward one another. Stable, tunable single-mode lasers considering the state of today's optical technology if not realizable are quite costly, therefore, not suitable for networks.

A receiver in a WDMA system must be able to select the desired optical signal and reject interference from unwanted adjacent channels. This has been achieved by a narrow-band optical band-pass filter based on Fabry-Perot interferometric techniques. The filter is electrically tunable. It permits simple demodulation of the incoming FSK signal by converting it into an amplitude-modulated wave that can be readily detected. The central message in this discussion is that by using optical FDMA schemes these networks will offer total throughputs of thousands of Gb/s while serving a community of thousands of users. However, the technology required to achieve this explosive advancement is not fully available yet, and certain key components, such as tunable lasers have proven difficult to realize. Without having such lasers WDMA networks will suffer from a poor signal-to-interference ratio due to unstability and wide linewidth of lasers.

At the same time, subcarrier multiplexing demonstrates potential to be a convenient and efficient technique for transmission of analog or digital information.

Variety of new information distribution systems using Subcarrier Multiplexing (SCM) have been proposed, recently.

Darcie and Bodeep [8] claim subcarrier transmission of multi-channel AM-VSB signals may find widespread application in Video distribution systems. They study performance of these systems and the limitations imposed by laser nonlinearity and noise.

Olshansky [9] argues that independence of microwave carriers makes simultaneous transmission of analog and digital modulation signals possible. Systems built today can exploit low-cost analog electronics and still be capable of evolving in steps with anticipated future requirements to transmit both digital and high-definition video signals.

Analog subcarrier modulation technique is becoming attractive because of wide bandwidth capabilities of semiconductor lasers. However, these techniques require the laser light intensity be a linear function of the drive current, under large signal modulation. Nonlinearities introduce distortions which can severely limit the system performance [10]

Recent fiber optic experiments have demonstrated feasibility of combining subcarrier

multiplexing (SCM) technique with coherent detection to provide multichannel transmission and improved sensitivity. Regardless of the way of detection; such systems suffer from Intermodulation Distortion (IMD). However, in the direct detection case, IMD is caused by laser or external modulation nonlinearities and in the coherent case IMD is a fundamental characteristic of the modulation/demodulation process.

Optical FDMA and SCM schemes are emerging as promising techniques in multiple-access lightwave systems for high-bit rate and low-bit rate applications, respectively. However, these schemes are sensitive to any type of interference. In systems exploiting optical FDMA, poor signal-to-interference ratio is due to optical frequency drift or wide linewidth of lasers. In SCM systems, the interfering signals are due to external modulation or laser nonlinearities in direct detection case and is an inherent characteristic of the modulation/demodulation process in coherent detection case.

By contrast, Code Division Multiple Acces (CDMA) is robust against interference. The most common form of CDMA is Direct-Sequence Spread-Spectrum Multiple Access (DS/SSMA) in which each user is assigned a particular code sequence which modulates, the carrier along with digital data. The DS/SSMA techniques are characterized by the use of a high-rate code (i.e., many code symbols per data symbol) having the effect of spreading the bandwidth of the data signal.

Spread spectrum technique can be used to reduce interference. Traditionally, it has been used for suppressing the effect of interference due to jamming, interference from other users of the same channel, and self-interference due to multipath propagation. This technique can also be used for suppressing the effect of interference due to optical frequency drift in optical FDMA systems or interference due to harmonics and Intermodulation Products (IMPs) caused by laser nonlinearity in subcarrier multiplexing schemes.

CDMA in optical systems can be exploited to ease the optical technology challenges. Stable, tunable lasers with accurate wavelength control are not required. The optical carriers are allowed to wander randomly anywhere over the optical frequency range, because by using spread spectrum technique the effect of interfering adjacent channel signals is

suppressed.

A hybrid scheme that combines FDMA and CDMA in such a way that resulting network is robust against interference and is more spectrally efficient than CDMA seems very interesting. Vannucci [16] presents many of implementation details of a combined CDM/FDMA system and demonstrates feasibility with today's optical technology.

In this thesis we will examine the capability of hybrid CDMA/FDMA system at subcarrier level in suppressing the effect of laser nonlinearity. At the same time, the required spreading of the spectrum in order to support a certain number of users is much less than that for asynchronous CDMA; if a limited number of FDM subcarriers are emplyed.

The major goal of this thesis will be to examine the potential capability of the proposed CDM/FDMA scheme in suppressing the effect of laser nonlinearities, while by employing microwave subcarrier multiplexing we are taking advantage of wide-bandwidth capabilities of semiconductor lasers.

In discussing implementation issues, we will suggest several alternatives which are very cost efficient for low-bit rate users of the proposed LAN. However, our results are not limited to the proposed set of components. The results are not limited to those devices and techniques that are currently available or practical. Lasers with a very high modulation bandwidth will be available in the future, however, laser nonlinearity is a fundamental characteristic in a light generation process. From rate equations it can be seen that the stimululated emission term, is a nonlinear coupling of electron and photon densities.

Having described the general motivations, we now state the contributions and outline of the thesis in the next two sections.

1.2 Contributions

Subcarrier multiplexing has proven potential in multiple-access lightwave systems, specially for low-bit rate applications. Laser nonlineariy is the main source of impairment

in such systems. In this work, a new CDMA/FDMA subcarrier scheme for the purpose of reducing nonlinearity distortion has been proposed.

Several possible configurations for the hybrid CDMA/FDMA subcarrier fiber optic LAN has been discussed. In our proposed systems, conventional spreading sequences can be used. For all these sequences the shift-and-add property holds. It has been shown that using these sequence sets to spread the signals prior to subcarrier frequency modulation, IMPs and harmonics have a similar interference-like effect as the non-matching sequences.

The power suppression of each order of IMPs and harmonics has been evaluated while a code sequence of length N is employed. Data bit rate in the suggested system is limited by the maximum laser modulation rate. However, there is possibility of using external modulation to support high-bit rate users. Our results are valid in either case.

A detailed design of a transmitter and a receiver has been provided and the suggested subsystems have been exprimentally realized. A good agreement has been observed between theoretical and experimental results. By using the proposed receiver which is a SAW filter-based type, one may make the system as spectrally efficient as FDMA systems while benefiting from robustness of CDMA against interference and as a mode of access.

1.3 Outline of the Thesis

Next chapter will provide review material. Three different LAN topologies are introduced. Problems associated with optical LAN topologies are discussed. A background is provided on optical network devices . A number of design considerations of subcarrier multiplexed lightwave systems related to our work are explained.

A major part of Chapter 3 consists of background materials on CDMA scheme and spread spectrum sequences. In this chapter different code sequence sets, generation method of these codes and their properties are described. After discussing the properties of the sequences in detail and using their properties, we derive the variance of the product of an arbitrary number of these sequences, since, these products correspond to transformed

IMPs and harmonics in our proposed LAN.

In Chapter 4 several configurations are introduced for the LAN . Advantages and disadvantages of each is stated. After modelling the proposed system using Gaussian distribution assumption on the multiple-access interference term, the average error probability performance is evaluated. Results obtained under the Gaussian assumption are compared to exact results obtained from numerical computations. In numerical evaluations, Gauss Quadrature Rule (GQR) integration is used as the method of probability density function (pdf) computation. Then, performance of the system is examined for two different sequence sets, namely; Gold sequences of length 127 and Kasami sequences of length 255.

In chapter 5, a detailed design of subsystems, i.e., transmitter and receiver is described. Results of a preliminary experiment on performance of the system is presented. Lastly, Chapter 6 outlines the conclusions reached with some suggestions for further research.

Chapter 2

Optical LANs and Subsystems – SCM Lightwave Systems Design Issues

2.1 Overview of Optical LANs and Devices

In this chapter we provide a relevent background on different optical LAN topologies and problems associated with them. We then overview optical devices. After providing the necessary background we investigate releverant design considerations of subcarrier multiplexed (SCM) lightwave systems.

2.2 LAN Topologies

Fiber as a transmission medium offers a combination of wide bandwidth and low-loss. In high-capacity LAN applications, where distances are relatively short, the extremely low propagation loss of fiber is not the main advantage of fiber. Fiber high bandwidth, measured in tens of terahertz is the most important advantage of this medium. Construction of multiple access networks carrying a total traffic of perhaps 5×10^4 Gb/s is conceivable. Today, of course we are far from realizing this potential. The fundamental processes that limit the network performance have not been fully elucidated, and the devices likely to be required do not yet exist. The fiber can not be simply substituted in place of copper to upgrade the capacity of a wire-based LAN; there are great differences between photonic and electronic regimes. Compared with copper networks, fiber-based systems are characterized by:

(1.) Severely limited signal power

(2.) Abundant transmission bandwidth

Two basic problems in lightwave LANs is arising from these two characteristics. The

power problem and electronic bottleneck. The severity of the power division problem is a strong function of network topology. The most common toplogies for local networks are the ring, bus and star.

2.2.1 Ring Topology

Typically, the ring structure consists of a closed loop of point-to-point links. Such a configuration with point-to-point links (signal regeneration at each node) suffers from no power division problems. However, in a ring structure with no optical regeneration at each node, the usable bandwidth is necessarily limited to the eletronic processing capability of a single node, i.e., roughly 1 Gb/s or less. This situation is electronic bottleneck. A more significant disadvantage of the ring topology is that, if a subset of users wish to operate at very high data rates, all others must be able to operate at similar rates. This requirement is unattractive economically for users interested in low bit rate applications.

2.2.2 Star Topology

The function of passive star coupler is to accept signals from all the transmitters simultaneously and broadcast them to all receivers. Thus, each receiver has access to all transmitted signals and selects out the messages intended for him.

Assume that signal power P is available from each of the N transmitters and that the fibers are lossless. The star coupler uniformly distributes these signals across its N output fibers, so that each one delivers to its receiver a contribution P/N from each transmitter.

2.2.3 Bus Topology

In a unidirectional bus each user injects signal into the so called talk side of the bus, via directional couplers. These signals are distributed to the receivers on other side of

bus called listen side, via a second set of couplers. Obviously, a true network would need two such buses, one for each direction. The power division issue would be the same for each bus, so we consider only one. In an $n-$user network with ideal couplers to inject and broadcast the optical signals, only $\frac{P}{N^2}$ useful power is delivered to each receiver. This is due to the fact that the sum of the fraction of powers coupled to each coupler output is less than 1. Since this signal must then be distributed among N receivers, it is attenuated by $\frac{1}{N}$, resulting in an overall transmitter-to-receiver attenuation of $\frac{1}{N^2}$.

The disadvantage of the bus topology, namely; poor energy efficiency, can be overcome with a suitable optical amplifier to compensate for the high signal attenuation in the network. However, there are two characteristics of an optical amplifier that limit its usefulness in LAN applications: maximum output power and internal noise generation.

2.3 Optical Network Devices

In this section, we review some optical devices for networks and we express the relative advantages and disadvantages of these components.

2.3.1 Light Sources

Essentially, there are two devices commonly used to generate light for fiber optic communications systems. Light-Emitting Diodes (LEDs) and Injection Laser Diodes (ILDs). Both devices have advantages and disadvantages and selection of one device over the other is determined by system requirements.

Light-Emitting Diodes

A light-emitting diode (LED) is simply a P-N junction diode. It is usually made from a semiconductor material such as Aluminum Gallium Arsenide (AlGaAs) or Gallium Arsenide Phosphide (GaAsP). LEDs emit light by spontaneous emission; light is emitted

as a result of the recombination of electrons and holes.

Injection Laser Diode

The word *laser* is an acronym for Light Amplification by Stimulated Emission of Radiation. Lasers are constructed from many different materials, including gases, liquids, and solids, although the type used most often for fiber optic communications is semiconductor laser. The ILD is similar to LED. In fact, below a certain threshold current an ILD acts like an LED. Above the threshold current, an ILD oscillates and lasing occurs.

The construction of an ILD is similar to that of an LED except that the ends are highly polished. The mirror-like ends trap the photons in the active region and, as they reflect back and forth, they stimulate free electrons to recombine with holes at a higher-than-normal energy level. This process is called *lasing*.

In the following, we summarize the advantages and disadvantages of ILDs over LEDs:

Advantages of ILDs

(1.) Because ILDs have a more direct radiation pattern, it is easier to couple their light into an optical fiber. This reduces the coupling losses and allows smaller fibers to be used.

(2.) The radiant output power from an ILD is greater than that of an LED. A typical output power for an ILD is $5mW(7dBm)$ and $0.5mW(-3dBm)$ for LEDs. This allows ILDs to provide a higher drive power.

(3.) ILDs can be used at higher bit rates than LEDs.

(4.) ILDs generate monochromatic light, which reduces chromatic or wavelength dispersion.

Disadvantages of ILDs

(1.) ILDs are typically by an order of 10 times more expensive than LEDs.

(2.) Because ILDs operate at higer powers, they typically have a much shorter lifetime than LEDs.

(3.) ILDs are more temperature dependent than LEDs.

The most important relevant disadvantage of lasers is that they are much more nonlinear than LEDs. The nonlinear characteristics of injection lasers have been extensively investigated. We briefly summarize some of the important results.

Nonlinearity Modeling

(1.) Static Nonlinearity

A memoryless nonlinearity [43] is the simplest model for a laser diode, but it is valid only for a very restricted operating condition. A memoryless nonlinearity can be observed directly from the light-versus-bias ($L - I$) curve, or its slope dL/dI. The optical power ratio of a second order nonlinear distortion term to the fundamental carrier is proportional to (d^2L/dI^2); the optical power ratio of a third order nonlinear distortion and a fundamental carrier is proportional to (d^3L/dI^3) [44].

(2.) Intrinisic Dynamic Nonlinearity

In addition to a static nonlinearity, a semiconductor laser exhibits a dynamic nonlinearity that is intrinsic to the nonlinear photon-electron interaction mechnanism. Using a small-signal analysis of the laser rate equations, Lau and Yariv [41] first showed that the calculated two-tone third order IMD from a GaAs laser matches well with experimental data. Their results were later extended to InGaAsP lasers [10]. Although the closed-form analysis is restricted to two closely spaced microwave carriers, the

result shows clearly the frequency-dependent nonlinear characteristics. Their analysis shows that the nonlinear distortions become larger when the modulating frequencies are closer to the resonance frequency.

2.3.2 Optical Fibers

Essentially, there are three types of optical fiber configurations: single-mode step index, multimode step-index, and multimode graded-index.

(1.) Single-mode Step-Index Fiber

This fiber has a core that is sufficiently small so that there is essentially only one path that light may take as it propagates.

(2.) Multimode Step-Index Fiber

This fiber is similar to the single-mode configuration except that the core is much larger. This type of fiber has a larger light-to-fiber aperture and, consequently, allows more light to enter the cable. Hence, this kind of fiber is suitable for use in systems that utilize a LED as light source.

(3.) Multimode Graded-Index Fiber

This fiber is characterized by a central core that has a nonuniform refractive index; it is maximum at the center and decreases gradually toward the outer edge. As the light rays propagate down the fiber, the light rays that travel in the outermost area of the fiber travel a greater distance than the rays travelling near the center. Because the refractive index decreases with distance from the center and the velocity is inversely proportional to the refractive index, the light rays traveling farthest from the center propagate at a higher velocity. Consequently, they take approximately the same amount of time to travel the length of the fiber.

Before comparing these fibers, we explain the modal dispersion phenomenon.

Modal Dispersion

Modal dispersion, or pulse spreading, is caused by the difference in the propagation times of light rays that take different paths down a fiber. Obviously, modal dispersion can occur only in multimode fibers. It can be reduced considerably by using graded index fibers and almost eliminated by using single-mode step-index fibers.

Comparison of Three Optical Fibers

Single-Mode Step-Index Fiber

Advantages

(1.) There is minimum dispersion. Because all rays propagating down the fiber take approximately the same path, they take approximately the same amount of time to travel down the cable. Consequently, a pulse of light entering the cable can be reproduced at the receiving end, accurately.

(2.) Because of the high accuracy in reproducing transmitted pulses at the receive end, larger bandwidths and higher information transmission rates are possible with single-mode step-index fibers than with other types of fibers.

Disadvantages

(1.) Because the central core is very small, it is difficult to couple light into and out of this type of fiber. The source-to-fiber aperture is the smallest of all the fiber types.

(2.) Again, because of the small central core, a highly directive light source such as a laser is required to couple light into a single-mode step-index fiber.

(3.) Single-mode step-index fibers are expensive and difficult to manufacture.

Multimode Step-Index Fiber

Advantages

(1.) Multimode step-index fibers are inexpensive and simple to manufacture.

(2.) It is easy to couple light into and out of these fibers; they have a relatively large source-to-fiber aperture.

Disadvantages

(1.) Light rays take many different paths down the fiber with large differences in their propagation times. Because of this, rays traveling down this type of fiber have a tendency to spread out. Consequently, a pulse of light propagating down a multimode step-index fiber is distorted more than in the other two types of fibers.

(2.) Bandwidth and rate of information transfer possible with this type of cable are each less than with the other types.

Multimode Graded-Index Fiber

Essentially, there are no outstanding advantages or disadvantages when it comes to this type of fiber. Multimode graded-index fibers are easier to couple light into and out of than single-mode step-index fibers but more difficult than with multimode step-index fibers. Distortion due to multiple propagation paths is greater than in single-mode step-index fibers but less than in multimode step-index fibers. Graded-index fibers are easier to manufacture than single-mode step-index fibers but more difficult than multimode step-index fibers. The multimode graded-index fiber is considered an intermediate fiber compared to other types.

2. Light Detectors

There are two devices that are commonly used for detecting light energy in fiber optic communications receivers; Positive-Intrinsic-Negative (PIN) diodes and Avalanche Photodiodes (APDs).

PIN Diodes

A PIN diode is a depletion-layer photodiode and is probably the most common device used as a light detector in fiber optic communications systems. Basically, a PIN photodiode operates just opposite of an LED. Most of the photons are absorbed by electrons in the valence band of the intrinsic material. When photons are absorbed, they add sufficient energy to generate carriers and allow current to flow through the device.

Avalanche Photodiodes

An APD is a *pipn* structure. Light enters the diode and is absorbed by the thin, heavily doped n-layer. This causes a high electric field intensity to be developed across the i-p-n junction. The high reverse-biased field intensity causes impact ionization to occur near the breakdown voltage of the junction. During impact ionization, a carrier gains sufficient energy to ionize other bounded electrons. These ionized carriers, in turn, cause more ionizations to occur. The process continues like an avalanche and is, effectively, equivalent to an internal gain or carrier multiplication. The most important characteristics of light detectors are:

(1.) Responsivity

This is a measure of the conversion efficiency of a photodector. It is the ratio of the output current of a photodiode to the input optical power and has the unit of amperes/watt. Responsivity is generally given for a particular wavelength or frequency.

(2.) Dark current

This is the leakage current that flows through a photodiode with no light input. Dark current is caused by thermally generated carriers in the diode.

(3.) Transit time

This is the time it takes a light-induced carrier to travel across the depletion area. This parameter determines the maximum bit rate possible with a particular photodiode.

(4.) Spectral response

This parameter determines the range or system length that can be achieved for a given wavelength. Generally, relative spectral response is graphed as a function of wavelength or frequency.

APDs compared to PIN diodes are more sensitive and require less additional amplification. The disadvantages of APDs are relatively long transit times and additional internally generated noise due the avalanche multiplication factor. They are also more nonlinear than PINs. We discuss this subject in design considerations of SCM schemes in the next section.

2.4 Design Considerations of SCM Lightwave Systems

Radio-frequency or microwave Subcarrier Multiplexing (SCM) has recently emerged as a potentially important multiplexing technique for future high-capacity lightwave systems. The terminology "subcarrier multiplexing" should be understood to encompass the multiplexing of both multichannel analog and/or digital signals. A number of baseband analog or digital signals are first frequency-division multiplexed by using local oscillators (LO's) of different radio frequencies. The upconverted signals are then combined to drive a high-speed light source (typically a laser diode). The LO frequencies are the so-called subcarriers in contrast to the optical carrier frequencies. At the receiver site, a user can re-

ceive any one of the FDM channels by tuning a local oscillator and downconvert the RF or microwave signals to baseband or IF frequencies, similar to the way we tune in radio or TV channels in radio systems. SCM systems have an advantage over time-division-multiplexed (TDM) baseband digital lightwave systems in that services carried by different subcarriers are independent of each other, and require no synchronization. In addition, SCM systems are presently still more cost-effective than high-capacity TDM lightwave systems-which is an attractive feature for near term deployment in broad-band subscriber loop systems.

In this section, we discuss the degradation due to laser-nonlinearity which limits the performance of these systems. We describe the APD nonlinearity and a phenomenon called beat-noise and we suggest solutions against this kind of noise.

Nonlinear Distortions

Harmonic and Intermodulation Distortions (IMD): For multichannel signals transmission through a nonlinear device such as a laser diode, second order IMD ($A - B$ or $A + B$ type where A and B stand for two arbitrary RF signals) are the dominant second order nonlinear distortions, and triple beat products specially $A+B-C$ type, which occurs within signal bands most frequently are the dominant third order nonlinear distortions. Also, the number of two-tone third order IMD ($2A - B$) increases as $N(N-1)$. The number of triple beat products increases as $\frac{N(N-1)(N-2)}{2}$. Therefore, triple beat nonlinear products are always the dominant third order nonlinear distortion products for large numbers of channels ($n > 7$). For RF and microwave signals occupying a bandwidth of more than one octave, the second order nonlinear distortions must be taken into account. Otherwise, only third order nonlinear distortions have to be considered.

If the RF/microwave carriers are totally uncorrelated and the total driving power is kept constant as the number of channels increases to N, the Optical Modulation Index (OMI) per channel must be decreased by a factor of $\frac{1}{\sqrt{N}}$. Therefore, the received carrier power for each channel is decreased by $\frac{1}{N}$. For a large number of channels, the dominant, third order nonlinear distortions is of the $A + B - C$ type, the power of which decreases

by a factor $\frac{1}{N^3}$; the dominant second order nonlinear distortions is of the $A+B$ type, whose power decreases by a factor of $\frac{1}{N^2}$. On the other hand, the number of beat products increases: for the channel suffering the highest $A+B-C$ type IMD which occurs at a midband channel, the number of IMD products that fall into that channel is increased to $\leq (\frac{3}{8}) \cdot N^2$ [45], [46]. For the channel suffering the highest $A-B$ type IMD which occurs at the lower band edge, the number of IMD products that fall into that channel is increased to $\leq N$. Therefore, the final power ratio of carrier to $A+B-C$ type IMD, C/IM_{A+B-C}, is changed by a factor $(\frac{1}{N})/((\frac{1}{N^3}) \cdot \frac{3}{8} \cdot N^2)$, which is a constant, and the final power ratio of carrier to $A-B$ type IMD, C/IM_2 is changed by a factor of $(\frac{1}{N})/((\frac{1}{N^2}) \cdot N)$ which is also a constant. Hence, we can see that as long as the driving power is kept constant, the difference of C/IMD both for a small number of channels $N \geq 7$ and for a large number of channels is small.

APD Nonlinearity: Due to the sharp increase of the avalanche gain with increasing bias voltage, an APD receiver usually exhibits nonlinear distortions at either high optical power, or in the high gain region.

At this point, we address a phenomenon called beat-noise. SCM systems with multiple lasers can experience impairments when the wavelengths of two lasers drift to within an RF bandwidth of each other [39]. This problem can be avoided by keeping the laser wavelengths well separated or by using stable lasers. Of course, LEDs don't cause this problem because of their short-coherent length. Reference [22] suggests using short-coherence self-pulsating lasers. Their linewidth is in the order of 2 nm. This minimizes optical beat noise, which has been shown to limit subcarrier networks using conventional, high-coherence lasers [38]. They also state that short-coherence lasers allow the use of low-cost multimode fiber components without concern for modal noise generation.

Now, having pointed to some problem areas in realizing SCM lightwave systems; in the next chapter, we introduce the CDMA scheme.

Chapter 3
Spread Spectrum in a Multiuser Network

3.1 Overview and Introduction to DS/SSMA System

Many real-world communications channels are accurately modeled as stationary Additive White Gaussian Noise (AWGN) channels. Therefore, most of the modulation/demodulation techniques have been designed to communicate digital information from one place to another as efficiently as possible in a stationary white Gaussian noise (AWGN) environment. The transmitted signals are selected to be relatively efficient in their use of communication resources, namely; power and bandwidth. Modulations are designed to yield minimum bit error probability for the given transmitted signal in AWGN. Quantative comparisons are made using the bandwidth and the E_b/N_o required at the receiver to achieve a specified bit error probability.

There are some other important channels which do not fit the AWGN model. Consider, for example, when there are multiple propagation paths between a transmitter and a receiver. The receiver interferes with itself via a delayed reception of its own signal. This phenomenon is called multiple reception and is a problem in microwave digital radios such as those used for long-haul telephone transmission and in urban mobile radio, among other places. The interference in these cases can not be modeled as a stationary AWGN.

Another type of interference which does not fit this model occurs when in a Frequency Subcarrier Multiplexing Optical Local Area Network (LAN) several data modulated subcarriers intensity modulate a light source like a laser which introduces intermodulation products (IMPs) interfering with original signals.

Spread spectrum techniques can be used to overcome the effects of the described types of interference. The technique is called spread-spectrum because the transmission bandwidth employed is much greater than the minimum bandwidth required to transmit

the digital information. To be classified under a spread-spectrum system, the modulator and the demodulator must have the following characteristics:

(1.) Transmitted signal energy must occupy a bandwidth which is larger than the information bit rate (usually much larger) and which is independent of the information bit rate.

(2.) Demodulation must be accomplished, in part, by correlation of the received signal with a replica of the signal used in the transmitter to spread the information signal.

Spread-spectrum techniques can be very useful in solving a wide range of communications problems. To be specific, spread spectrum signals are used for the purpose of (1) suppressing the effect of interference due to jamming, interference arising from other users of channel, and self-interference due to multipath propagation, (2) hiding a signal by transmitting it at a low power and making it difficult for an unintended listener to detect it in presence of background noise, and (3) achieving message privacy in presence of other listeners.

The amount of performance improvement achieved through the use of spread spectrum is defined as the processing gain of the spread spectrum system. Processing gain is the gain difference between system performance with spread-spectrum techniques and system performance without spread-spectrum techniques, all else being equal. An often used approximation for processing gain is the ratio of spread bandwidth to the information rate. That is, the bandwidth expansion factor $B_c = W/R$, where the spread spectrum signal bandwidth W is much greater than the information rate R in bits per second. The large redundancy inherent in spread spectrum signals is required to overcome the severe levels of interference.

As we have mentioned before, one of the most important impairments in frequency-subcarrier multiplexing optical systems is interference of IMPs - caused by laser nonlinearity - with main data-modulated signals. In section 3.3, we will show how spread spectrum can be used to overcome this problem.

Before getting into any further details in section 3.3, we introduce a class of techniques known as code-division multiple access (CDMA). The CDMA techniques are those methods in which the multiple-access capability is due primarily to coding. In these techniques all users are sharing the same channel bandwidth.

Interference from other users arises in multiple-access communications systems in which a number of users share a common channel bandwidth. At any given time, a subset of these users may transmit information simultaneously over the common channel to corresponding receivers. Assuming that all users employ the same code for the encoding and decoding of their respective information sequences, the transmitted signals in this common spectrum may be distinguished by superimposing a different pseudo-random pattern, also called a code, on each transmitted signal. Thus, a particular receiver can recover the transmitted information intended for it by knowing the pseudo-random pattern, i.e., the key, used by the corresponding transmitter. This type of communication technique which allows multiple users to simultaneously use a common channel for transmission of information, is called code division multiple access (CDMA).

The most common form of CDMA is Direct-Sequence Spread-Spectrum Multiple Access (DS/SSMA) in which each user is assigned a particular code sequence modulating the carrier along with the digital data. The DS/SSMA techniques are characterized by the use of a high rate code (i.e., many code symbols per data symbol) having the effect of spreading the bandwidth of data signal. The two most common forms of SSMA are:

(1.) Phase-coded SSMA (also known as direct-sequence spread-spectrum)

(2.) Frequency-hopped SSMA

We are concerned only with direct-sequence spread-spectrum in this work.

Direct-Sequence Spread-Spectrum

One method of spreading the spectrum of a data-modulated signal is to modulate the

signal a second time using a very wideband spreading signal. This second modulation is usually some form of digital phase modulation, although analog amplitude or phase modulation is conceptually possible. The spreading signal is chosen to have properties which facilitate demodulation of the transmitted signal by the intended receiver, and which make demodulation by an unintended receiver as difficult as possible. These same properties will also make it possible for the intended receiver to discriminate between a communication signal and a jamming signal.

Bandwidth spreading by direct modulation of a data-modulated carrier by a wideband spreading signal or code is called direct-sequence (DS) spread spectrum. Other types of spread spectrum systems exist in which the spreading code is used to control the frequency or time of the data-modulated carrier. Thus, indirectly modulating the data-modulated carrier by a spreading code.

Direct sequence spread spectrum utilizes the most common form of spread spectrum. As we stated earlier, it employs digital phase modulation as the spreading modulation and that is why DS spread-spectrum is also known as phase-coded SSMA. In phase-coded SSMA the carrier is phase-modulated by the digital data sequence and the code sequence.

Direct sequence spread spectrum multiple access technique, shown in Fig. 3.1, is probably the most common form of spread spectrum modulation. Here, the carrier is phase modulated by the information data bit stream and the code sequence

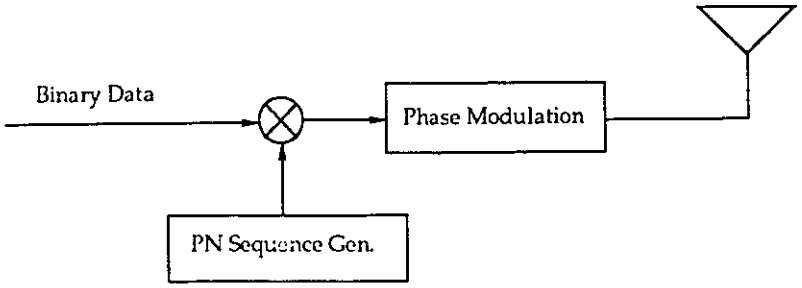

a) Transmitter

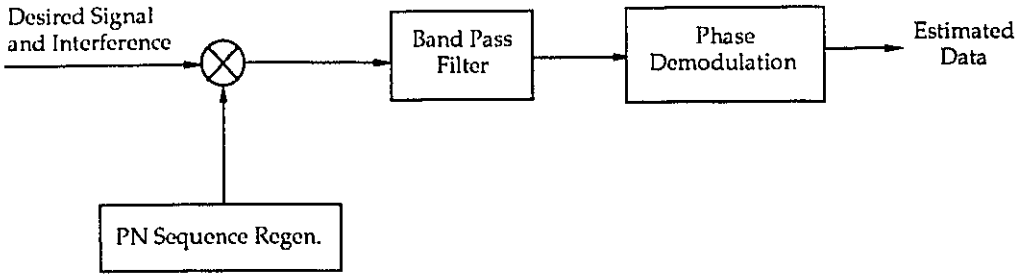

b) Receiver

Fig. 3.1. (a) Transmitter (b) Receiver

In order to understand how a spread-spectrum multiple access system operates, it is necessary to know the required properties of the direct sequence codes. Therefore, in the next section we introduce these code parameters and properties.

3.2 Direct Sequence Codes for CDMA Applications

3.2.1 Direct Sequence Code Parameters

Spread-spectrum communications systems require sets of signals which have the following two properties:

(1.) each signal in the set is easy to distinguish from a time-shifted version of itself;

(2.) each signal in the set is easy to distinguish from a possibly time-shifted version of every other signal in the set.

The signals employed in these systems are periodic. This is primarily because of the simplifications in system implementation that typically results from the use of periodic signals. The signals of interest for this particular application are periodic signals which consist of sequences of time-limited pulses. These pulses are all of the same shape, so that the signal can be written as

$$x(t) = \sum_{n=-\infty}^{+\infty} x_n P_{T_c}(t - nT_c) \tag{3.1}$$

where $P_{T_c}(t)$ is a unit amplitude rectangular pulse and T_c is the time duration of this pulse. If $x(t) = x(t+T)$ for all t, then T must be a multiple of T_c and the sequence (x_n) must be periodic with a period which is a divisor of T/T_c. Suppose $x(t)$ and $y(t)$ are periodic signals, as described above. One of the most common and most useful measures of distinguishability between two signals is the mean-square difference. For our purpose, two signals $x(t)$ and $y(t)$ are easy to distinguish if and only if the mean-squared differences between them is large, and we will require not only that $x(t)$ is easy to distinguish from $y(t)$ but also that $-x(t)$ is easy to distinguish from $y(t)$. Both $+x(t)$ and $-x(t)$ must be considered because modulation processes are involved. Thus the measure of distinguishing is

$$T^{-1} \int_0^T [y(t) \pm x(t)]^2 dt$$

$$= T^{-1}\left\{\int_0^T [y^2(t) + x^2(t)]dt \pm 2\int_0^T x(t)\ y(t)\ dt\right\} \tag{3.2}$$

The first integral on the right-hand side of eq.(3.2) is the energy in $x(t)$, $0 \leq t \leq T$, plus the energy in $y(t)$, $0 \leq t \leq T$. Thus for a fixed signal energy, $y(t)$ is easy to distinguish from both $+x(t)$ and $-x(t)$ if and only if the magnitude of the quantity

$$r = \int_0^T x(t)\ y(t)\ dt \tag{3.3}$$

is small.

Now, if $x(t)$ has the form of eq.(3.1) and $y(t)$ is given by

$$y(t) = \sum_{n=-\infty}^{+\infty} y_n P_{T_c}(t - nT_c) \tag{3.4}$$

It is easy to show that parameter r of (3.3) is given by

$$r = T_c \sum_{n=0}^{N-1} x_n\ y_n \tag{3.5}$$

In general, according to eq. (3.5), the inner product of the continuous time periodic signals $x(t)$ and $y(t)$ is proportional to the inner product of the corresponding vectors $(x_0, x_1, ..., x_{N-1})$ and $(y_0, y_1, ..., y_{N-1})$. Furthermore, if $\tau = lT_c$, eq. (3.5) generalizes to

$$r_{x,y}(\tau) = T_c \sum_{n=0}^{N-1} x_n\ y_{n+l} \tag{3.6}$$

The above discussion motivates the consideration of the periodic crosscorrelation function for sequences (x_n) and (y_n) which is defined by

$$\theta_{x,y}(l) = \sum_{n=0}^{N-1} x_n y_{n+l} \tag{3.7}$$

From eq. (3.6) we see that $r_{x,y}(\tau) = T_c\theta_{x,y}(l)$ whenever $\tau = lT_c$. In addition, for arbitrary values of τ, $r_{x,y}(\tau)$ can be determined from the periodic crosscorrelation function. For instance, for $0 \leq \tau < T$,

$$r_{x,y}(\tau) = T_c\ \theta_{x,y}(l') + (\tau - l'T_c)[\theta_{x,y}(l'+1) - \theta_{x,y}(l')] \tag{3.8}$$

where l' is the largest integer such that $l'T_c \leq \tau$.

Since the periodic crosscorrelation parameters for the continuous-time signals $x(t)$ and $y(t)$ of eqs. (3.1) and (3.4) are compeletly determined by the crosscorrelation function, the signal requirements described at the beginning of this section reduce to the problem of having sets of periodic sequences with the following two properties:

(1.) for each sequence $x = x(n)$ in the set, $|\theta_{x,x}(l)|$ is small for $1 \leq l \leq N-1$.

(2.) for each pair of sequences $x = x(n)$ and $y = y(n)$, $|\theta_{x,y}(l)|$ is small for all l.

In spread-spectrum communications, aperiodic correlation parameters for sequences in addition to the periodic correlation parameters are of particular interest.

In the following, we mention the aperiodic and periodic properties of pseudorandom and related sequences. The particular correlation parameters considered are those that are motivated by applications in spread-spectrum and code-division multiple-access communications areas.

In much of the literature on periodic sequences, the terms pseudorandom sequences, pseudonoise (PN) sequence, and maximal-length linear feedback shift-register sequence (m-sequence) are used synonymously. However, recently the term pseudorandom sequence or pseudonoise sequence has been employed as generic name for sequences from some imprecisely defined large class that includes certain non-maximal-length linear feedback shift-register sequences in addition to the m-sequences.

Before discussing the different properties of several classes of periodic sequences such as m-sequences and some nonmaximal-length linear feedback shift-register sequences like Gold and Kasami sequences, we first define the periodic and aperiodic correlation functions (autocorrelation and crosscorrelation) for general sequences.

We note that in our analysis, all PN sequences with elements $\{0, 1\}$ represented by a sequence α can be mapped into corresponding PN sequences with elements $\{-1, +1\}$ represented by a sequence a. In practice, the spreading is achieved if the information data

bits and the code sequence have elements $\{0, 1\}$, by adding each data bit modulo-2 to every chip in a full PN sequence. Conversely, if the data bits and the PN sequence have elements $\{-1, 1\}$, spreading is carried out by multiplying the chips by the data bit. This distinction will help to clarify the various notations used for denoting the PN sequence in this chapter.

Assume x, y and z denote sequences with length N where $x = (x_o, x_1, ..., x_{N-1})$. The inner product $< x, y >$ of two vectors x and y is defined by $< x, y >= x_o y_o + x_1 y_1 + ... + x_{N-1} y_{N-1}$. Note that, $< x, x >$ is a positive number for all nonzero vectors. Let T denote the operator which shifts vectors cyclically to the left by one place that is $Tx = (x_1, x_2, ..., x_{N-1}, x_o)$. If T is applied k times to x, the result is $T^k x$. We see that $T^k x = (x_k, x_{k+1}, ..., x_{N-1}, x_o, x_1, ..., x_{k-1})$ for $0 \leq k < N$, while $T^N x = x$. For larger values of k, $T^k x = T^{k'} x$ where $k' \equiv k \bmod N$. Similarly the operator T^{-1} shifts vectors cyclically to the right by one place, and it is easy to see that $T^{-k} x = T^{N-k} x$ for $0 \leq k < N$, and $T^{-N} x = x$. We also have that $\|T^k x\| = \|x\|$ and $\sum(T^k x) = \sum x$. The period of x is defined to be the least positive integer M such that $T^M x = x$. Although $T^i x \neq T^j x$ for $0 \leq i < j < M$, the vectors $x, Tx, T^2 x, ..., T^{N-1} x$ are cyclically equivalent; that is, they are cyclic shifts of each other. The sequences $x, Tx, T^2 x, ..., T^{N-1} x$ are called phases of x; they are generated by cyclically equivalent vectors.

For vectors x and y of length N we define the periodic crosscorrelation function $\theta_{x,y}(.)$ by

$$\theta_{x,y}(l) =< x, T^l y >, \qquad l \in z \tag{3.9}$$

It is easy to verify that for each $l \in z$

$$\theta_{x,y}(l) = \theta_{x,y}(l + N) \tag{3.10}$$

and

$$\theta_{x,y}(-l) = \theta_{y,x}(l) \tag{3.11}$$

The periodic autocorrelation function $\theta_x(.)$ for the sequence x is just $\theta_{x,x}(.)$. Notice

that, $\theta_x(0) =< x, x >$ and for each $l \in z$, $\theta_x(l) = \theta_x(l+N)$, $\theta_x(-l) = \theta_x(l)$, and also

$$|\theta_x(l)| \leq \|x\|^2 =< x, x >= \theta_x(0). \tag{3.12}$$

At times, an alternative notation $\theta(x,y)(.)$ is used for $\theta_{x,y}(.)$.

θ_c and θ_a denote the peak cross-correlation magnitude and the peak out-of-phase autocorrelation magnitude respectively, so that

$$\theta_c = max\{|\theta_{x,y}(l)| \quad : \quad 0 \leq l \leq N-1 \quad , \quad x \neq y\} \tag{3.13}$$

and

$$\theta_a = max\{|\theta_x(l)| \quad : \quad 1 \leq l \leq N-1\} \tag{3.14}$$

θ_{max} is the maximum correlation function defined by

$$\theta_{max} = max\{\theta_a, \theta_c\}$$

So far, we have mentioned only the periodic crosscorrelation properties of the code sequences, however, the need for considering aperiodic crosscorrelation properties in order to analyze an asynchronous phase-coded spread spectrum multiple access (SSMA) system performance can not be avoided. We also mention that, one of the most desirable features of a direct sequence SSMA system is its asynchronous multiple access capability. Therefore, in the following we discuss some of the aperiodic crosscorrelation properties of sequences which are relevent to our work.

Assume $a_k(t)$ is a code sequence waveform which consists of a periodic sequence of unit amplitude, positive and negative, rectangular pulses of duration T_c. If a_j^k is the corresponding sequence of elements of $\{+1, -1\}$, then we write $c_k(t)$ as

$$a_k(t) = \sum_{j=-\infty}^{+\infty} a_j^k \; P_{T_c}(t - jT_c) \tag{3.15}$$

where $P_{T_c}(t)$ for $0 \leq t < T_c$ and $P_{T_c}(t) = 0$, otherwise. It is assumed that the Kth code sequence c_j^k has a period $N = T/T_c$. Now, let $a_i(t)$ and $a_j(t)$ be two different code

waveforms as described above, then, the continuous-time partial cross-correlation functions $R_{k,i}(.)$ and $\hat{R}_{k,i}(.)$ are defined as

$$R_{k,i}(\tau) = \int_0^{\tau} a_k(t-\tau)a_i(t)dt$$

$$\hat{R}_{k,i}(\tau) = \int_{\tau}^{T} a_k(t-\tau)a_i(t)dt \tag{3.16}$$

for $0 \leq \tau \leq T$. It is easy to see that for $0 \leq lT_c \leq \tau \leq (l+1)T_c \leq T$, these two cross-correlation functions can be written as

$$R_{k,i}(\tau) = C_{k,i}(l-N)T_c + [C_{k,i}(l+1-N) - C_{k,i}(l-N)](\tau - lT_c) \tag{3.17}$$

and

$$\hat{R}_{k,i}(\tau) = C_{k,i}(l)T_c + [C_{k,i}(l+1) - C_{k,i}(l)](\tau - lT_c) \tag{3.18}$$

where the discrete aperiodic cross-correlation function $C_{k,i}$ for the sequences $(a_j^{(k)})$ and $(a_j^{(i)})$ is defined by

$$C_{k,i}(l) = \begin{cases} \sum_{j=0}^{N-1-l} a_j^{(k)}\ a_{j+l}^{(i)}, & 0 \leq l \leq N-1 \\ \sum_{j=0}^{N-1+l} a_{j-l}^{(k)}\ a_j^{(i)}, & 1-N \leq l \leq 0 \\ 0. & |l| \geq N \end{cases} \tag{3.19}$$

Since the term,

$$\begin{aligned} V &= \frac{1}{T}\sum_{\substack{k=1 \\ k\neq i}}^{K} \int_0^T R^2{}_{k,i}(\tau) + \hat{R}_{k,i}^2(\tau)d\tau \\ &= \frac{1}{T}\sum_{\substack{k=1 \\ k\neq i}}^{K}\sum_{l=0}^{N-1} \int_{lT_c}^{(l+1)T_c} R^2{}_{k,i}(\tau) + \hat{R}_{k,i}^2(\tau)d\tau \end{aligned} \tag{3.20}$$

appears in the variance of the noise component of the output of the i^{th} receiver in our proposed Local Area Network (LAN) we find an appropriate expression for such a term. We substitute for $R_{k,i}(\tau)$ and $\hat{R}_{k,i}(\tau)$ from eqs. (3.17) and (3.18) into (3.20). Upon evaluation of the resulting integral we find that

$$V = \frac{T^2}{3N^2}(\sum_{\substack{k=1 \\ k\neq i}}^{K} r_{k,i}) \tag{3.21}$$

where

$$r_{k,i} = \sum_{l=0}^{N-1} \Big\{ C_{k,i}^2(l-N) + C_{k,i}(l-N)C_{k,i}(l-N+1) + C_{k,i}^2(l-N+1) + C_{k,i}^2(l) + C_{k,i}(l)C_{k,i}(l+1) + C_{k,i}^2(l+1) \Big\}$$

This last expression can be written in terms of the crosscorrelation $\mu_{k,i}(n)$ which are defined by

$$\mu_{k,i}(n) = \sum_{l=1-N}^{N-1} C_{k,i}(l)C_{k,i}(l+n) \tag{3.22}$$

Notice that;

$$\mu_{k,i}(0) = \sum_{l=1-N}^{N-1} C_{k,i}^2(l) = \sum_{l=0}^{N-1} C_{k,i}^2(l-N) + C_{k,i}^2(l) = \sum_{l=0}^{N-1} C_{k,i}^2(l-N+1) + C_{k,i}^2(l+1)$$

and

$$\mu_{k,i}(1) = \sum_{l=1-N}^{N-1} C_{k,i}(l)\ C_{k,i}(l+1) = \sum_{l=0}^{N-1} C_{k,i}(l-N)\ C_{k,i}(l-N+1) + C_{k,i}(l)\ C_{k,i}(l+1)$$

Therefore,

$$r_{k,i} = 2\mu_{k,i}(0) + \mu_{k,i}(1)$$

and

$$V = \frac{T^2}{3N^3} \sum_{\substack{k=1 \\ k \neq i}}^{K} [2\mu_{k,i}(0) + \mu_{k,i}(1)]$$

Finally, we should mention a preliminary system design can be done based on the following approximation [28]:

$$2\mu_{k,i}(0) + \mu_{k,i}(1) \approx 2N^2$$

consequently;

$$V \approx \frac{T^2}{3N^3}(K-1)2N^2 = \frac{2}{3}(K-1)\frac{T^2}{N} \tag{3.23}$$

3.2.2 Properties of m-Sequences

The sequences that have received the most attention in the literature are the binary maximal-length linear feedback shift-register sequences which we refer to as m-sequences. As the name suggests these are precisely the sequences of maximum possible period $N = 2^n - 1$ from an n-stage binary shift-register with linear feedback. In this section, we shall restrict our attention to binary sequences. This is primarily because binary sequences are employed in our application. In addition, the restriction to binary sequences simplifies much of the discussion in this section. Let $h(x) = h_0x^n + h_1x^{n-1} + ... + h_{n-1}x + h_n$ denote a binary polynomial of degree n where $h_0 = h_n = 1$ and the other h_i's take on values 0 and 1. A binary sequence u is said to be a sequence generated by $h(n)$ if for all integers j

$$h_0u_j \oplus h_1u_{j-1} \oplus h_2u_{j-2} \oplus .... \oplus h_nu_{j-n} = 0 \tag{3.24}$$

Here $\oplus$ denotes addition modulo 2 (i.e., the EXCLUSIVE-OR operation). Replacing j by $j + n$ in eq. (3.24), and using the fact that $h_0 = 1$, we obtain

$$u_{j+n} = h_nu_j \oplus h_{n-1}u_{j+1} \oplus ... \oplus h_1u_{j+n-1}$$

From this, it follows that the sequence u can be generated by an n-stage binary linear feedback shift register. For example, the shift register in Fig. 3.2 corresponds to $h(x) = x^5 + x^4 + x^3 + x^2 + 1$.

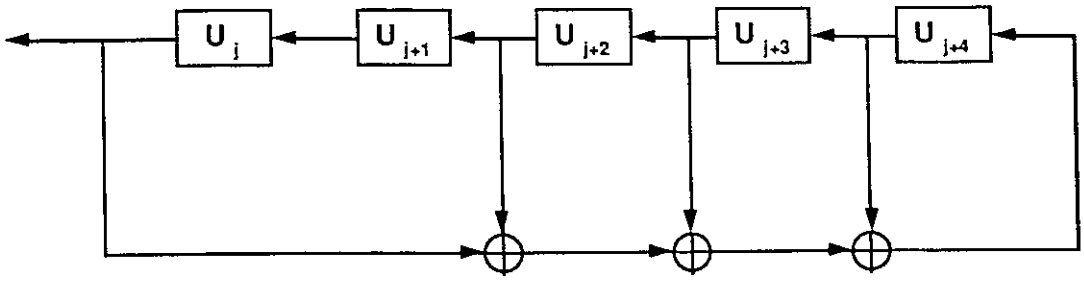

Fig. 3.2. Maximal Length Sequence Generator

An n^{th}-order polynomial $h(x)$ is *irreducible* if it is not divisible by any polynomial of degree less than n but greater than 0. The period of sequence u generated by the polynomial $h(x)$ is at most $N = 2^n - 1$. If $h(x)$ is an irreducible polynomial of degree n, sequence u has this maximal period $N = 2^n - 1$ and is called an m-sequence and $h(x)$ is called a *primitive* binary polynomial of degree n.

Some properties of m-sequences which are useful in their application to spread-spectrum and relevant to our work are:

Property I. The period of an m-sequence u is $N = 2^n - 1$.

Property II. There are exactly N nonzero sequences generated by $h(x)$, and they are just the N different phases of u; namely $u, Tu, T^2u, ..., T^{N-1}u$.

Property III. Given distinct integers i and j, $0 \leq i, j \leq N$, there is a unique integer k, distinct from both i and j, such that $0 \leq k \leq N$ and

$$T^i u \oplus T^j u = T^k u$$

where this property is known as the shift-and-add property.

Property IV. A maximal-length sequence contains one more "one" than "zero". The number of ones in the sequence which is called $wt(u)$ is $\frac{1}{2}(N+1)$.

$$wt(u) = 2^{n-1} = \frac{1}{2}(N+1)$$

Property V. The periodic autocorrelation function $\theta_u(l)$ is two -valued and is given by

$$\theta_u(l) = \begin{cases} N, & if \ \ l \equiv 0 \ \ mod \ \ N \\ -1, & if \ \ l \not\equiv 0 \ \ mod \ \ N. \end{cases}$$

Property VI. Let u denote an m-sequence of period $N = 2^n - 1$, generated by $h(x)$ and q denote a positive integer, and consider the sequence v formed by taking every qth bit of u (i.e., $v_i = u_{qi}$ for all i). The sequence v is said to be a decimation by q of u, and will be denoted by $u[q]$. Then, if $u[q]$ is not identically zero, $u[q]$ has period $N/gcd(N,q)$, and is generated by the polynomial $\hat{h}(x)$ whose roots are the qth powers of the roots of $h(x)$; where $gcd(a,b)$ denote the greatest common divisor of the integers a and b.

Property VII. Let u and v denote m-sequences of period $N = 2^n - 1$. Many properties of crosscorrelation function $\theta_{u,v}(.)$ follow immediately from previous results in this chapter. We have that $\theta_{u,v}(l) = \theta_{u,v}(l+N)$ and $|\theta_{u,v}(l)| \leq N$ for all l. Other results are:

$$\sum_{l=0}^{N-1} \theta_{u,v}(l) = +1 \tag{3.25}$$

&

$$\sum_{l=0}^{N-1} |\theta_{u,v}(l)|^2 = N^2 + N - 1 \tag{3.26}$$

Another point is that a bound due to [30] implies that for at least one integer l,

$$|\theta_{u,v}(l)| > -1 + 2^{(n+1)/2} \tag{3.27}$$

Although we can find pairs of sequences for which the periodic crosscorrelation function is relatively small in magnitude, for our application which is code-division multiple-access communications, large sets of sequences are needed. One pair of m-sequences which has good crosscorrelation properties is the so called preferred pair. The crosscorrelation of these pairs is three-valued and θ_c for these pairs is small.

Maximal Connected Sets of m-Sequences

A connected set of m-sequences is a collection of m-sequences which has the property that each pair in the collection is a preferred pair. A largest possible connected set is called a maximal connected set and the size of such a set is denoted by M_n. Listed in Table 3.1 are the values of M_n and the peak periodic crosscorrelation magnitudes $t(n)$ for a maximal connected set for $3 \leq n \leq 16$. For purposes of comparison, Table 3.1 also lists the size of the set of all m-sequences of each period, and the peak period crosscorrelation θ_c for this set.

Maximal connected sets of m-sequences are useful in those applications which require only a few sequences with excellent crosscorrelation and autocorrelation properties. However, most applications such as spread-spectrum multiple-access communications, for example require much larger sets of sequences. Unfortunately, large sets of m-sequences generally have quite a poor crosscorrelation properties, and thus are inadequate for such applications. It is therefore desirable to obtain larger sets of sequences of period $N = 2^n - 1$ which have the same bound θ_c on the peak periodic crosscorrelation as for maximal connected sets. Since the larger sets like Gold and Kasami sequences must contain some nonmaximal-length sequences, their peak periodic autocorrelation θ_a must exceed 1.

n	$N = 2^n - 1$	Number of m-sequences	θ_c for set of all m-sequences	M_n	$t(n)$
3	7	2	5	2	5
4	15	2	9	0	9
5	31	6	11	3	9
6	63	6	23	2	17
7	127	18	41	6	17
8	255	16	95	0	33
9	511	48	113	2	33
10	1023	60	383	3	65
11	2047	176	287	4	65
12	4095	144	1407	0	129
13	8191	630	≥ 703	4	129
14	16383	756	≥ 5631	3	257
15	32767	1800	≥ 2047	2	257
16	65535	2048	≥ 4095	0	513

TABLE 3.1

Maximal-Length Sequence Design

We use a preferred pair of m-sequences in our experiment and in general it is often necessary to design circuits that generate m-sequences having a particular number of stages. Since finding the primitive polynomials used to generate these sequences is difficult, a number of authors have generated tables of primitive polynomials for quick reference. In particular, Peterson, et al. [47] have an extensive table of polynomials in their Appendix C. The use of this table is described here since it provides a large selection of primitive polynomials which will be useful to the spread-spectrum system designer.

In the table, all polynomials are specified by an octal number which defines the coefficients of $h(x)$. The table also defines some polynomials which are not primitive and therefore will not yield a maximal-length sequence. An example entry in the table is

DEGREE 6	1 103F	3 127B	5 147H	7 111A
	9 015	11 155E	21 007	

The letters E, F, and H mean the polynomials 103, 147, and 155 are primitive while A and B indicate nonprimitive polynomials. Now, suppose the m-sequence u is generated by the polynomial 103. Then u[3] that stands for a sequence formed by taking every third bit of u ($u[3]$ is a decimation by 3 of u) is generated by the polynomial 127, $u[5]$ is generated by 147, etc. According to property VI, $u[3]$ has a period $63/gcd(63,3) = 21$, and thus is not an m-sequence; while $u[5]$ has a period 63 and is an m-sequence. The corresponding polynomials 127 and 147 are clearly indicated as nonprimitive and primitive, respectively. The octal number gives the coefficients of $h(x)$ beginning with h_0 on the right and proceeding to h_n in the last nonzero position on the left.

3.2.3 Gold Sequences

One important class of periodic sequences which provides larger sets of sequences with good periodic crosscorrelation is the class of Gold sequences. A set of Gold sequences of period $N = 2^n - 1$ consists of $N + 2$ sequences for which

$$\theta_{max} = t(n) \stackrel{\triangle}{=} 1 + 2^{\lfloor (n+2)/2 \rfloor}$$

where $\lfloor y \rfloor$ denotes the integer part of the real number y. Thus, for instance, each class of 129 Gold sequences of period 127 has a correlation bound of 17. In contrast, the largest possible set of m-sequences of period 127 for which this bound holds contains only 6 sequences. Gold sequences have a three-valued correlation function taking on values from $\{-1,\ -t(n),\ t(n) - 2\}$. A set of Gold sequences can be constructed from appropriately selected m-sequences as described below.

Suppose a shift register polynomial $f(x)$ factors into $h(x)\hat{h}(x)$ where $h(x)$ and $\hat{h}(x)$ have no factors in common. Then the set generated by $f(x)$ is just the set of all sequences of the form $\alpha \oplus \beta$ where α is generated by $h(x)$ and β is generated by $\hat{h}(x)$. Now, suppose that $h(x)$ and $\hat{h}(x)$ are two different primitive binary polynomials of degree n that generate the m-sequences u and v, respectively, of period $N = 2^n - 1$. If y denotes a nonzero sequence generated by $f(x) = h(x)\hat{h}(x)$, then, from the above and property II of m- sequences, we

get either

$$y = T^i u$$

or

$$y = T^j v$$

or

$$y = T^i u \oplus T^j v$$

where $0 \leq i, j \leq N-1$, and where, $T^i u \oplus T^j v$ denotes the sequence whose kth element is $u_{i+k} \oplus v_{j+k}$. From this, it follows that y is some phase of some sequence in the set $G(u,v)$ defined by

$$G(u,v) \triangleq \{u, v, u \oplus Tv, u \oplus T^2 v, ..., u \oplus T^{N-1} v\}. \tag{3.28}$$

Note that, $G(u,v)$ contains $N+2 = 2^n + 1$ sequences of period N. It is not difficult to show that if we have two sequences y_1 and y_2 generated by $f(x)$, then $T^i y_1 \oplus T^j y_2$ is some phase of some sequences of this set. Since,

$$T^i y_1 \oplus T^j y_2 \tag{3.29}$$

from (3.25) is equal to:

$$\begin{aligned} & T^i(u \oplus T^{i_1} v) \oplus T^j(u \oplus T^{i_2} v) \\ &= (T^i u \oplus T^i T^{i_1} v) \oplus (T^j u \oplus T^j T^{i_2} v) \\ &= (T^i u \oplus T^j u) \oplus (T^i T^{i_1} v \oplus T^j T^{i_2} v) \\ &= (T^i u \oplus T^j u) \oplus (T^{i+i_1} v \oplus T^{j+i_2} v) \end{aligned} \tag{3.30}$$

and from property III of m-sequences:

$$T^i u \oplus T^j u = T^k u$$

thus, eq. (3.30) is equal to:

$$T^k u \oplus T^{k'} v$$

$$= u \oplus T^{k'-k} v \in G(u, v)$$

which is a phase of another sequence from the same polynomial. As we have stated earlier, each sequence with elements $\{0, 1\}$ represented by the sequence $\alpha = (\alpha_0, ..., \alpha_N)$ is mapped to a sequence with elements $\{1, -1\}$ represented by the sequence $a = (a_0, ..., a_N)$ where $a_i = (-1)^{\alpha_i}$ for $0 \leq i \leq N-1$; then, adding modulo-2 of the sequences with elements $\{0, 1\}$ corresponds to multiplying of the sequences with elements $\{1, -1\}$. Therefore, from above, product of two Gold sequences with an arbitrary shift is still another Gold sequence from the same set. In other words, shift-and-add property also holds for Gold sequences. In our numerical computations we use a set of Gold sequences described in [29]. Therefore, in the following we consider this example.

Example 3.1:

For $n = 7$, the polynomials 211 and 217 are a preferred pair of primitive polynomials. Their product is the polynomial

$$\begin{aligned} f(x) &= (x^7 + x^3 + 1)(x^7 + x^3 + x^2 + x + 1) \\ &= x^{14} + x^9 + x^8 + x^6 + x^5 + x^4 + x^2 + x + 1 \end{aligned}$$

which is represented in octal by 41567, as illustrated in Fig. 3.3.

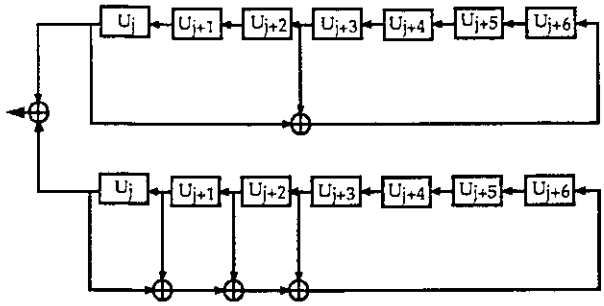

a) Double Shift-Registers Representation

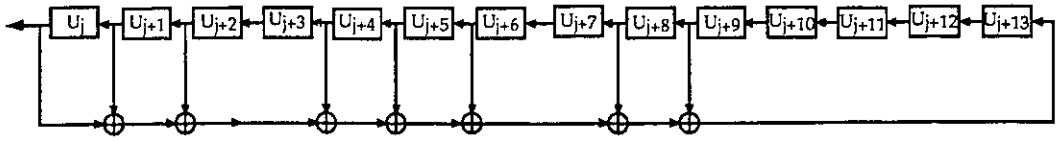

b) Single Shift-Register Representation

Fig. 3.3. Gold Code Generation

According to Gold's theorem, in this design, the corresponding shift register will generate 129 i.e., 2^7+1 different linear sequences of period length 127 i.e., 2^7-1. The maximum correlation value for this set of sequences is 17. The generated codes in this example have three-valued autocorrelation function sidelobes and a three-valued crosscorrelation taking on values from the set (-1,-17,15).

3.2.4 Kasami Sequences

Let n be even and let u denote an m-sequence of period $N = 2^n - 1$ generated by $h(x)$. the sequence $w = u[s(n)] = u[2^{n/2}+1]$. It follows from property VI that w is a sequence of period $2^{n/2}-1$ which is generated by a polynomial of degree $n/2$, w is an m-sequence of period $2^{n/2}-1$. Now, consider the sequences generated by the polynomial $h(x)h'(x)$ of degree $3n/2$. Clearly, any such sequence must be of one of forms $T^iu, T^jw, T^iu \oplus T^jw, 0 \leq i < 2^{n-1}, 0 \leq j < 2^{n/2}-1$. Thus, any sequence y of period $2^n - 1$ generated by $h(x)h'(x)$

is some phase of some sequence in the set $K_s(u)$ defined by

$$K_s(u) \triangleq \{u, u \oplus w, u \oplus Tw, ..., u \oplus T^{2^{n/2}-2}w\}$$

This set of sequences is called the small set of Kasami sequences. The correlation functions for sequences belonging to $K_s(u)$ take on values in the set $\{-1, -s(n), s(n) - 2\}$. Consequently, for the set $K_s(u)$,

$$\begin{aligned} \theta_{max} &= s(n) \\ &= 1 + 2^{n/2} \end{aligned} \tag{3.31}$$

Notice that, θ_{max} for the set $K_s(u)$ is approximately one half of the value of θ_{max} acheived by the sets of Gold sequences. On the other hand, $K_s(u)$ contains only $2^{n/2} = (N+1)^{1/2}$ sequences, while the sets of Gold sequences contain $N + 2$ sequences.

Now, let $\hat{h}(x)$ denote the primitive polynomial which generates the sequence v. As we noted earlier, the polynomial $h(x)\hat{h}(x)$ generates the set of Gold sequences $G(u, v)$. All sequences generated by $f(x) = h(x)\hat{h}(x)h'(x)$ are of the form $a \oplus b \oplus c$ where a, b and c are generated by $h(x), \hat{h}(x)$ and $h'(x)$, respectively. The set of sequences of period N generated by $h(x)\hat{h}(x)h'(x)$, is called the large set of Kasami sequences and is denoted by $K_L(u)$. This set contains both a small set of Kasami sequences and a set of Gold sequences as subsets. More interestingly, the correlation bound $\theta_{max} = max\{\theta_a, \theta_c\} = t(n)$ is the same as that for the latter subset.

It is not difficult to see that shift-and-add property for both small and large set of Kasami sequences holds.

In our simulation, we have also used a small set of Kasami sequences of period 255, therefore, we explain the design of these sequences as an example.

Example 3.2:

For $n = 8$ we can form the product of polynomial $h(x) = x^8 + x^4 + x^3 + x^2 + 1$ and the polynomial $\hat{h}(x) = x^4 + x + 1$ as illustrated in Fig. (3.4) to obtain the polynomial

$f(x) = x^{12} + x^9 + x^7 + x^6 + x^5 + x^4 + x^2 + x + 1$ which is 11367 in octal. The 12-stage linear feedback shift register corresponding to this polynomial generates a set of 16 sequences of period 255 with a periodic correlation bound of 17.

This small class of Kasami sequences consists of the m-sequence $\alpha = \alpha_{(16)}$ together with all $2^{n/2} - 1$ sequences of the form $\alpha \oplus T_j\beta$ for $0 \leq j \leq 2^{n/2} - 2$, where β is generated by $\hat{h}(x)$.

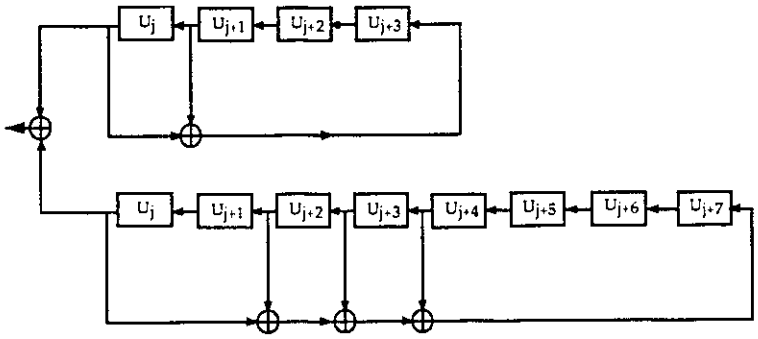

a) Double Shift-Registers Representation

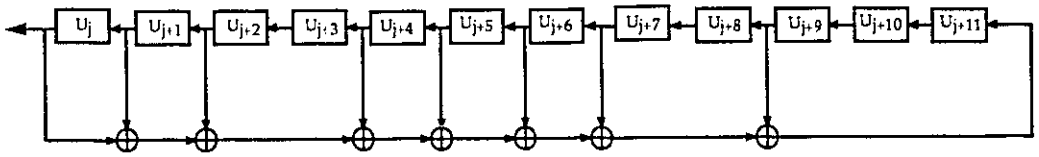

b) Single Shift-Register Representation

Fig. 3.4. Kasami Code Generation

3.3 Maximal-Length, Gold and Kasami Sequence Through Nonlinear Systems

Let $a_i(t)$, $a_j(t)$ and $a_k(t)$ be three different code sequence waveforms of the same period length T defined as in eq. (3.15). Assume these code waveforms are not synchronous, so that $a_j(t)$ has the delay of τ_I compared to $a_k(t)$ and $a_k(t)$ is delayed by τ compared to $a_i(t)$ where $0 \leq \tau, \tau_I \leq T$.

The product of two waveforms $a_k(t)$ and $a_j(t)$ shown by a'_{kj} is a periodic waveform of the same period T. The continuous-time partial crosscorrelation functions for this waveform and $a_i(t)$ are defined by

$$R_{kj,i}(\tau) = \int_0^{\tau} a'_{kj}(t-\tau)a_i(t)dt$$

$$\hat{R}_{kj,i}(\tau) = \int_{\tau}^{T} a'_{kj}(t-\tau)a_i(t)dt \tag{3.32}$$

Then:

$$E_{(\tau)}\{R_{kj,i}(\tau) + \hat{R}_{kj,i}(\tau)\}^2 =$$

$$\frac{1}{3}E\{R^2{}_{l,i}(\tau) + R^2{}_{l+1,i}(\tau)\} + \frac{1}{3}E\{\hat{R}^2_{l,i}(\tau) + \hat{R}^2_{l+1,i}(\tau)\}$$

where $R_{l,i}(.)$, $\hat{R}_{l,i}(.)$, $R_{l+1,i}(.)$ and $\hat{R}_{l+1,i}(.)$ stand for continous-time partial cross-correlation functions of two waveforms $a_i(t)$ and $a_l(t)$, or $a_i(t)$ and $a_{l+1}(t)$, where $a_l(t)$ and $a_{l+1}(t)$ are two sequence waveforms of the same set as $a_i(t)$.

In the following we prove the above statement. From Fig. 3.5 it is apparent that the product of two code waveforms $a_k(t)$ and $a_j(t)$, shown by $a'_{kj}(t)$ is a periodic waveform of the same period T,

and it is not difficult to see that

$$a'_{kj} = \begin{cases} (T^{l+1}a_j(t))\ a_k(t) & mT_c < t \leq mT_c + \tau'_l \\ (T^l a_j(t))\ a_k(t) & mT_c + \tau'_l \leq t \leq (m+1)T_c \end{cases} \tag{3.33}$$

where $0 \leq m \leq N-1$ is an integer, T^l stands for a circular shift to the right by l and τ'_l is defined so that $\tau'_l = \tau_l - lT_c$ where $0 \leq \tau'_l \leq T_c$ and l is an integer. The corresponding sequence of elements of $\{+1, -1\}$, to sequence waveform $(T^{l+1}a_j(t))\ a_k(t)$ is $(T^{l+1}a_m^{(j)})\ a_m^{(k)}$ where $a_m^{(j)} = (a_0^j, a_1^j, \ldots, a_{N-1}^j)$ and $a_m^{(k)} = (a_0^k, a_1^k, \ldots, a_{N-1}^k)$ are corresponding sequences to $a_j(t)$ and $a_k(t)$, respectively.

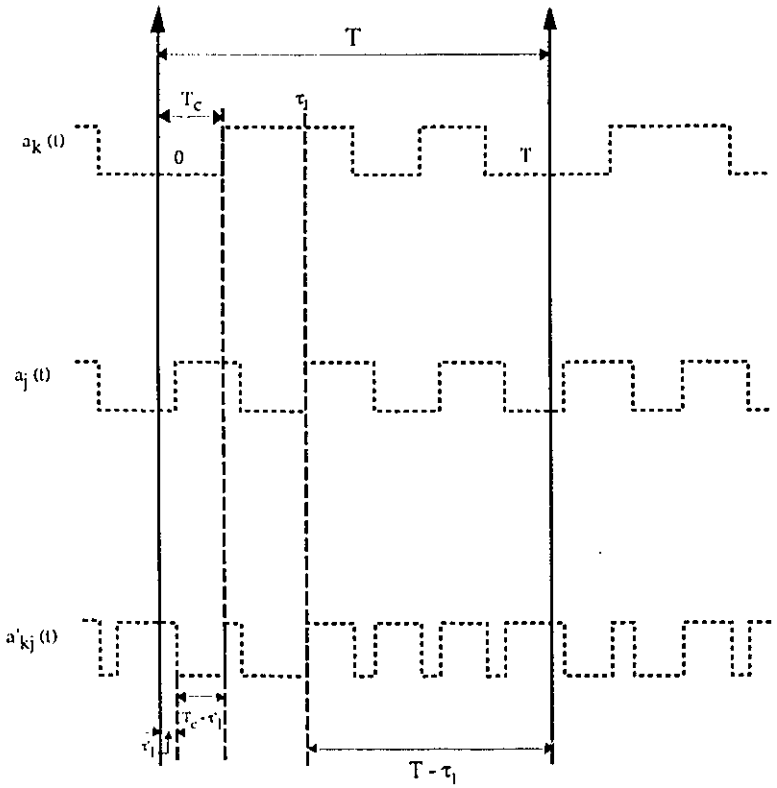

Fig. 3.5. Product of Two Sequence Waveforms

In section 3.1, we show that for Gold and Kasami sequences as well as maximal connected set of m-sequences, shift-and-add property holds. Since the product of sequences of elements $\{+1, -1\}$ corresponds to modulo-2 addition of sequences of elements $\{0, 1\}$, $(T^l a_m^j)a_n^k$ and $(T^{l+1}a_m^j)a_m^k$ are two sequences belonging to the same set of sequences as

a_m^j and a_m^k. For simplicity, we denote:

$$(T^l a_m^j)\ a_m^k = a_m^l$$

and

$$(T^{l+1}\ a_m^j)\ a_m^k = a_m^{l+1} \quad m = 0, 1, \ldots, N-1$$

Obviously, the corresponding waveforms are:

$$(T^l\ a_j(t))\ a_k(t) = a_l(t)$$

and

$$(T^{l+1}\ a_j(t))\ a_k(t) = a_{l+1}(t)$$

We point out that in a direct-sequence SSMA communication system the k^{th} data signal $b_k(t)$ which is a sequence of unit amplitude, positive and negative, rectangular pulses of duration T; are modulated onto the phase-coded carrier $cr_k(t)$, which is given by

$$\begin{aligned} cr_k(t) &= \sqrt{2p}\ \sin(\omega_c t + (\pi/2)a_k(t)) \\ &= \sqrt{2p}\ \ a_k(t)cos(\omega_c t + \theta_k). \end{aligned}$$

Thus, the transmitted signal for the k^{th} user is

$$\begin{aligned} s_k(t) &= \sqrt{2p}\ \sin(\omega_c t + \theta_k + (\pi/2)a_k(t)b_k(t)) \\ &= \sqrt{2p}\ \ a_k(t)b_k(t)cos(\omega_c t + \theta_k). \end{aligned}$$

In the above expressions, θ_k represents the phase of the kth carrier, ω_c represents the common center frequency, and p represents the common signal power.

From above, we notice the sign of $b_j(t)$ may differ before and after τ_I, and correspondingly the sign of $a'_{k_j}(t)$ may be different before and after τ_I.

To substitute eq. (3.33) in eq. (3.32) we have to consider two possible relationships between τ and τ_I, where τ is the delay of $a'_{k_j}(t)$ compared to $a_i(t)$. Fig. 3.6 shows the first possible relation when $\tau + \tau_I < T$.

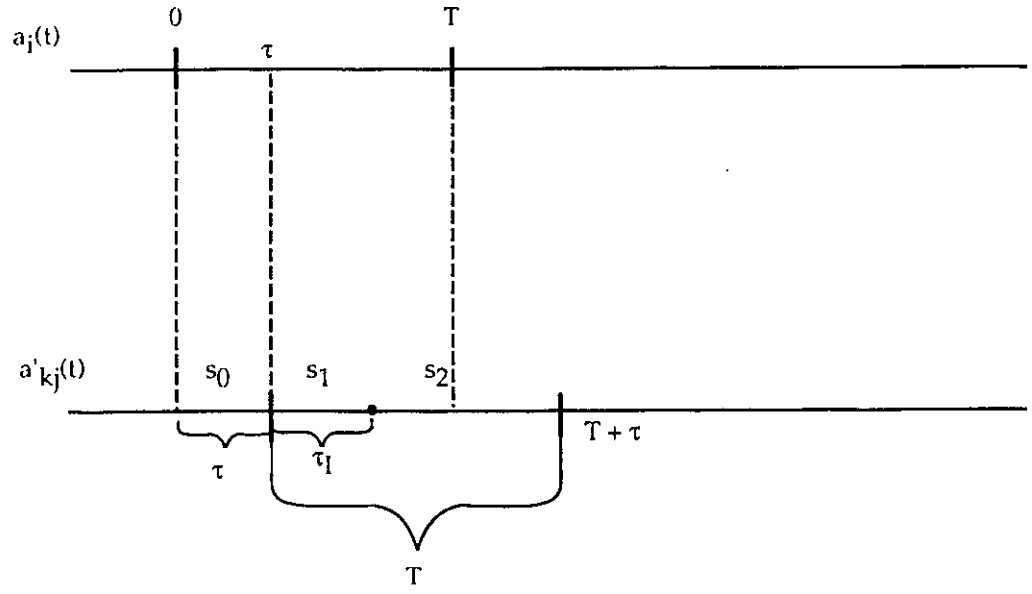

Fig. 3.6. $a'_{kj}(t)$ Compared to $a_i(t)$ Where $\tau + \tau_I < T$

In Fig. 3.6 s_0 denotes the sign of product of $a_i(t)$ and $a'_{kj}(t)$ for $0 \leq t \leq \tau$, s_1 denotes it for $\tau \leq t \leq \tau + \tau_I$ and s_2 for $\tau + \tau_I \leq t \leq T$.

By substituting eq. (3.33) in eq. (3.32) when $\tau + \tau_I < T$, we get:

$$R_{kj,i}(\tau) = s_0 \left[\int_0^{\tau} (1-\alpha) a_l(t-\tau)\ a_i(t) dt + \int_0^{\tau} \alpha a_{l+1}(t-\tau) a_i(t)\ dt \right]$$

$$\hat{R}_{kj,i}(\tau) = s_1 \left[\int_{\tau}^{\tau+\tau_I} (1-\alpha) a_l(t-\tau) \alpha_i(t) dt + \int_{\tau}^{\tau+\tau_I} \alpha a_{l+1}(t-\tau) a_i(t) dt \right]$$
$$+ s_2 \left[\int_{\tau+\tau_I}^{T} (1-\alpha) a_l(t-\tau) a_i(t)\ dt + \int_{\tau+\tau_I}^{T} \alpha a_{l+1}(t-\tau) a_l(t) dt \right]$$

where $\alpha = \frac{\tau'_I}{T_c}$.

When $\tau + \tau_I > T$, from Fig. 3.7:

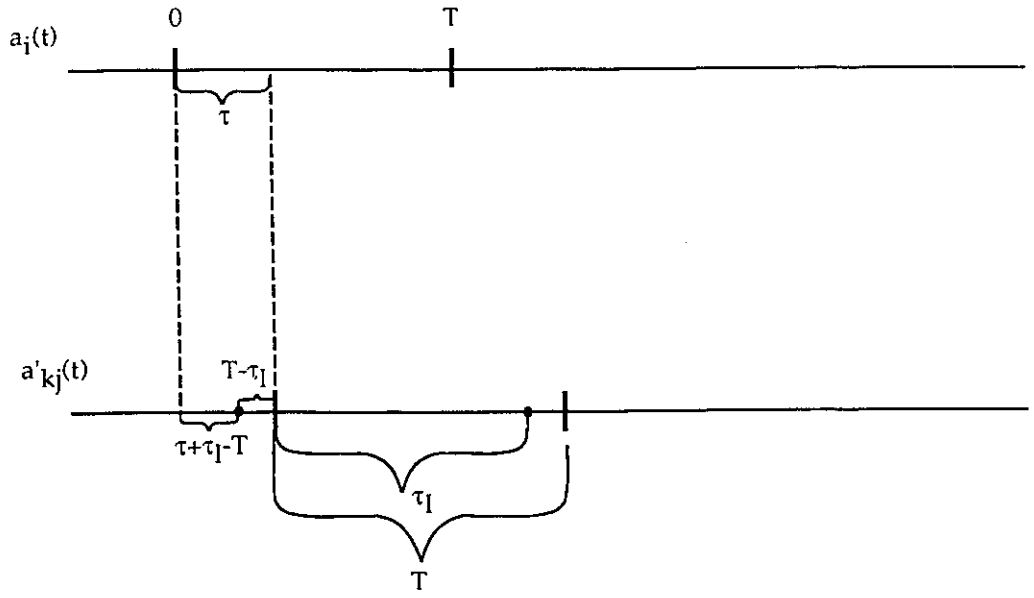

Fig. 3.7. $a'_{kj}(t)$ Compared to $a_i(t)$ Where $\tau + \tau_I > T$

$$R_{kj,i}(\tau) = s_1\left[\int_0^{\tau+\tau_I-T}(1-\alpha)a_l(t-\tau)a_i(t)dt + \int_0^{\tau+\tau_I-T}\alpha a_{l+1}(t-\tau)a_i(t)dt\right] + s_2\left[\int_{\tau+\tau_i-T}^{\tau}(1-\alpha)a_l(t-\tau)a_i(t)dt + \int_{\tau+\tau_I-T}^{\tau}\alpha a_{l+1}(t-\tau)a_i(t)dt\right]$$

$$\hat{R}_{kj,i}(\tau) = s_0\left[\int_{\tau}^{T}(1-\alpha)a_l(t-\tau)a_i(t)dt + \int_{\tau}^{T}\alpha a_{l+1}(t-\tau)a_i(t)dt\right]$$

We notice s_0, s_1, and s_2 are independent and also $E[s_0] = E[s_1] = E[s_2] = 0$. Therefore, for both cases,

$$\begin{aligned} &E[R_{kj,i}(\tau) + \hat{R}_{kj,i}(\tau)]^2 \\ &= \left[\int_0^{\tau}(1-\alpha)a_l(t-\tau)a_i(t)dt\right]^2 + \left[\int_0^{\tau}\alpha a_{l+1}(t-\tau)a_i(t)dt\right]^2 \\ &+ \left[\int_{\tau}^{T}(1-\alpha)a_l(t-\tau)a_i(t)dt\right]^2 + \left[\int_{\tau}^{T}\alpha a_{l+1}(t-\tau)a_i(t)dt\right]^2 \\ &+ 2\left[\int_0^{T}(1-\alpha)a_l(t-\tau)a_i(t)dt \cdot \int_0^{T}\alpha a_{l+1}(t-\tau)a_i(t)dt\right] \end{aligned} \tag{3.34}$$

It can be easily seen that:

$$\int_0^{T} a_l(t-\tau)a_i(t)dt = [(1-\alpha')\theta_{i,l}(n) + \alpha'\theta_{i,l}(n+1)]T_c$$

where $nT_c < \tau < (n+1)T_c$ and $\alpha' = \tau - nT_c$. The average of right hand side of last equation over α' is uniformly distributed over [0,1]. Therefore, the average value of last term in eq. (3.34) over n from eq. (3.25) is equal to $2(\frac{1}{N} \cdot \frac{1}{N})T_c^2 = \frac{2T^2}{N^2}$. It is worth mentioning that eq. (3.25) is true not only for m-sequences but also for Gold and Kasami sequences. The first four terms in eq. (3.34) are equal to:

$$(1-\alpha)^2 R_{l,i}^2(\tau) + \alpha^2 R_{l+1,i}(\tau)$$

$$+(1-\alpha)^2 \hat{R}_{l,i}(\tau) + \alpha^2 \hat{R}_{l+1,i}(\tau)$$

The average of these terms over α is equal to:

$$\frac{1}{3}\left[R_{l,i}^2(\tau) + \hat{R}_{l,i}^2(\tau)\right] + \frac{1}{3}\left[R_{l+1,i}^2(\tau) + \hat{R}_{l+1,i}^2(\tau)\right]$$

consequently;

$$V' = \frac{1}{T}\int_0^T E[R_{kj,i}(\tau) + \hat{R}_{kj,i}(\tau)]^2 dt$$

Using eq. (3.23)

$$V' = \frac{1}{3}\left[\frac{2}{3}\frac{T^2}{N}\right] + \frac{1}{3}\left[\frac{2}{3}\frac{T^2}{N}\right] + \frac{2T^2}{N^4}$$

where obviously the last term is negligible for a large N. Therefore,

$$V' \approx \frac{2}{3}[V] = \frac{2}{3}\left[\frac{2}{3}\frac{T^2}{N}\right]$$

As an extension, the product of three or more sequence waveforms of period T is also a periodic waveform of the same period T consisting of three or more sequences expressable by an equation like eq. (3.33). The continuous time partial cross-correlation functions from this product waveform and an arbitrary sequence waveform $a_i(t)$ are defined in a similar way like in eq. (3.32) and the same term like V' for such partial cross-correlation functions is linearly proportional to the number of multiplying waveforms, so that

$$V'(n) \approx \frac{n}{3} \cdot \left(\frac{2}{3}\frac{T^2}{N}\right) \tag{3.35}$$

where n is the number of multipling waveforms.

Chapter 4

Systems Configuration and Performance Evaluation

4.1 System Configuration

In this section, we will describe an optical LAN architecture that we have analyzed in this work. This architecture has several advantages over other possible ones.

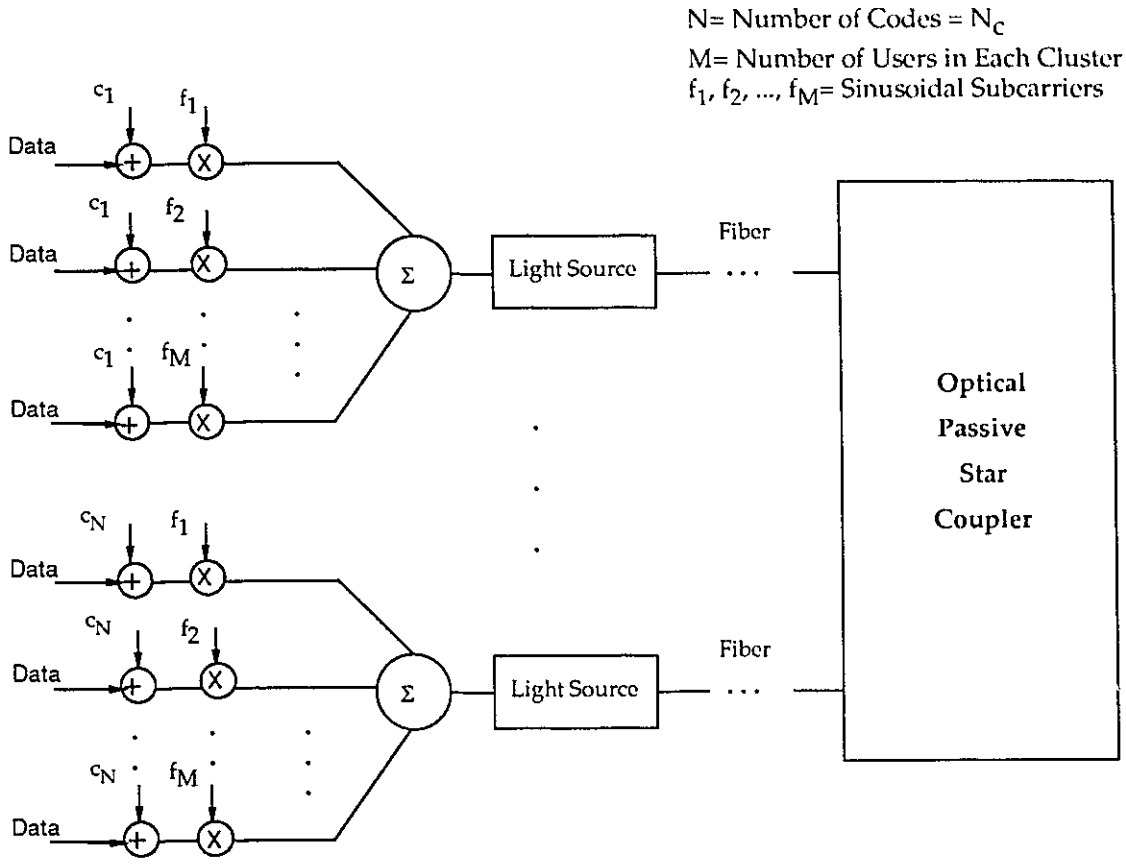

Fig. 4.1. LAN Configuration (1)

Fig. 4.1 illustrates a block diagram of the proposed LAN subsystems. A sequence of chips is added to the information bits and the spread data signals modulate FDM subcarriers. Sum of the FDM signals intensity modulate a light source. Emitted light is

guided to a passive star coupler via an optical fiber.

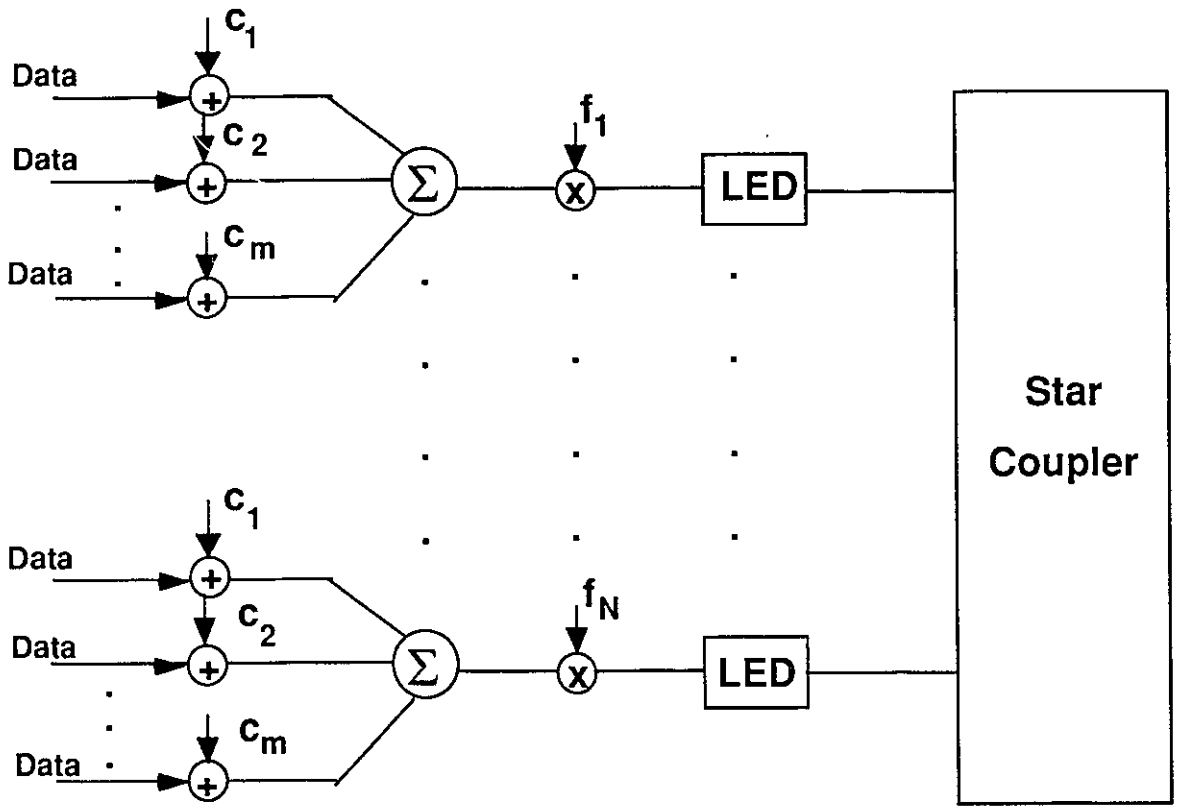

Fig. 4.2. LAN Configuration (2)

Fig. 4.2 illustrates a block diagram of another architecture. A sequence of chips is added to the information bits. The sum of the spread signals phase modulates the carrier. The modulated carrier intensity modulates a light source. Emitted light is guided to a passive star coupler. The sum of the spread data signals is no longer a binary signal, and the modulator output is no longer a binary phase modulated carrier. The output of the adder is a multi-level sequence. The number of levels depends on the number of users in one cluster. The frequency content of the new signal is much more than each of the user spread data signals because the transmitters are not synchronous.

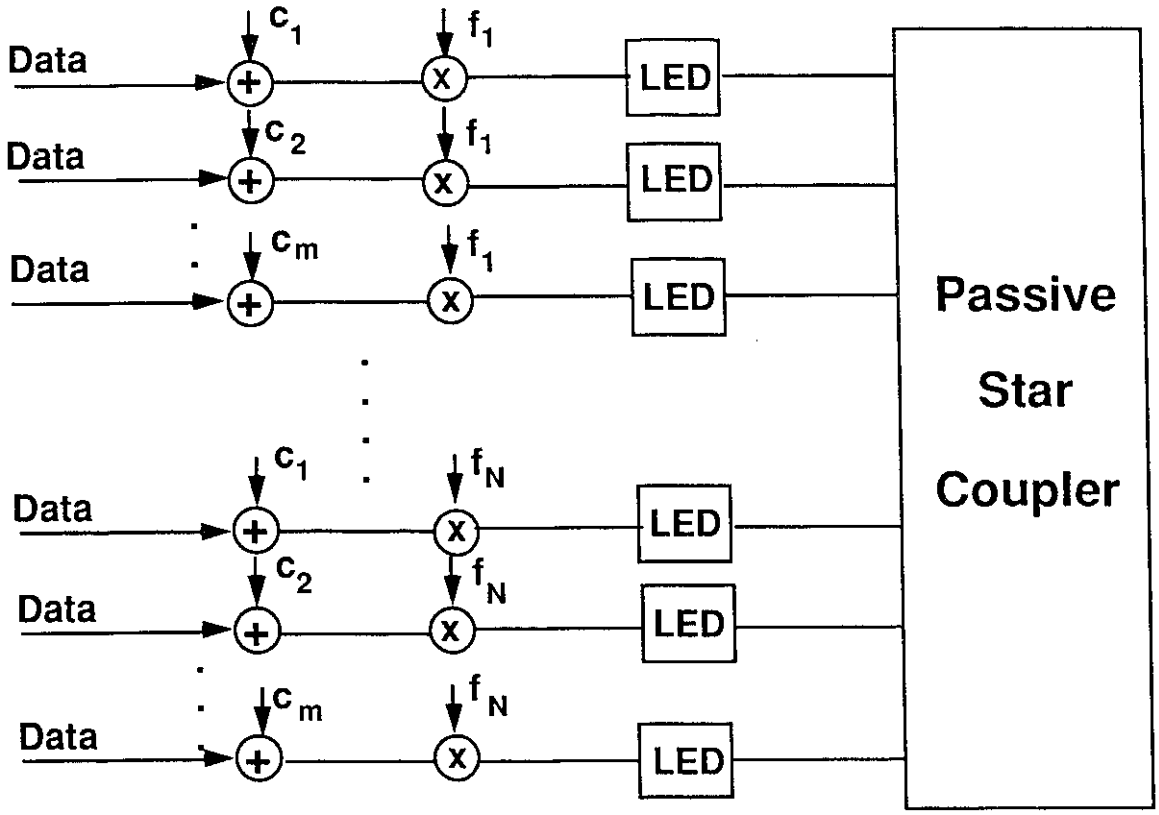

Fig. 4.3. LAN Configuration (3)

Fig. 4.3 illustrates a block diagram of another LAN configuration. In this configuration, the spread signal phase modulates a carrier and the modulated carrier intensity modulates the light source. This architecture is not efficient in terms of number of light sources, however it is quite immune to electromagnetic interference. In all these configurations, passive star coupler acts as a broadcast medium; distributing signals among a number of output ports connected to LAN users by fiber.

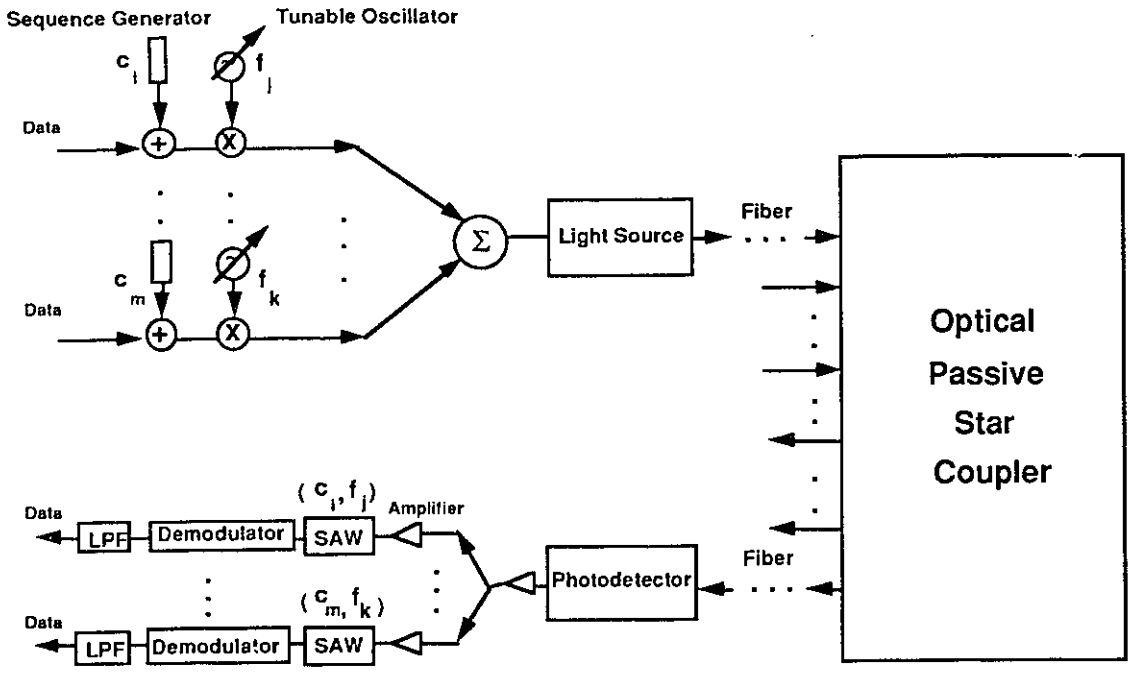

Fig. 4.4. Proposed LAN Configuration

Fig. 4.4 provides a more detailed illustration of the proposed passive star LAN. Every transmit terminal has a tunable oscillator capable of generating several discrete frequencies ranging from 45 to 700 MHz. It also has a sequence generator capable of generating PN sequences traditionally used in CDM applications

Every receiver is uniquely defined by a pair (c_i, f_j) where f_j corresponds to center frequency of a Surface Acoustic Wave (SAW) matched-filter and c_i is a finite-length sequence prefabricated in the SAW device. To reach a certain receive terminal, the transmitter has to generate the code sequence unique to the user and use the subcarrier frequency of the receiver for modulation by its baseband signal. Generated sequence spreads the narrow band of data. The tunable oscillator subcarrier signal is modulated by the spread data. A group of data terminals signals could share the same light source. The calls are mutually protected by the difference in either the code or the frequency of the subcarrier. Only call pairs to the same receiver would have identical codes and subcarrier frequencies, however, these calls would be blocked by a busy receiver signal. On the transmit side, if a number of users share a single light source, this number is limited by the nonlinearity

of the source. Total intermodulation products power will limit the number of subcarriers. Using very long spreading sequences may not be spectrally efficient. Hence, we seek an optimum combination of spread sequence length and the required subcarrier number, given a fixed modulating band of inexpensive light sources. On the receive side, each user has a SAW matched-filter with a very high-Q and a unique pre-programmed sequence. Each SAW only responds to the call tuned to its center frequency and with the matching code. Other concurrent calls are rejected by the SAW. Since through a passive coupler all transmitted signals are optically available to the receiving ports, use of the SAW provides a double layer of security in discriminating against unintended calls. Again, it is possible to share one photodetector among a number of users. To make the scheme very bandwidth efficient, we use the high-Q property of the SAW transfer characteristics. As long as the subcarriers are spaced by one narrow band data rate apart, practically there will be no interference between the shared bands. For example, at a data rate $80kbps$, using a chip rate of $10mcps$, the required $20MHz$ double-sided subcarrier modulation band can be reused by the subcarriers, as long as they are by $80kHz$ apart. For example, subcarriers at 120, 120.08, 120.16 MHz, etc. although for the most part reuse the 20 MHz band, create no significant interference to one another even if they all carry the same spread sequence. This is because a SAW filter has a Sinc Function transfer magnitude response with nulls on each side of the main lobe by one data rate away from the center [1]. Hence, even SAW's programmed to the same sequence but with different center frequencies will provide sufficient discrimination among signals.

4.2 Model of Suggested System

The system model that we will consider is shown in Fig. 4.4. During each T second symbol interval, the i^{th} transmitting laser is amplitude-modulated by the summation of modulated signals of different users in a cluster and the modulated signal for each user is the product of data which takes on values $\{1, -1\}$, a Gold or a Kasami sequence and a sinusoidal subcarrier. Sequences are specified by the values they take on in N equal-length

subintervals (chips) [0,T]. As in [12], we define $b_k(t)$ as the k^{th} user's information which is a sequence of rectangular pulses taking on values from the set $\{\pm 1\}$ over a T-second time interval. Hence,

$$b_k(t) = \sum_{j=-\infty}^{+\infty} b_j^k P_T(t - jT) \tag{4.1}$$

where b_j^k represents the k^{th} user data at the j^{th} timing interval and $P_T(.)$ is a rectangular waveform of T-second duration. The k^{th} user is assigned a code waveform $a_k(t)$ that consists of a periodic sequence of rectangular chips taking on values from the set $\{\pm 1\}$ each of T_c seconds duration. If a_i^k represents the i^{th} chip value of the k^{th} user,

$$a_k(t) = \sum_{j=-\infty}^{+\infty} a_j^k P_{T_c}(t - jT_c) \tag{4.2}$$

Each user is assigned a periodic sequence with a period $N = T/T_c$.

After spreading the information signal and biphase modulating it onto a carrier signal, $cos(\omega_c t + \theta_k)$- where the carrier level is 1, ω_c is the nominal carrier frequency and θ_k is the carrier phase that is assumed to be uniformly distributed between 0 and 2π - the modulated signal of the k^{th} user becomes:

$$S_k(t) = a_k(t)b_k(t)cos(\omega_c t + \theta_k) \tag{4.3}$$

Without any loss in generality, we will set the quantum efficiency of the photodetector to unity, as this affects the distribution of the number of received photons in form of intensity attenuation. For similar reasons, we neglect the fiber loss and coupling losses in the passive star coupler.

We define M as the number of users in each cluster, N_s as the number of clusters, N_c as the number of spreading codes, N_f the number of frequencies, N_u the number of users which is equal to $N_f.N_c$ and N as already discussed is the sequence-length.

The instantaneous optical power of each laser is:

$$P(t) = \bar{P}_T \left[1 + m \sum_{k=1}^{M} S_k(t) \right] \tag{4.4}$$

where m is optical modulation index.

Given the signal levels in eq. (4.3) are normalized to unity, for proper optical intensity modulation, it is necessary that:

$$0 < m \leq \frac{1}{M}$$

By assuming a lossless communication system, the RF photocurrent corresponding to the desired signal at each receiver is:

$$\pm A cos(\omega_c t + \theta) = \frac{\pm R \bar{P}_T m}{N_s} cos(\omega_c t + \theta)$$

So,

$$A = \frac{R \bar{P}_T m}{N_s} \tag{4.5}$$

and we know,

$$E_b = \frac{A^2 T}{2} \tag{4.6}$$

thus;

$$E_b = \frac{R^2 \bar{P}_T^2 m^2}{2 N_s^2} T \tag{4.7}$$

The maximum achievable values of A and E_b corresponding to $m = \frac{1}{M}$ and photodetector responsivity $R = 1$ are:

$$A = \frac{\bar{P}_T}{M N_s} = \frac{\bar{P}_T}{N_u} \tag{4.8}$$

$$E_b = \frac{\bar{P}_T^2}{M^2 N_s^2} \cdot \frac{T}{2} = \frac{\bar{P}_T^2}{N_u^2} \cdot \frac{T}{2} \tag{4.9}$$

Calculation of Average Error Probability

Now, regardless of the number of users in each cluster; since each receiver is using one frequency and rejecting others, the number of interference signals is equal to the number of codes used. Hence, the received signal after the photodetector can be expressed as:

$$r(t) = \sum_{k=1}^{N_c} S_k(t - \tau_k) + \sum_{l=1}^{L} S_l'(t - \tau_l) + n(t) \tag{4.10}$$

where τ's are uniformly distributed over $[0, T]$ because users are independently sending their signals. The first term in eq. (4.10) includes different user signals, $n(t)$ is a white gaussian noise with a double-sided spectral density of $\frac{N_0}{2}$ height and the last term includes sum of harmonics and intermodulation products (IMPs) falling around the center frequency f_c. From eq. (4.3)

$$\begin{aligned} r(t) = A\sum_{k=1}^{N_c} a_k(t-\tau_k)b_k(t-\tau_k)cos(\omega_c t + \Theta_k) + n(t) \\ + A\sum_{l=1}^{L} w_l a_l'(t-\tau_l)cos(\omega_c t + \Theta_l) \end{aligned} \tag{4.11}$$

where $\Theta_k = -\omega_c\tau_k + \theta_k$ and θ_1 is assumed to be zero with no loss in generality. The parameter w_l in the last term represents the weight of each IMP or harmonic. The weights of harmonics are 6 dB less than the weights of IMPs of the same order. The weight for higher than third order harmonics and IMPs is usually too small to be considered in performance analysis of a system. Levels -40 dB, -60 dB and -100 dB are typical second, third and higher order harmonic and IMP weights, respectively [8]. The $a_l'(t)$ is a waveform like in eq. (3.33) for second order IMP and would be an extended form of this equation in the case of higher order IMPs. In the case of Gold, Kasami and m-sequences, harmonics affect the performance of the system in the same way as IMPs because for these sets of sequences cross-correlation and autocorrelation functions have the same sidelobes and take on values from the same set. For instance, we consider the two following transmitted signals:

$$S_k(t) = a_k(t-t_k)b_k(t-t_k)cos(\omega_k t + \theta_k)$$

$$S_j(t) = a_j(t-t_j)b_j(t-t_j)cos(\omega_j t + \theta_j)$$

It is obvious that the amplitude of the second order IMP is proportional to

$$a_k(t-\tau_k)b_k(t-\tau_k)a_j(t-\tau_j)b_j(t-\tau_j)$$

which is an analytical representation of Fig. 3.5. Under Gaussian assumption, $n(t)$ is a white gaussian noise with a double-sided spectral density of $\frac{N_0}{2}$ height, where:

$$N_0 = \frac{4KTF}{R_L} + 2eI_D + (RIN)I_D^2 \tag{4.12}$$

In eq. (4.12), K is the Boltzmann's constant ($1.38 \times 10^{-23} j/K$), T is the absolute temperature ($290°K$), e is an electron charge ($1.602 \times 10^{-19} e$), F is the electronic receiver amplifier noise figure and R_L is the photodiode load resistor with a 50 ohm nominal value.

After the despreading that collapses the wideband coded signal into a narrowband modulated signal and then the demodulation process, a signal sample at the receiver low-pass filter output can be expressed as:

$$\xi = \int_0^T r(t) a_1(t) cos(\omega_c t) dt \tag{4.13}$$

By using eq. (4.11) we obtain:

$$\begin{aligned} \xi = & A \sum_{k=1}^{N_c} \int_0^T a_k(t-\tau_k) b_k(t-\tau_k) a_1(t) cos(\omega_c t + \Theta_k) cos(\omega_c t) dt \\ & + A \sum_{l=1}^{L} w_l \int_0^T a'_l(t-\tau_l) a_1(t) cos(\omega_c t + \Theta_k) cos(\omega_c t) dt \\ & + \int_0^T n(t) a_1(t) cos(\omega_c t) dt \end{aligned} \tag{4.14}$$

where the last integral is a sample of Gaussian noise with a zero-mean and an $\frac{N_0 T}{4}$ variance.

The assumption of phase and delay locking of the receiver to the first desired modulated signal that is received enables one to rewrite eq. (4.14) as:

$$\begin{aligned} \xi = & \frac{A}{2} \int_0^T a_1^2(t) b_1(t) dt \\ & + \frac{A}{2} \sum_{k=2}^{N_c} \int_0^T a_k(t-\tau_k) b_k(t-\tau_k) a_1(t) cos(\Theta_k) dt \\ & + \sum_{l=1}^{L} \left(\frac{A}{2}\right) w_l \int_0^T a'_l(t-\tau_l) a_1(t) cos(\Theta_l) dt + \eta \end{aligned} \tag{4.15}$$

where $\Theta_k = \theta_k - \omega_c \tau_k$ and η is equal to the last term in eq. (4.14).

We notice that, from eq. (4.4)

$$b_1(t) = \sum_{j=-\infty}^{\infty} b_j^1 P_T(t - jT)$$

and therefore, by using eq. (3.16); eq. (4.15) can be written as

$$\begin{aligned}\xi = \frac{AT}{2}b_0^1 + \frac{A}{2}\sum_{k=2}^{N_c}[b_{-1}^k R_{k,1}(\tau_k) + b_0^k \hat{R}_{k,1}(\tau_k)]cos\Theta_k \\ + \frac{A}{2}\sum_{l=1}^{L} w_l \int_0^T a_l'(t-\tau_l)a_1(t)cos(\Theta_l)dt + \eta\end{aligned} \tag{4.16}$$

where b_0^1 represents the information bit being detected and b_{-1}^1 is the previous bit. We refer to reference term as z; so that:

$$z = \frac{A}{2}\sum_{k=2}^{N_c}\left[b_{-1}^k R_{k,1}(\tau_r) + b_0^k \hat{R}_{k,1}(\tau_k)\right]cos(\Theta_k) \tag{4.17}$$

4.3 Probability of Error Expression

4.3.1 Gaussian Assumption

We assume all the multiuser interference terms, harmonics and IMPs are Gaussian distributed. Under Gaussian assumption, the power of interference term and also the harmonic and IMP terms is equal to the variance of these terms. The first term in eq. (4.16) is the signal term and it has an average power of $\left\{\frac{AT}{2}\right\}^2$, or from eq. (4.8) average power of $\frac{P_T^2}{4M^2N_s^2}T^2$. The rest of the terms in eq. (4.16) are mutually independent. To calculate the total power of the interference term, we must evaluate a mean-squared term like,

$$\epsilon^2 = \frac{E[\alpha_{-1}R(t_1) + \alpha_0\hat{R}(t_1)]^2}{T^2} \tag{4.18}$$

where $\alpha_i = \pm 1,\ i = -1, 0$ are independent binary variables. In eq. (4.18), ϵ^2 according to eq. (3.23) has the value $\frac{2}{(3N)}$, where N is the length of sequences. The total power of the last term of eq. (4.16) which is the variance of harmonics and IMP terms according to eq. (3.35) is equal to:

$$\sum_{l=1}^{L}\frac{A^2}{4}w_l^2\frac{n_l}{3}\left(\frac{2}{3}\frac{T^2}{N}\right)$$

where n_l is the order of l^{th} IMP or harmonic. Therefore;

$$\text{signal power} = \left(\frac{AT}{2}\right)^2 = \frac{\bar{P}_T^2}{4M^2N_c^2}T^2 = \frac{\bar{P}_T^2}{4N_u}T^2$$

$$\text{interference power} = \left(\frac{AT}{2}\right)^2 (N_c-1)\frac{\epsilon^2}{2} = \frac{\bar{P}_T^2}{8M^2N_c^2}T^2(N_c-1)\epsilon^2$$

$$= \frac{\bar{P}_T^2}{8N_u^2}T^2(N_c-1)\epsilon^2$$

$$\text{nonlinearity term power} = \left(\frac{AT}{2}\right)^2 \sum_{l=1}^{L} n_l w_l^2 \frac{\epsilon^2}{3} = \frac{\bar{P}_T^2}{12N_u^2}\epsilon^2 \sum_{l=1}^{L} n_l w_l^2$$

$$\text{noise power} = N_0\frac{T}{4}$$

For binary PSK modulation, the error probability is given by:

$$P(e) = \frac{1}{2}erfc(\sqrt{\gamma_b}) \tag{4.19}$$

where γ_b is the bit energy-to-noise density ratio.

Note that, in eq. (4.19) γ_b is half of the signal-to-noise plus interference power ratio; hence,

$$SNR = 2\gamma_b = \frac{\bar{P}_T^2}{(N_c-1)\frac{1}{3N}\bar{P}_T^2 + (\sum_{l=1}^{L} n_l w_l^2)\frac{2}{9N}\bar{P}_T^2 + N_0\frac{1}{T}N_u^2} \tag{4.20}$$

where we have set the modulation index m to $\frac{1}{M}$, responsivity of the photodetector R to unity, B is the bandwidth of the signal, N is the spreading sequence length and N_c is the number of the sequences that we have used.

By using eq. (4.9):

$$SNR = \frac{E_b}{(N_c-1)\frac{1}{3N}E_b + \sum_{l=1}^{L} n_l w_l^2 \frac{2}{9N}E_b + \frac{N_0}{2}} \tag{4.21}$$

4.3.2 Average Error Probability with Moments Method

The objective of the detector is to compare the received sample in eq. (4.16) with a threshold in order to make a decision on the polarity of the transmitted data bit being

detected, that is, b_0^1. The detector makes a wrong decision if ξ is negative while $b_0^1 = +1$ or if ξ is positive when $b_0^1 = -1$. We note that during the detection interval of b_0^1 the other two data bits in eq. (4.16), namely, b_{-1}^k and b_0^k, $k \neq 1$ can independently take on $\{\pm 1\}$. Hence, the conditional error probability is expressed by:

$$\begin{aligned} P_{e|z} = & \frac{1}{2} Pr\left\{ \frac{AT}{2} + \frac{AT}{2} z + \eta < 0 | b_0^1 = +1 \right\} \\ & + \frac{1}{2} Pr\left\{ -\frac{AT}{2} + \frac{AT}{2} z + \eta > 0 | b_0^1 = -1 \right\} \end{aligned} \tag{4.22}$$

We can rewrite eq. (4.22) as:

$$P_{e|z} = \frac{1}{4}\left\{ erfc\left[\frac{\frac{AT}{2} + \frac{AT}{2} z}{\sigma\sqrt{2}} \right] + erfc\left[\frac{\frac{AT}{2} - \frac{AT}{2} z}{\sigma\sqrt{2}} \right] \right\} \tag{4.23}$$

where

$$erfc(\mu) = \frac{2}{\sqrt{\pi}} \int_{\mu}^{\infty} e^{-y^2} dy$$

and σ is the standard deviation of the Gaussian noise.

We notice that, the data symbols have a zero mean, therefore, all the odd moments of z are equal to zero. Now, to evaluate the average error probability we will apply the moments of interference term to a numerical Gauss Quadrature Rules integration routine [12]. Using this method, for an even distribution, there are symetrical nodes around zero with the same weight [12]. Now, it is not difficult to observe that instead of using eq. (4.23) we can use the following, due to symmetry:

$$P_{e|z} = \frac{1}{2} erfc\left\{ \frac{\frac{AT}{2}(1 - z)}{\sigma\sqrt{2}} \right\} \tag{4.24}$$

Recalling;

$$\sigma = \frac{\sqrt{N_0 T}}{2}$$

and observing a bit energy,

$$E_b = \frac{A^2 T}{2} = \frac{\bar{P}_T^2}{N_u^2} \frac{T}{2}$$

we can express eq. (4.24) as

$$\begin{aligned} P_{e|z} &= \frac{1}{2} erfc\left\{ \sqrt{\frac{E_b}{N_o}}(1-z) \right\} \\ &= \frac{1}{2} erfc\left\{ \sqrt{\frac{1}{N_u^2}\frac{\bar{P}_T^2 T}{2N_0}}(1-z) \right\} \end{aligned} \tag{4.25}$$

Now using Gauss Quadrature Rules integration [19] the average error probability can be obtained numerically, by averaging the conditional probability in eq. (4.25) over the interference term, z. This is accomplished by first evaluating the $N_m = 2N_{n,\omega}+1$ moments of z which are applied in evaluation of the $N_{n,\omega}$ nodes and weights of the Quadrature Rule [31]. Hence, the average probability of error is:

$$P_e = \frac{1}{2}\sum_{j=1}^{N_{n,\omega}} W_j \; erfc\left\{ \sqrt{\frac{E_b}{N_0}}(1-\xi_j) \right\} \tag{4.26}$$

4.3.3 Moment-Generating Approach

The average probability of error expression in eq. (4.26) assumes $2N_c + 1$ moments of random variable z which is a function of independent random parameters: τ_k, Θ_k and b_i^k.

Furthermore, z_k's are independent and symmetrically distributed; hence the odd moments of z are all zero. Therefore, having the even moments of z, in this section we derive the moments of z. Since,

$$z = \sum_{k=2}^{K} z_k$$

where

$$z_k = \frac{1}{T}\{b_{-1}^k R_{k,1}(\tau_k) + b_0^k \hat{R}_{k,1}(\tau_k)\} cos\Theta_k$$

then

$$E\{z_k^{2m}\} = \frac{1}{T^{2m}} E[cos\Theta_k]^{2m} \cdot [b_{-1}^k R_{k,1}(\tau_k) + b_0^k \hat{R}_{k,1}(\tau_k)]^{2m} \tag{4.27}$$

To evaluate the second expectation of the right-hand side of eq. (4.27) since Θ_k is an independent random variable, we can deal with it separately.

That is, we first evaluate

$$E\{[cos\Theta_k]^{2m}\} = \frac{\binom{2m}{m}}{4^m}$$

and then find the second expectation of eq. (4.27) as

$$H = \frac{\binom{2m}{m}}{4^m} E\{[b_{-1}^k R_{k,1}(\tau_k) + b_0^k \hat{R}_{k,1}(\tau_k)]^{2m}$$

$$= \frac{\binom{2m}{m}}{4^m} \cdot \frac{1}{T} \cdot \int_0^T [b_{-1}^k R_{k,1}(\tau_k) + b_0^k \hat{R}_{k,1}(\tau_k)]^{2m} d\tau_k$$

where the expectation in H is over the random delay τ_k.

Now we can expand the latter integral over N chips period. Hence,

$$H = \frac{\binom{2m}{m}}{4^m} \cdot \frac{1}{T} \sum_{n=0}^{N-1} \int_{nT_c}^{(n+1)T_c} [b_{-1}^k R_{k,1}(\tau_k) + b_0^k \hat{R}_{k,1}(\tau_k)]^{2m} d\tau_k$$

We can then use eqs. (3.17) - (3.19) to evaluate the correlation functions. This is accomplished by assuming rectangular chips and noting that for any $0 \leq nT_c \leq \tau \leq (n+1)T_c \leq T$, as shown by eqs. (3.17) and (3.18),

$$\begin{cases} R_{k,1}(\tau) = A_{n_{k,1}} T_c + B_{n_{k,1}}(\tau - nT_c) \\ \hat{R}_{k,1}(\tau) = \hat{A}_{n_{k,1}} T_c + \hat{B}_{n_{k,1}}(\tau - nT_c) \end{cases} \tag{4.28}$$

where

$$\begin{cases} A_{n_{k,1}} = C_{k,1}(n - N) \\ B_{n_{k,1}} = C_{k,1}(n + 1 - N) - C_{k,1}(n - N) \\ \hat{A}_{n_{k,1}} = C_{k,1}(n + 1) - C_{k,1}(n) \qquad k = 1, 2, \ldots, K \\ \hat{B}_{n_{k,1}} = C_{k,1}(n + 1) - C_{k,1}(n) \end{cases} \tag{4.29}$$

where the discrete aperiodic cross-correlation term $C_{k,1}(\cdot)$ is related to chip sequences a_j^k and a_j^1 via

$$C_{k,1}(n) = \begin{cases} \sum_{j=0}^{N-1-n} a_j^k a_{j+n}^1 & 0 \leq n \leq N-1 \\ \sum_{j=0}^{N-1+n} a_{j-n}^k a_j^1 & -(N-1) \leq n \leq 0 \\ 0 & \text{else} \end{cases} \tag{4.30}$$

Therefore, H becomes

$$\begin{aligned} H = & \frac{1}{T}\frac{\binom{2m}{m}}{4^m}\sum_{n=0}^{N-1}\sum_{r=0}^{m}\binom{2m}{2r} \\ & \cdot \int_{nT_c}^{(n+1)T_c} [A_{n_{k,1}}T_c + B_{n_{n,k}}(\tau_k - nT_c)]^{2r} \\ & \cdot [\hat{A}_{n_{k,1}}T_c + \hat{B}_{n_{k,1}}(\tau_k nT_c)]^{2(m-r)} d\tau_k. \end{aligned} \tag{4.31}$$

Notice that, in deriving eq. (4.31), because of the even moments, b_{-1}^k and b_0^k are averaged to one. Now, in eq. (4.31), by changing $\tau_k - nT_c$ to WT_c, H becomes

$$\begin{aligned} H = & T_c^{2m+1}\frac{\binom{2m}{m}}{4^m}\sum_{n=0}^{N-1}\sum_{r=0}^{m}\binom{2m}{2r} \\ & \cdot \left\{\int_0^1 [A_{n_{k,1}} + B_{n_{k,1}}W]^{2r} \cdot [\hat{A}_{n_{k,1}} + \hat{B}_{n_{k,1}}W]^{2(m-r)} dW\right\} \end{aligned} \tag{4.32}$$

Therefore, to determine H we have to solve

$$\Gamma_{m,r,n} = \int_0^1 [A_{n_{k,1}} + B_{n_{k,1}}W]^{2r} \cdot [\hat{A}_{n_{k,1}} + \hat{B}_{n_{k,1}}W]^{2(m-r)} dW \tag{4.33}$$

This can be done recursively, using integration by parts, and the result is

$$\begin{aligned} \Gamma_{m,r,n} = & \sum_{i=0}^{2r}(-1)^i \frac{(B_{n_{k,1}})^i}{(\hat{B}_{n_{k,1}})^{i+1}} \cdot \frac{1}{(i+1)} \cdot \frac{\binom{2r}{i}}{\binom{2(m-r)+i+1}{i+1}} \\ & \cdot \{(A_{n_{k,1}} + B_{n_{k,1}})^{2r-i} \cdot (\hat{A}_{n_{k,1}} + \hat{B}_{n_{k,1}})^{2(m-r)+i+1} \\ & - (A_{n_{k,1}})^{2r-i} \cdot (\hat{A}_{n_{k,1}})^{2(m-r)+i+1}\} \end{aligned} \tag{4.34}$$

For H in eq. (4.32) we now have

$$H = \frac{T_c^{2m+1}}{T}\frac{\binom{2m}{m}}{4^m}\sum_{n=0}^{N-1}\sum_{r=0}^{m}\binom{2m}{2r}\Gamma_{m,r,n}$$

and for $E\{z_k^{2m}\}$ in eq. (4.27),

$$E\{z_k^{2m}\} = \frac{\binom{2m}{m}}{4^m} \cdot \frac{1}{N^{2m+1}}\sum_{n=0}^{N-1}\sum_{r=0}^{m}\binom{2m}{2r}\Gamma_{m,r,n}. \tag{4.35}$$

To find the moments of

$$z = \sum_{k=2}^{K} z_k$$

we can use a three-step method prescribed in [11], where from the cumulants of random variable $z_k, \gamma_m(z_k)$, the moments of z are arrived at. This simple algorithm is outlined below.

The first step is to find

$$M_{2m} = E\{z_k^{2m}\}$$

and then

$$\gamma_{m+1}(z_k) = M_{m+1}(z_k) - \sum_{r=0}^{m-1} \binom{m}{r} \gamma_{r+1}(z_k) \cdot M_{m-r}(z_k)$$

with

$$\gamma_1(z_k) = M_1(z_k) = 0 \tag{4.36}$$

The second step is to find

$$\gamma_m(z) = \sum_{k=2}^{K} \gamma_m(z_k) \tag{4.37}$$

The third step is to find

$$M_{m+1}(z) = \gamma_{m+1}(z) + \sum_{r=0}^{m-1} \binom{m}{r} \gamma_{r+1}(z) \cdot M_{m-r}(z)$$

4.4 Discussion and Numerical Results

In this section, the average error probability as a function of signal-to-noise for each transceiver pair in Fig. 4.4 is evaluated. We will first discuss the parameters which are critical in designing our proposed LAN in Fig. 4.4 and then we will exhibit the analytical average error probability and numerical results of calculating average error probability, obtained using Gauss Quadrature Rule integration.

To calculate the average error probability under the Gaussian assumption, we use the error probability expression eq. (4.21) developed in section 4.3.1. The effect of light source

nonlinearity in eq. (4.21) appears as

$$E_b \sum_{l=1}^{L} n_l \omega_l^2 \frac{2}{9N}$$

From above, the power suppression of second order harmonics and IMPs is equal to $4/9N$ and the third order IMPs and harmonics are suppressed by the factor $6/9N$ and in general the n^{th}-order components are suppressed by a factor $2n/9N$.

It has been shown that the distortion level from a laser is only dependent on the signal level [8][26]. Therefore, once we have results for a laser for two channels and a particular channel spacing, it is not necessary to have another set of results for a different number of channels. The number of IMPs and harmonics increases with an increase in the number of channels but the power of each of these components decreases by the same factor. More specifically, the number of second order products increases with the square of the number of channels, and the power of each component decreases with the same factor. Likewise, the number of third order intermodulation products increases with the cube of the number of channels, but the power of each component is reduced by the cube of the number of channels. The total signal power of N channels is given as follows:

$$\text{Signal Power} = \frac{1}{2}(m\bar{P}_T R)^2 N R_L$$

where m is the optical modulation index and $\bar{P}_T$ corresponds to driving laser current bias, R is the responsivity of photodiode and R_L is taken to be 50Ω. Therefore, to obtain the same distortion level, we can trade N, the number of channels with m, the optical modulation index.

Darcie [10] has presented a theoretical and experimental study of intermodulation and harmonic distortion in high speed 1.3 and $1.5\mu m$ InGaAsP lasers modulated at frequencies up to 8 GHz. The measured results show that all lasers, including Fabry-Perot and distributed feedback lasers, generate approximately the same distortion levels for a given modulation depth and laser relaxation resonance frequency. In our proposed LAN shown in Fig. 4.4 the minimun detectable signal power or receiver sensitivity will limit the minimun

modulation index m and consequently the number of users in one cluster. The distortion level of harmonics and IMPs is a function of modulation index m. For a modulation depth m and relaxation resonance frequency f_r the weight of the second and third order harmonics and IMPs distortion level for each kind of laser is given. By having weight of all nonlinearity components (second and third order) we can calculate the total power of interfering products caused by light-source nonlinearity. In Appendix B, we present an example and we calculate the weights of second and third order IMPs and harmonics for a given m and a particular laser. Since the nonlinearity distortion level is a function of modulation index m and consequently a function of number of users in each cluster, calculating the exact nonlinearity distortion level is possible only when the number of users in each cluster and the type of light source are known. So far, we have calculated the signal to nonlinearity distortion improvement obtained using a spreading sequence of length N. We have also outlined the computation for a designed optical LAN for which all the required parameters are known.

For the rest of our work which is the performance study of the proposed system using different sequences and exploiting different methods, we do not consider nonlinear distortion. This would not affect our analysis because our goal is to make a comparison between different sequences or different methods while the nonlinear effects merely depend on the length of the sequence.

In our numerical evaluation we have used two sets of Gold and Kasami sequences.

4.4.1 Gold Sequences Results

Figs. 4.5-4.7 illustrate the performance of the SS/CMDA scheme where the codes employed are Gold codes of periodic length 127 and for different number of users. The Gold sequences are obtained by multiplying the two primitive polynomials described in example 3.1.

To find the actual codes, we used the initial loadings of [29]. These initial loadings are

shown to generate a class of Gold codes known as Auto-Optimal with Least Sidelobe Energy (AO/LSE). In our numerical evaluation we used ten initial loadings. Hence, this covers ten periodic code sequences for a hypothetical community of users sharing the common channel band on a spread-spectrum multiple-access basis. Once the code sequences are obtained, we compute the partial correlation coefficients of eq. (4.29), which are used in conjuction with eq. (4.27) in finding the moments of z as described in section 4.3.3. The BER performance curves for two users are shown in Fig. 4.5.

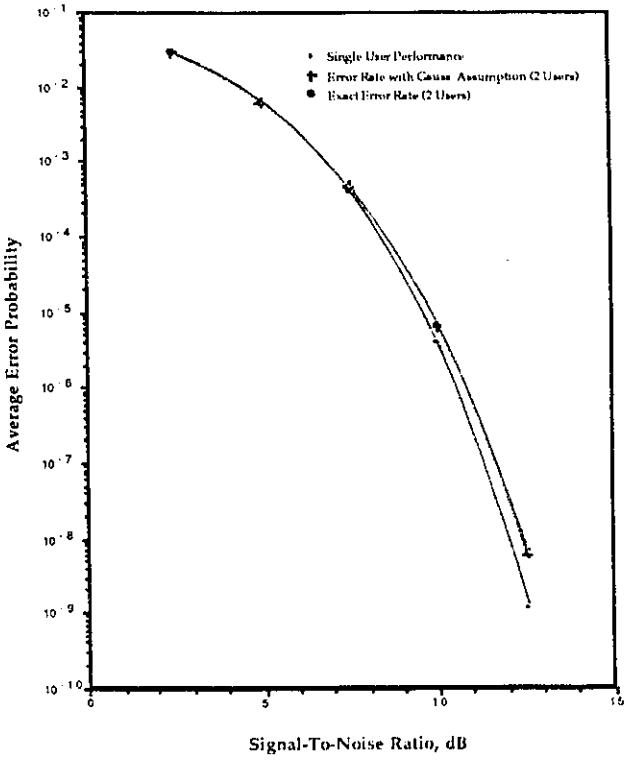

Fig. 4.5. Performance of DS/SSMA System with BPSK Modulation (Gold Sequence, N=127, $N_c = 2$ Users)

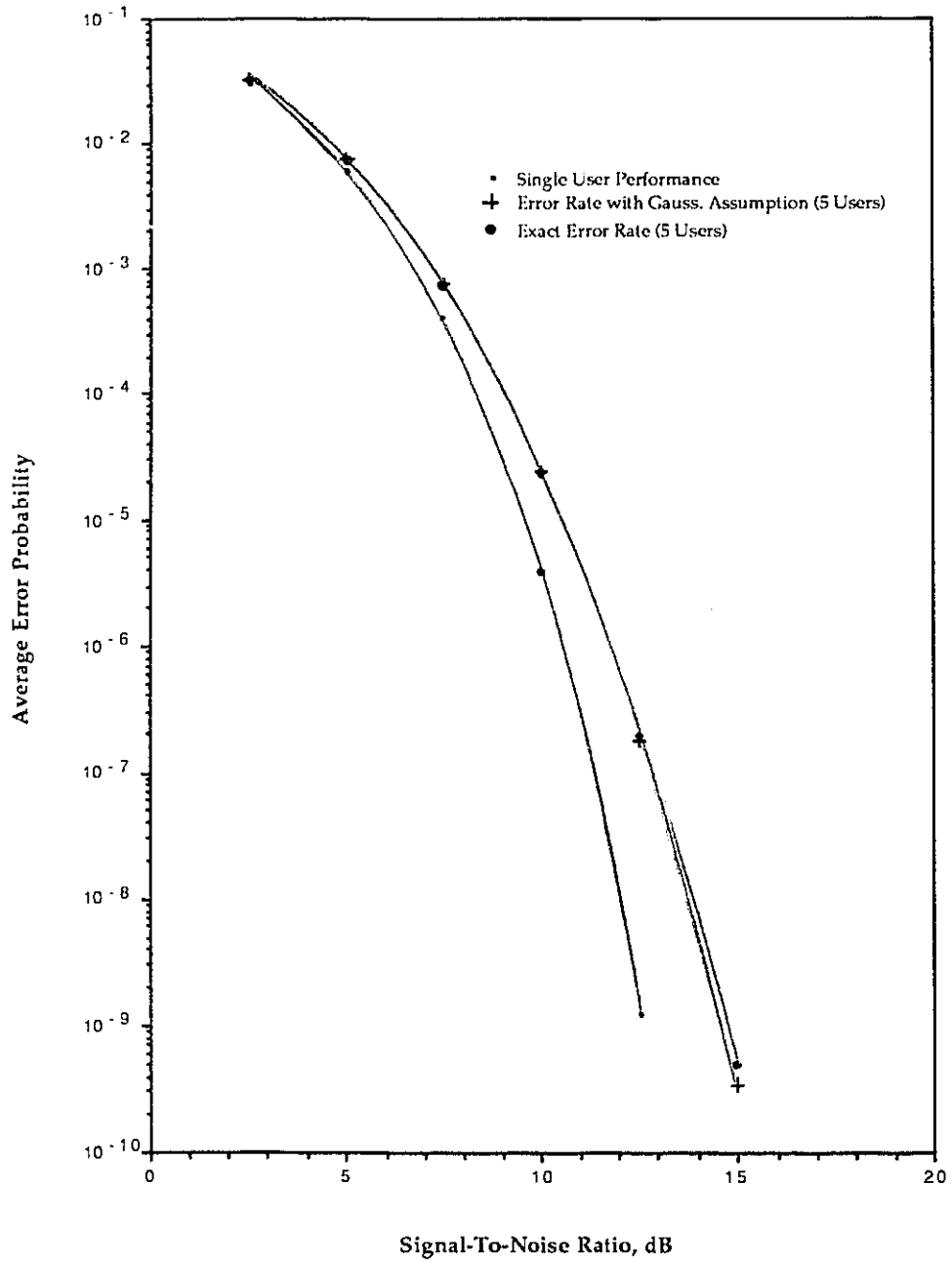

Fig. 4.6. Performance of DS/SSMA System with DPSK Modulation (Gold Sequence, N=127, $N_c = 5$ Users)

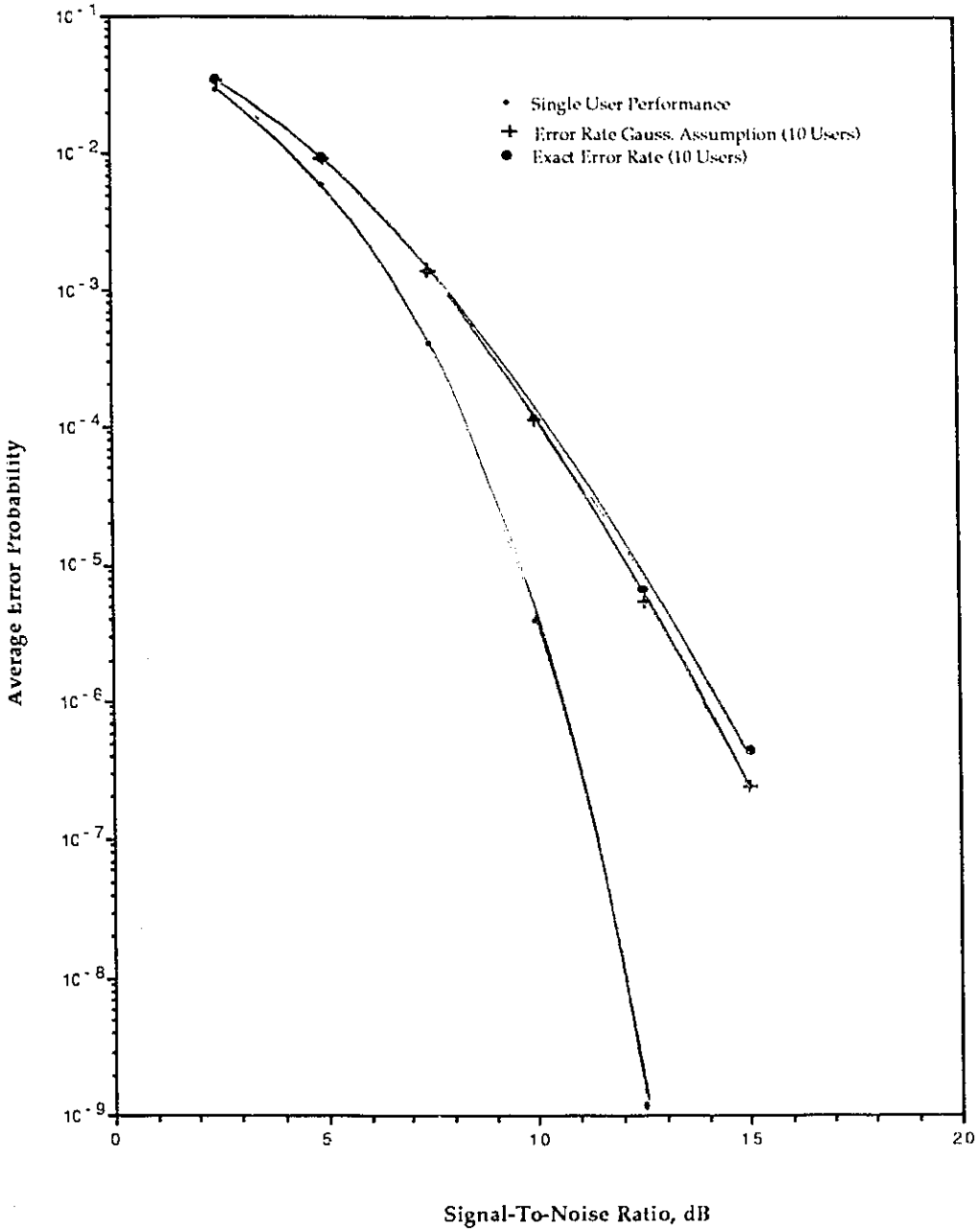

Fig. 4.7. Performance of DS/SSMA System with BPSK Modulation (Gold Sequence, N=127, $N_c = 10$ Users)

For a given probability of error, a signal-to-noise ratio $\frac{E_b}{N_0}$ is given. For a given density height noise which is according to eq.(3.12) a function of injected current bias, E_b is computable. Recalling

$$E_b = \frac{A^2 T}{2} = \frac{\bar{P}_T^2 m^2}{N_s^2} \frac{T}{2},$$

for a given optical power bias; to have a particular value of E_b, different pairs of number of clusters N_s and modulation index m can be found. By having m, number of users per cluster is limited by eq. (4.5). Finally, having number of clusters and number of users per cluster, the total number of users which can be served is determined.

Results show, the Gaussian assumption gives a good approximation of the average error probability in this case. Results obtained by Gaussian assumption are somewhat optimistic compared to the exact ones. This agrees with earlier findings of Mazo [20].

4.4.2 Kasami Sequences Results

Figures 4.8-4.12 illustrate the performance of the SS/CDMA scheme where the sequences employed are Kasami codes of periodic length 255 and different number of users. The Kasami sequences are obtained by multiplying the two polynomials described in example 3.2.

To find the actual codes, we used initial loadings from [29]. These initial loadings are shown to generate a class of Kasami codes known as Auto-Optimal with Least Sidelobe Energy (AO/LSE). In our numerical evaluation we used fifteen initial loadings. Hence, this covers fifteen periodic code sequences for a hypothetical community of users sharing the common channel band on a spread-spectrum multiple-access basis. Once the code sequences are obtained, the rest of the procedure to calculate error probability is identical to the previous case.

The BER performance curves for two users are shown in Figures 4.8.

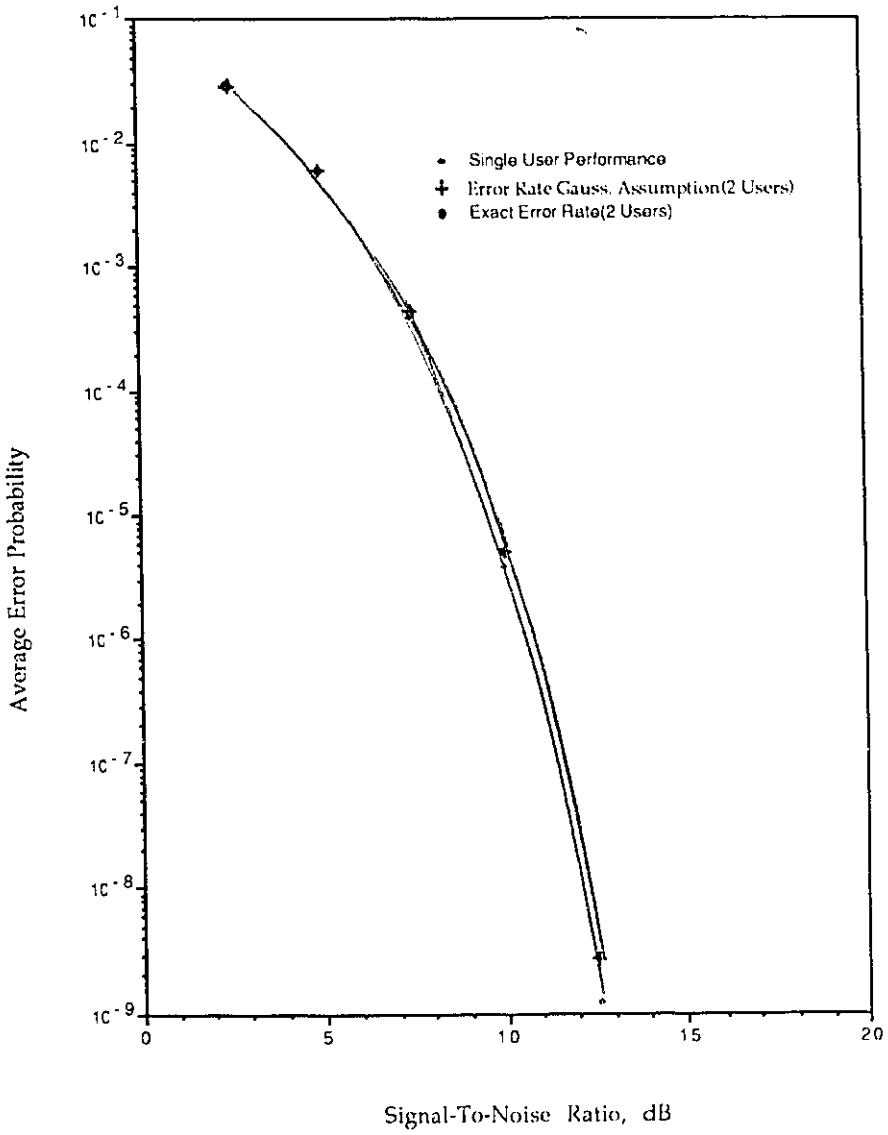

Fig. 4.8. Performance of DS/SSMA System with BPSK Modulation (Kasami Sequence, N=255, $N_c = 2$ Users)

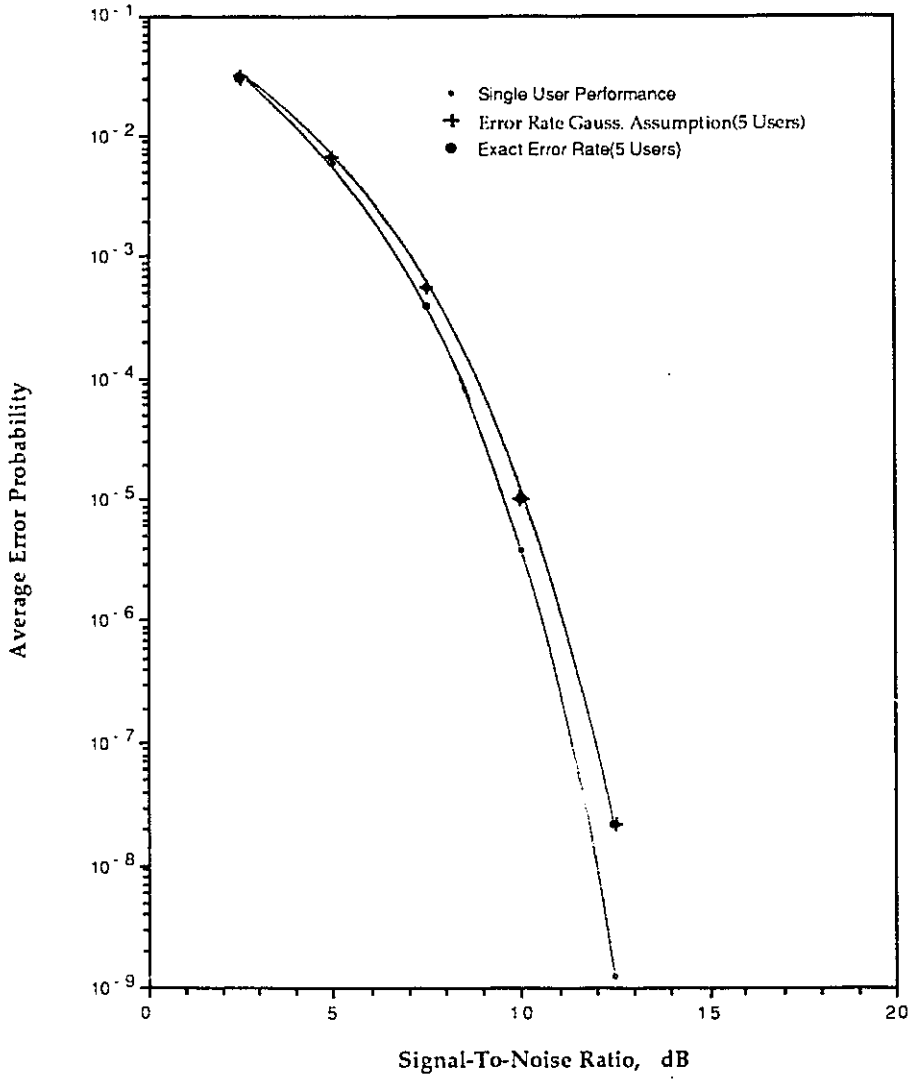

Fig. 4.9. Performance of DS/SSMA System with BPSK Modulation (Kasami Sequence, N=255, $N_c = 5$ Users)

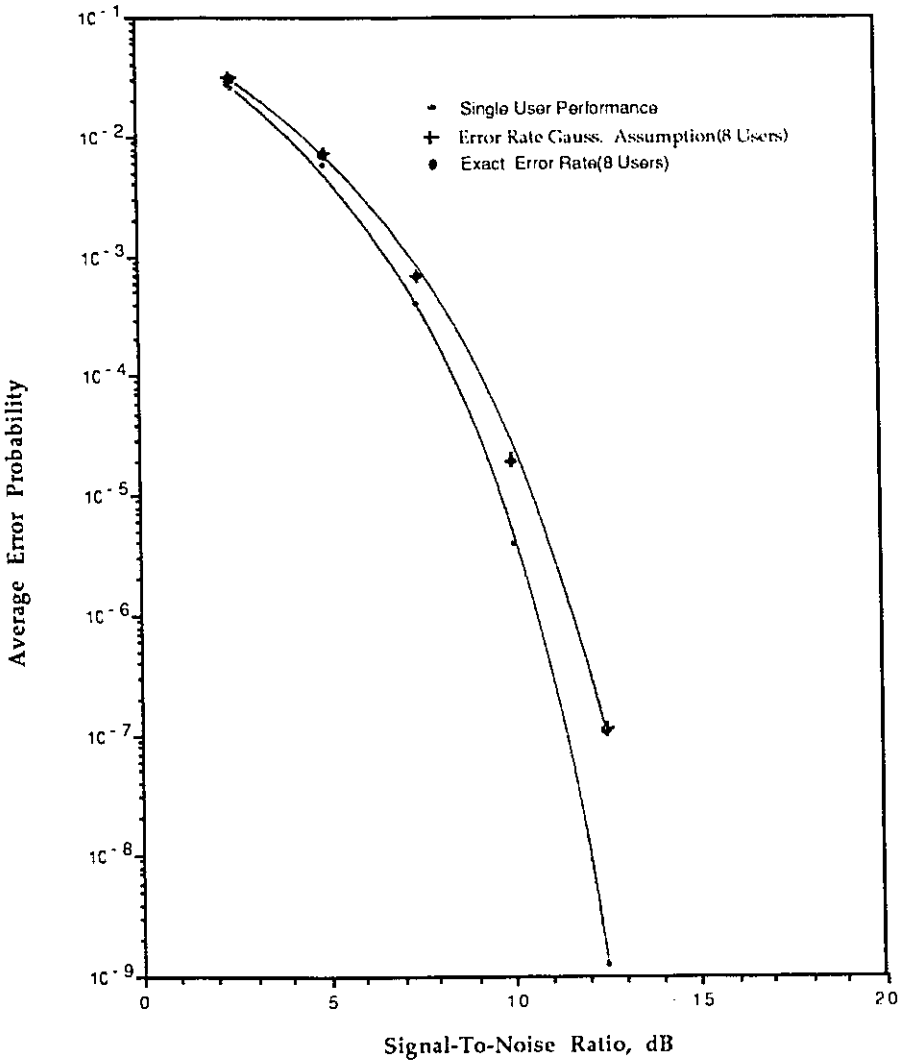

Fig. 4.10. Performance of DS/SSMA System with BPSK Modulation (Kasami Sequence, N=255, $N_c = 8$ Users)

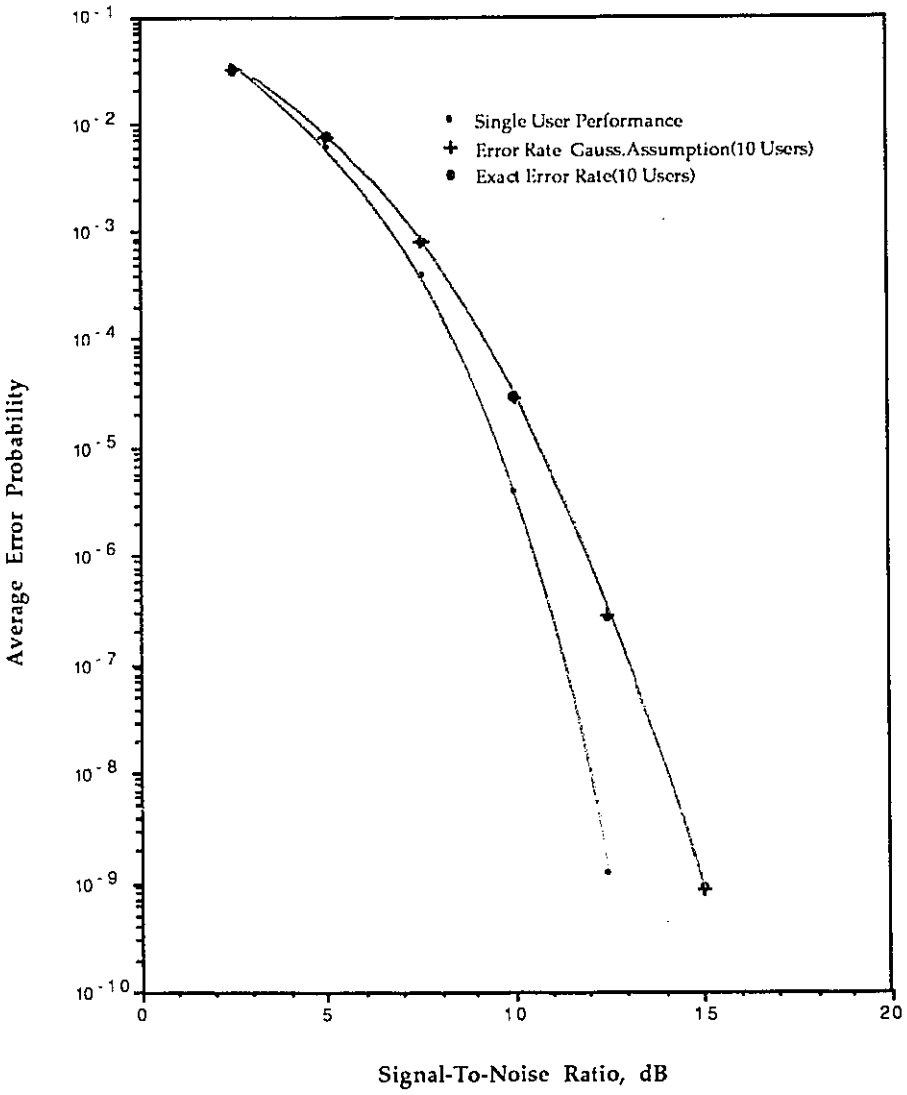

Fig. 4.11. Performance of DS/SSMA System with BPSK Modulation (Kasami Sequence, N=255, $N_c = 10$ Users)

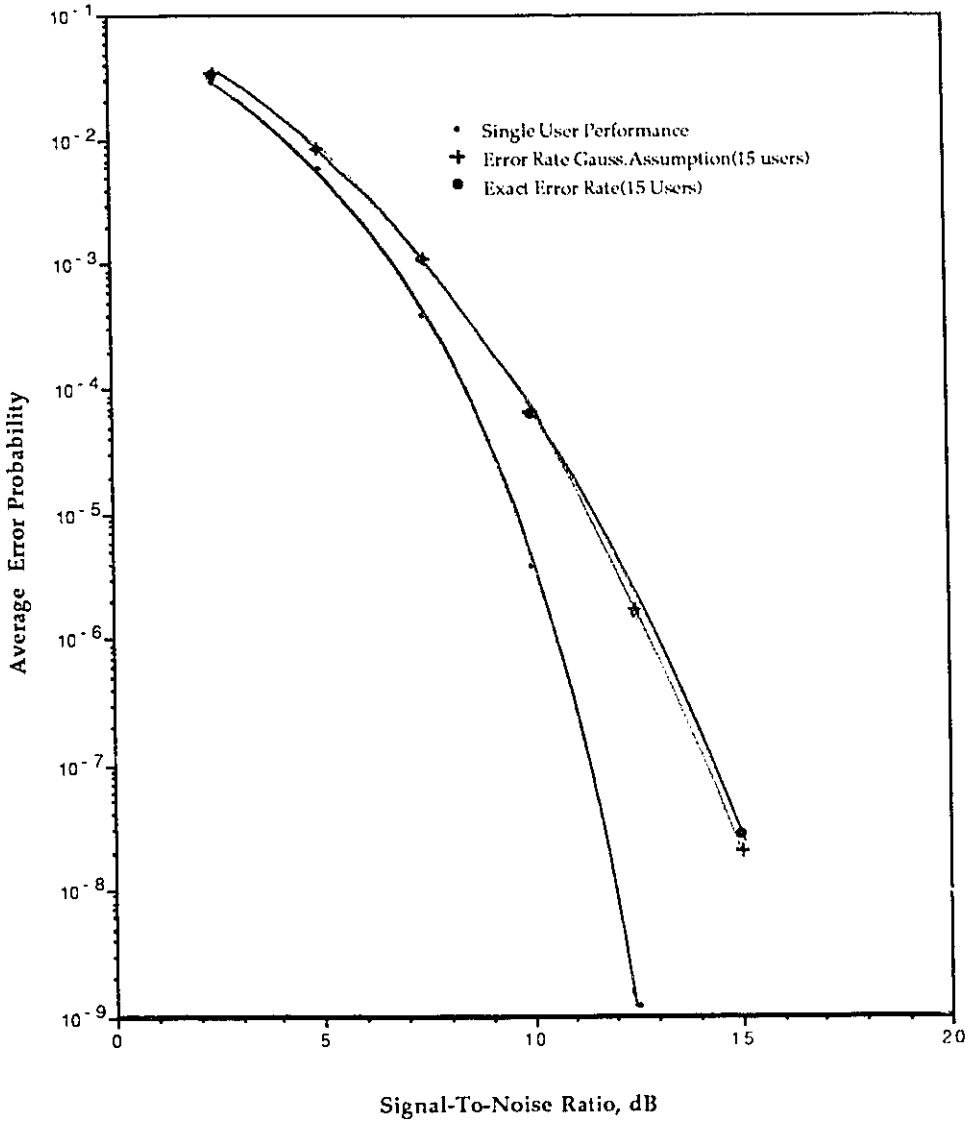

Fig. 4.12. Performance of DS/SSMA System with BPSK Modulation (Kasami Sequence, N=255, N_c = 15 Users)

4.4.3 Comparison Between Using Gold and Kasami Codes Sequence Sets

Comparison of the average error probability performance of the system using two code sequence sets with $N = 127$ for Gold type and $N = 255$ for Kasami type codes shows the scheme performs better when it employs the larger length codes set. The penalty is the larger bandwidth requirement. However, this is compensated by the larger set of individual codes which can accomodate more potential users.

Fig. 4.13 illustrates the number of simultaneous users per subcarrier which can be supported for a threshold bit error rate of 10^{-4}. That is, with this number of active users, the error rate will not exceed 10^{-4}.

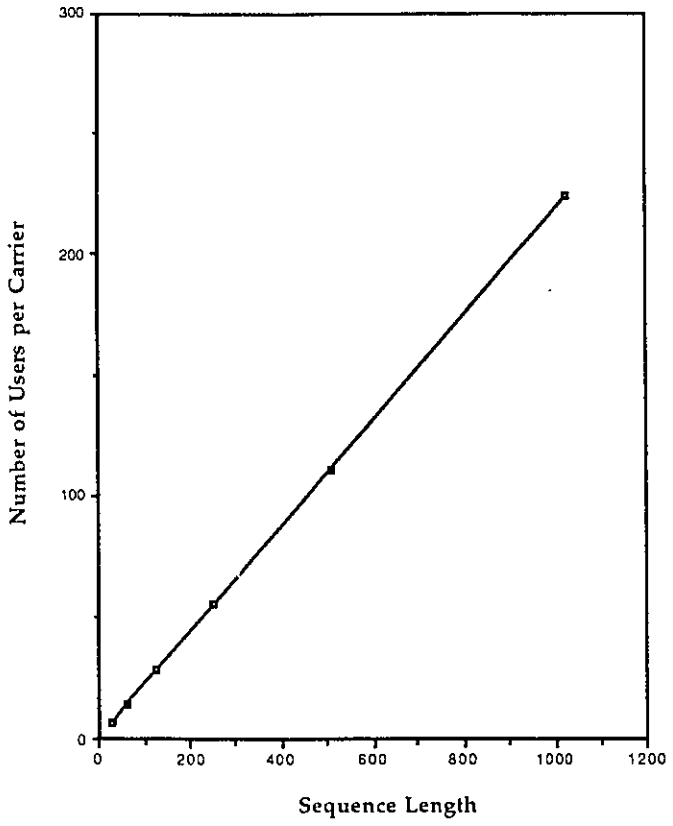

Fig. 4.13. Number of Simultaneous Users Per Subcarrier Versus Spread-Spectrum Sequence Length

Chapter 5

An Experiment on the Proposed Optical LAN

In this section, we present some preliminary experimental results on the LAN implementation as well as the corresponding transmission performance.

We will first discuss the subsystems of the experimental LAN.

5.1 Suggested Subsystems

In this section we describe the design and implementation of a Surface Acoustic Wave (SAW) filter-based receiver and transmitter of the proposed optical LAN. The system described is a direct-sequence spread-spectrum system using differential phase-shift keying (DPSK) modulation.

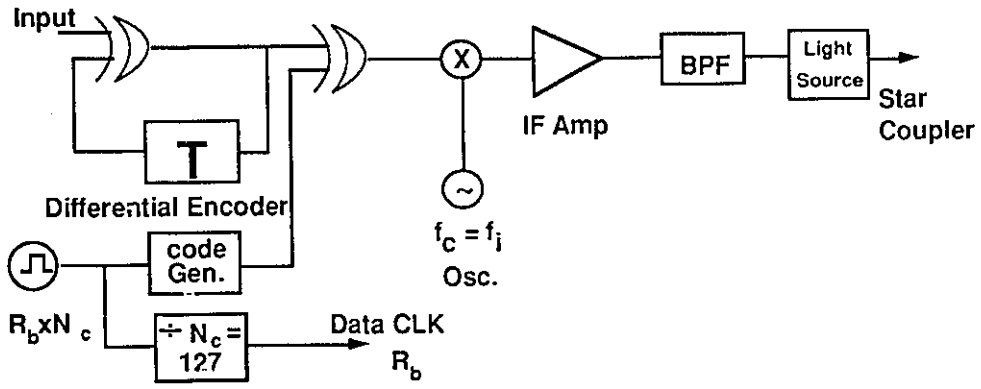

Fig. 5.1. Transmitter Block Diagram

In the transmitter, shown in Fig. 5.1, the code sequence chips are modulo-2 added to differentially encoded data bits. DPSK modulation is used to eliminate the need for synchronous carrier recovery at the receiver and to simplify the receiver design. The binary bit stream is then used to modulate a subcarrier Intermediate Frequency (IF) carrier. The DPSK signal intensity modulates a light source and the optical signal is then transmitted

via a fiber to a star coupler.

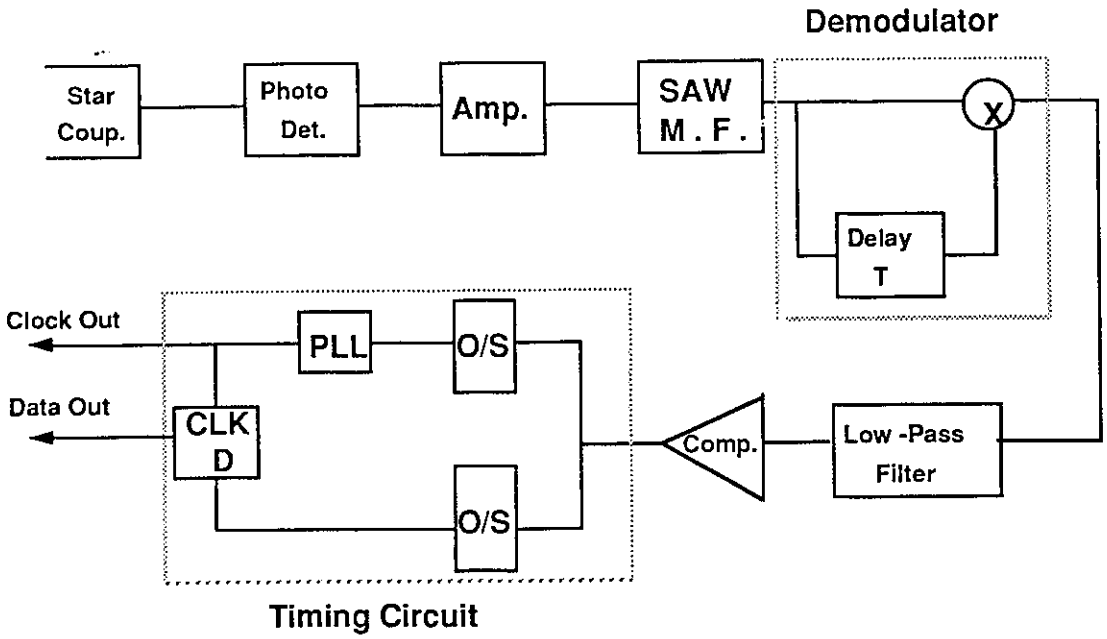

Fig. 5.2. Receiver Block Diagram

In the receiver, as shown in Fig. 5.2, the received optical signal is photodetected. The signal is then passed through a bandpass filter and a bandpass amplifier with an automatic gain control and on to the SAW Matched-Filter (SAW-MF). The center frequency of the SAW filter responds, with an autocorrelation peak, to a matching sequence. If there is no match, the SAW output is that of cross-correlation sidelobes. The SAW output is still a DPSK modulated signal. The DPSK signal is then demodulated and passed through a low-pass filter, to eliminate the harmonics.

The reference transmitter and an interfering transmitter that was designed to test the multiple access capability of the system are described in the next section. We will then discuss the receiver, the SAW matched-filter and the measured performance.

5.2 Experiment Subsystems

In this section, we elaborate on the main subsystems of the experimental LAN. The set-up was dictated mainly by availability of equipment. The experiment provides some preliminary insight into the LAN performance. A summary of this section can also be found in [24].

5.2.1 Transmitter Design

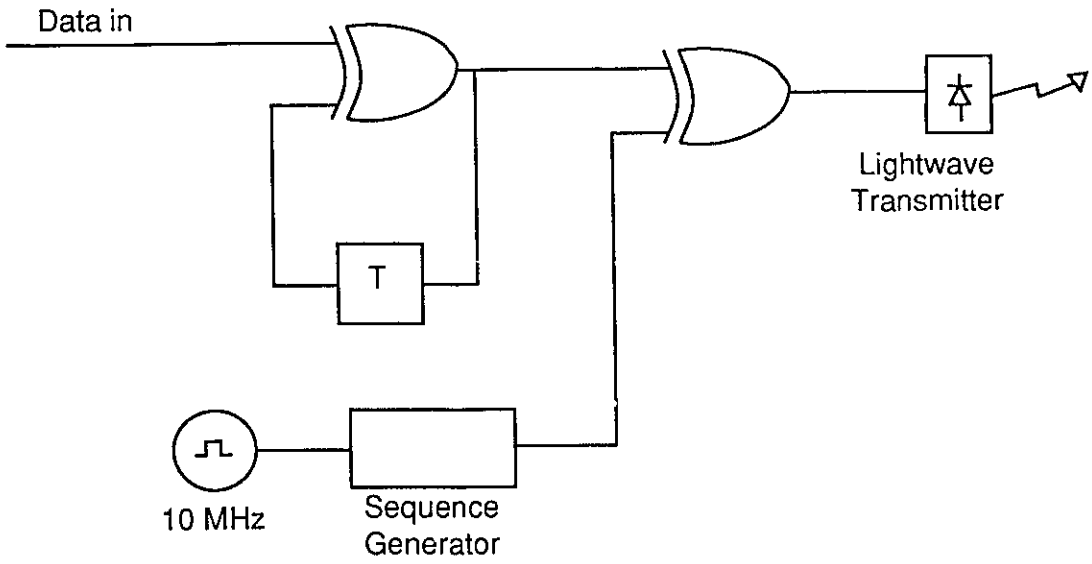

Fig. 5.3. Experimental Transmitter Block Diagram

A block diagram of the reference transmitter is shown in Fig. 5.3. It is essentially baseband section of a DPSK transmitter with the addition of a sequence generator and a modulo-2 adder. For the reference transmitter, the periodic sequence generated is a maximal length sequence [23] of 127 chips implemented by a shift register with linear feedback. The sequence is described by the polynomial $x^7 + x^3 + x^2 + x + 1$, octally represented by 217. The choice of this sequence was dictated by the availability of hardware for this experiment. In practice, a maximal length sequence would be inappropriate due to the limited number of available sequences. A more suitable choice would be the large

set of Kasami sequences [23].

The transmitter is implemented using standard TTL intergrated circuits. The input data is differentially encoded using an exclusive-OR gate and a one bit delay ($12.7\mu s$) from an Integrated Circuit (IC) shift register. A full sequence length, 127 chips, is then added to each differentialy encoded data bit.

The sequence gererator is clocked using a 10 MHz oscillator. A 78.8 kHz data clock is generated by detecting the last 7 chips of the sequence. For the octal 217 sequence used here the last seven bits are logic "ones" and are detected by AND gates. Generating the data clock this way ensures the proper phase relation between the data and a full length of the code sequence. The baseband rate (78.8 kHz) is the ratio of the chip rate (10 MHz) to the sequence length (127). Note that, given the above signal parameters, a baseband rate of 78.8 kHz is the only rate that can be inferred.

This spread spectrum signal is then used to modulate an AT&T Technologies lightwave transmitter model 1250A. The optical source used in the transmitter is a GaAlAs Light Emitting Diode (LED) emitting light at 0.875 micron.

A second transmitter was necessary for signal-to-interference ratio and multiple-access interference measurements. The only difference between the reference transmitter and the interference transmitter is in the sequence gererators. The generated sequence in the interfering transmitter is another 127 chips maximal length sequence represented by the polynomial $x^7 + x^3 + 1$. The selection of this sequence was totally arbitrary.

5.2.2 SAW Matched-Filter

SAW filters play an important role in many recent applications such as high-speed timing recovery circuits and spread-spectrum systems, to name a few. The SAW matched-filter in our system correlates its input with a preprogrammed matching sequence. Also, the device acts as a very high-Q bandpass filter. A plot of relative correlation peak amplitude versus frequency offset from the IF is shown in Fig. 5.4. The amplitude response is basically that

of a $|sin(x)/x|$ function with zero crossings on each side of the main lobe away from the center by $1/T$ where T is the data biy interval. The effect of frequency offset is illustrated in Fig. 5.4(b). As seen in this figure, it is possible to use the frequency offset property, however, the off-frequency interference, dispersed in time, raises the off-peak noise level to some extent.

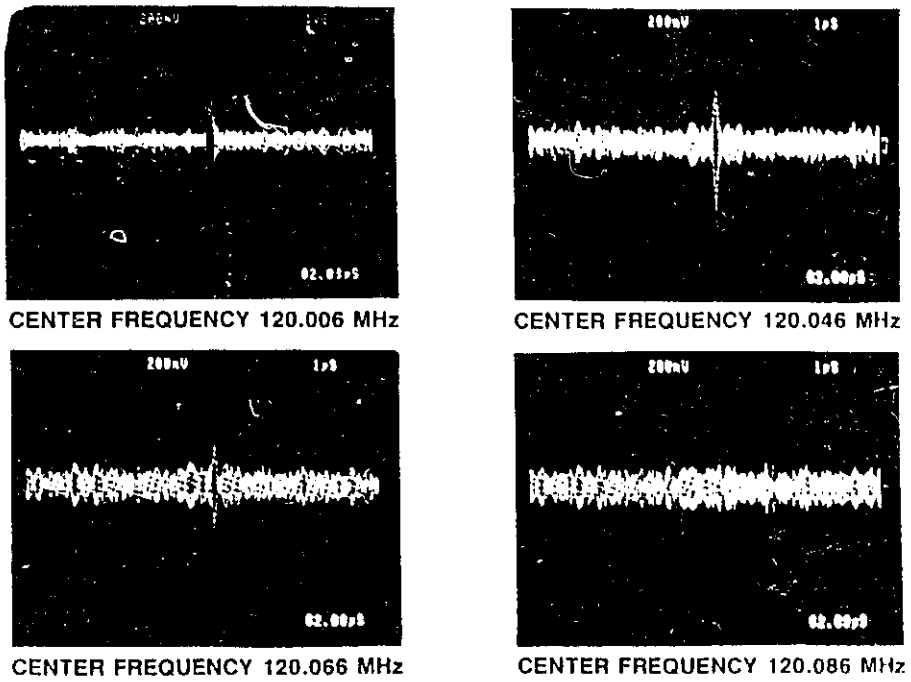

Fig. 5.4.(a) Effect of Center Frequency Shift on Correlation Peaks

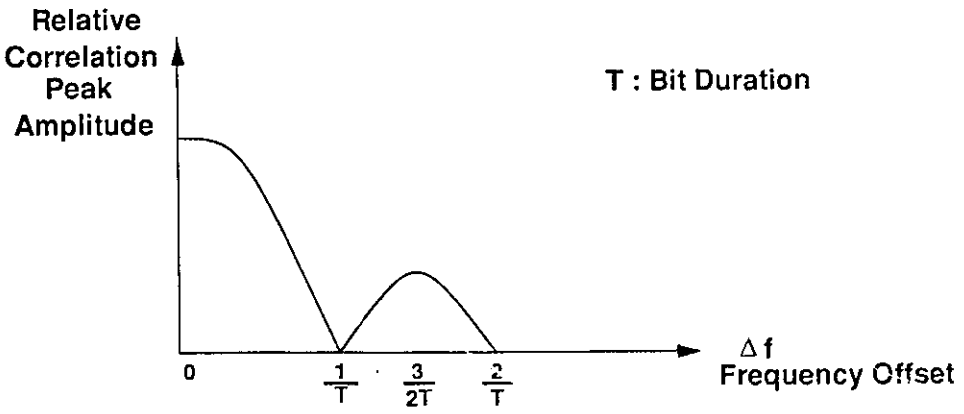

Fig. 5.4.(b) Effect of Frequency Shift on Correlation Peak of the SAW Filter, T= Data Bit Length

The SAW devices are implemented using a combination of thick film, bipolar LSI, and SAW technologies. The rather smal size of the SAW device (about 1.5 inch in this application) lends itself to integration into small receivers. With today's technology, SAW filters may have center frequencies up to 700 MHz. Depending on the spreading sequence, the processing gain (as will be defined later) of a state-of-the-art SAW filter can be as high as 60 dB. For multiuser applications as in our experiment, SAW matched-filters with different prefabricated masks need be developed, or else, programmable SAW filters could be used.

In order to develop a better understanding of the correlation measurements, we will review some basic terms here. When measuring a correlation function, we can have two distinct cases, namely; aperiodic and periodic correlations. In the aperiodic case we correlate two sequences, which may or may not be identical depending on whether we perform an auto or a cross correlation. However, these sequences occur once and only once. The aperiodic case is not relevant to our application. The even and odd periodic correlation functions are important here because of the nature of digital transmission. These two cases, even and odd periodic correlations, are shown in Fig. 5.5.

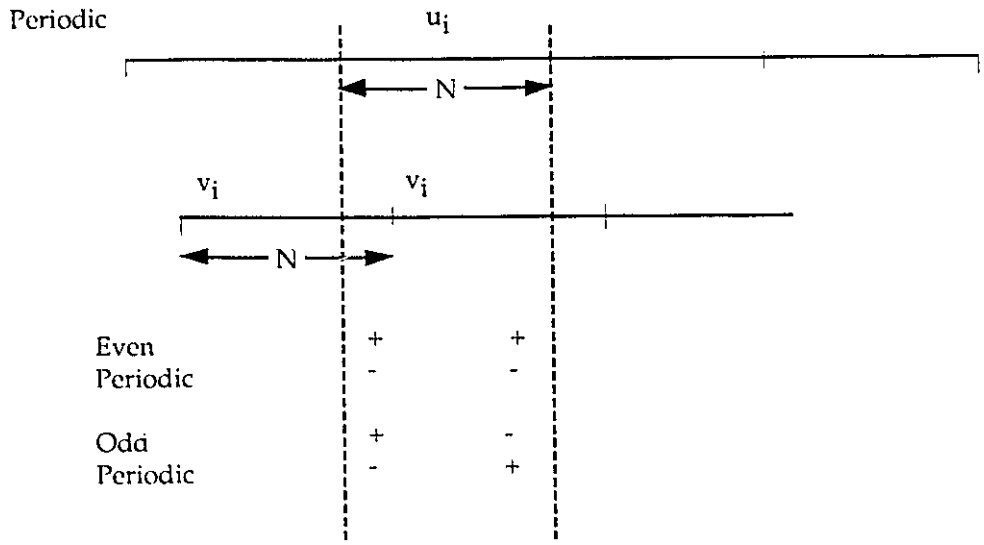

Fig. 5.5. Correlation Parameters for PN-Sequences

We have two periodic sequences u_j and v_j, direct-sequence added to random bipolar

bits of two binary streams, as shown, and v_j is correlated with u_j. If two adjacent bits of the second stream within correlation window have the same polarity, we obtain an even periodic correlation function. Otherwise, we will end-up with an odd periodic correlation function. Numerical evaluations of correlation parameters are available in [29] and are used here for a theoretical comparison. For the maximal length sequences used in this experiment (i.e., octal 211 and 217), the peak values are given as follows.

For the autocorrelation of the sequences corresponding to 217 and 217; even periodic sidelobe level is -1 and odd periodic sidelobe peak level is 15. For the cross-correlation of 217 and 211; even periodic sidelobe peak level is 17 and odd periodic sidelobe peak level is 33.

From these numerical evaluations we can calculate the worst case processing gain (PG) for the odd periodic sidelobe as 20 log (127/33) = 11.7 dB. For the even periodic sidelobe the worst case is 20 log (127/17) = 17.4 dB.

We have measured the average processing gain to be about 18 dB. This measured processing gain is the ratio of the autocorrelation peak of the reference signal to the rms of the cross-correlation sidelobes due to the interference transmitter. (See Fig. 5.6)

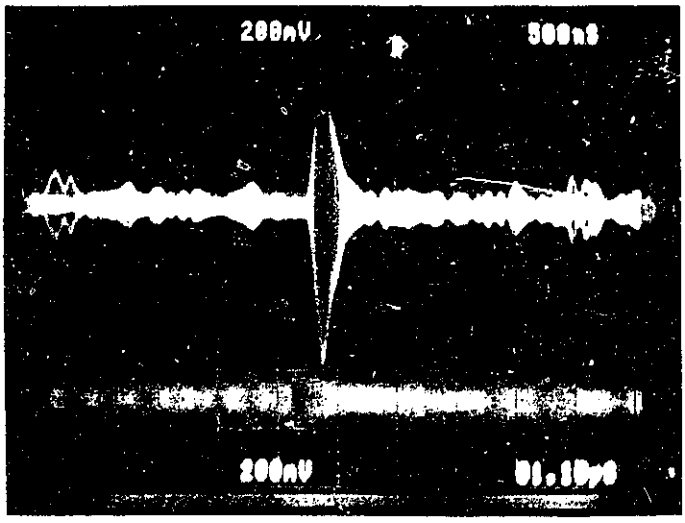

Fig. 5.6. Autocorrelation Peak and Cross-Correlation Sidelobes

5.2.3 Receiver Design

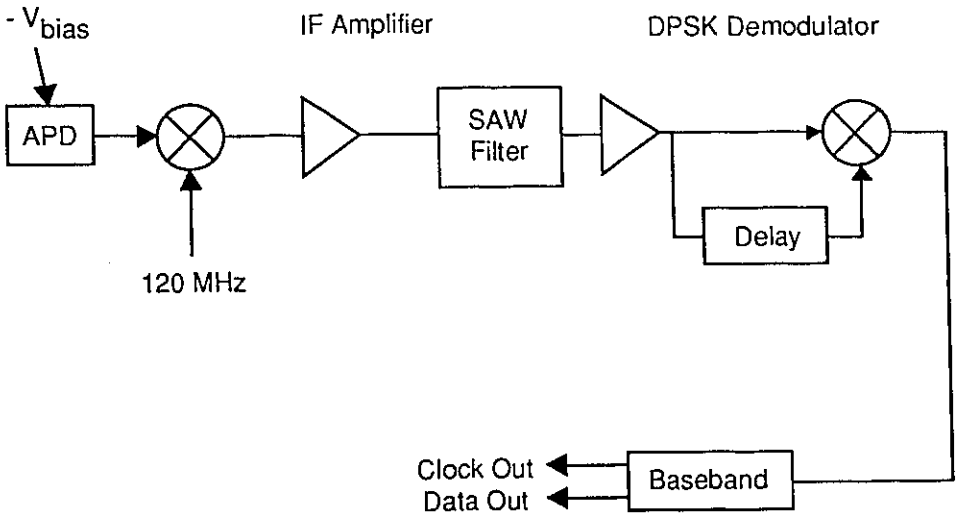

Fig. 5.7. Experimental Receiver Block Diagram

A block diagram of the receiver is shown in Fig. 5.7. Basically, it consists of an optical receiver which is the AT&T Technologies model 1350A using a silicon avalanche photodiode (APD), a SAW filter-based demodulator, a baseband timing circuit and a detector circuit. The data output of the receiver is a TTL compatible signal that is used to bi-phase modulate a 120 MHz signal through a balanced mixer. This modulation/up conversion is necessary to take advantage of the SAW matched-filter since its center frequency is at 120 MHz. In actual implementation as shown in Fig. 5.1 this modulation will take place in the transmitter. However, it was simpler to set this up as shown in Fig. 5.7.

The SAW matched-filter in our system correlates its input with the preprogrammed matching sequence.

The amplified IF signal is fed into the SAW matched-filter. Because of 17 dB insertion loss of the SAW, it is necessary to have a broadband amplifier prior to demodulation. DPSK modulation is used to eliminate the need for synchronous carrier recovery at the receiver and to simplify the receiver design and implementation. In the DPSK modulation loop a bandpass SAW delay line provides the one bit delay required in the demodulation.

The baseband signal at the demodulator output is still bipolar and we use a dual comparator as a window detector to detect its positive and negative peaks. For simplicity, one comparator is used to detect +1 binary pulses and convert them to logic "ones". A one-shot then stretches the pulse to 50 percent duty cyle and the signal is sent to a data latch. The second comparator is used to detect the −1 pulses to convert them to logic "zeros". The output of this comparator is positive pulses and is OR-gated with the output of the first comparator to form our receiver clock signal. The pulses are then stretched to 50 percent duty cycle and used to trigger a phase-locked loop in the clock recovery circuit.

5.3 Experiment and Results

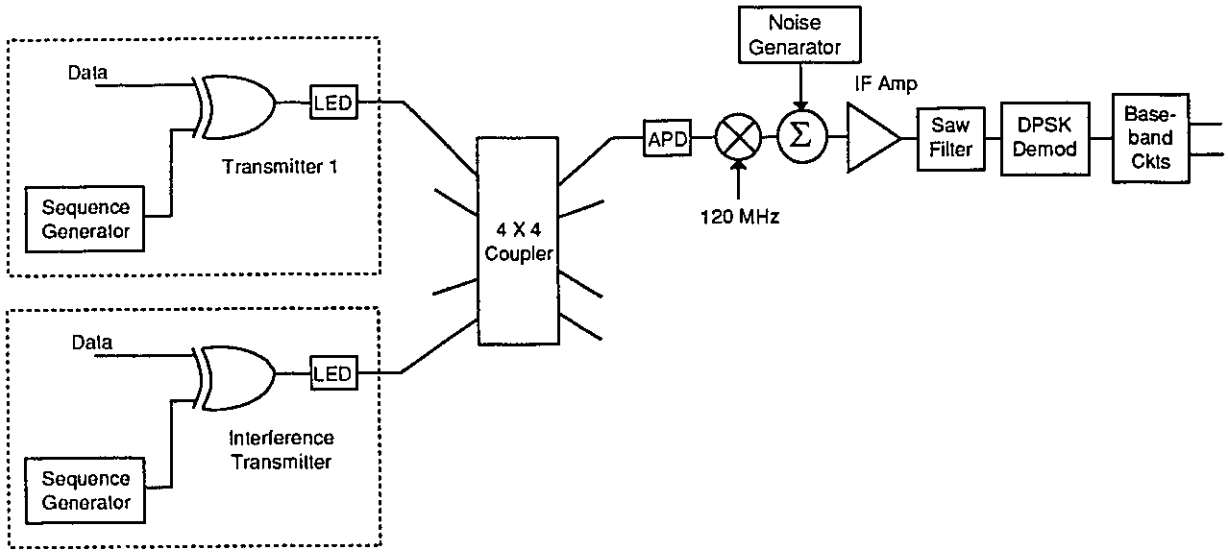

Fig. 5.8. Experiment Set-Up

Two optical transmitters and one optical receiver are connected to a 4 × 4 multimode passive optical star coupler, as shown in Fig. 5.8. Transmitter number 1 is adding a 127 bit PN sequence to each data bit, the same sequence the SAW matched-filter has been programmed to recognize. The second transmitter is adding another 127 bit PN sequence, randomly selected to generate interference. A noise source is also connected to the receiver IF amplifier. The noise source output is varied and the bit error rate is measured as a function of signal-to-noise ratio. This is shown in Fig. 5.9.

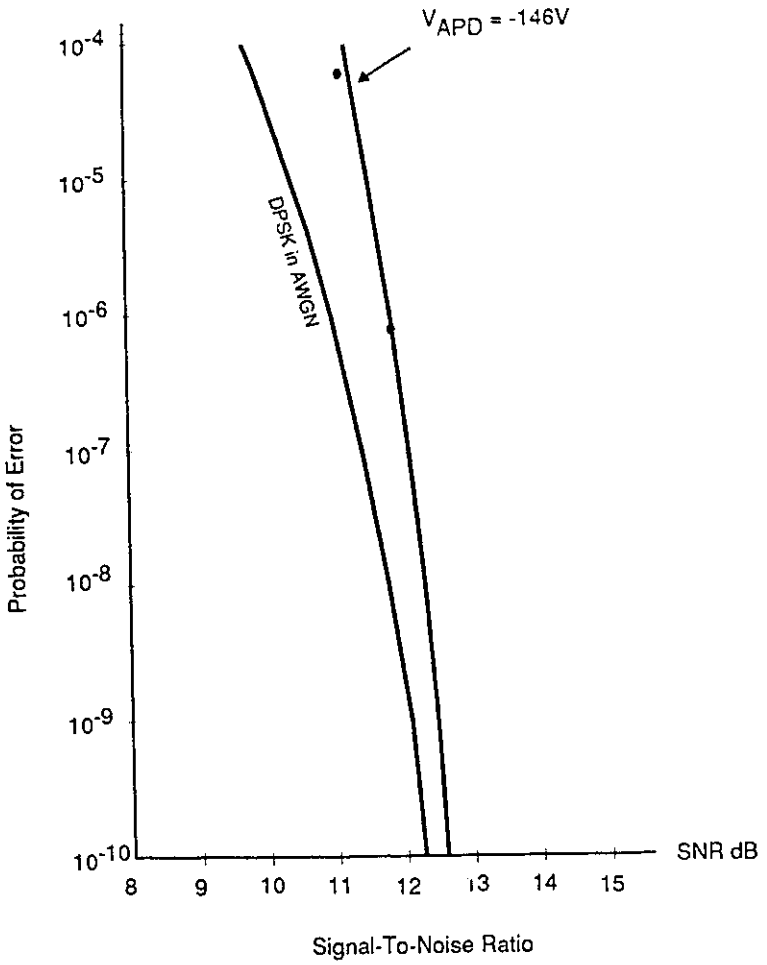

Fig. 5.9. Performance of Implemented System with DPSK Modulation (m-Sequences, $N = 127,\ N_c = 2$ Users)

On the figure, as a reference, there is also shown theoretical performance of the system for one user. This would basically represent performance of a DPSK signal in presence of additive Gaussian noise. The gap beween this curve and the measured curve is due to all implementation inaccuracies as well as the interfering signal. Therefore, from this figure we may conclude the technique has potential for LAN applications.

Chapter 6

Conclusions

6.1 Summary

This thesis began with the assertion that robustness of CDMA scheme against interference can be used to alleviate the effect of laser or external modulation nonlinearities in Optical LANs. Laser nonlinearity limits the performance of systems which exploit subcarrier multiplexing scheme. We have proposed a hybrid CDMA/FDMA subcarrier scheme so that the beneficial aspects of each scheme mitigate the impairments of the other one. The proposed scheme is robust against interference and is much more spectrally efficient than CDMA.

We have employed DS/SSMA as a form of CDMA and BPSK as modulation. In Section 3.4,we have shown that IMPs and harmonics have an interference-like effect as nonmatching sequences if sequence sets for which shift-and-add property holds are used to spread the data signal prior to subcarrier modulation. We have shown shift-and-add holds for traditional sequences; i.e., m-sequences, Gold and Kasami sequences. As a result, we have been able to calculate the total power of any order of IMP and harmonics. The second order harmonics and IMPs are suppressed by a factor $\frac{4}{9N}$ and third order components by $\frac{6}{9N}$ and in general for n^{th} order components, it becomes $\frac{2n}{9N}$ where N is the length of spreading sequences. By using the sequence of length $N = 127$ the second order components power is suppressed by 24.56 dB and third order components by 22.80 dB. Using the spreading sequence of length $N = 255$ the second order components power is suppressed by 27.59 dB and third order components by 25.83 dB.

We modeled the system and evaluated the average error probability performance of the proposed LAN for a transceiver pair. We examined the accuracy of the Gaussian Assumption on multiple-access interference distribution. The results show a great agreement between exact results and ones obtained under the Gaussian assumption as shown in Fig.

4.5-4.12.

In our numerical evaluation we have used the Gauss Quadrature Rule integration (GQR) method, to obtain an exact average error probability performance.

We compared the performance of the scheme for two different code sequence sets ($N = 127$ Gold and $N = 255$ Kasami codes) and determined that there is a significant advantage in deploying $N = 255$ Kasami sequence set. As a result, we were able to provide BER performance of the scheme as a function of:

(1.) Bit energy-to-noise ratio (E_b/N_o)

(2.) Number of users

We also computed the number of users per subcarrier frequency that can be supported by the system where the irreducable BER is less then 10^{-4}.

Among implementation issues, we have suggested using SAW filters as correlator in order to obtain a spectrum efficiency as subcarrier FDMA scheme.

A detailed design of transmitter and receiver has been provided. Two transmitters and one SAW filter-based receiver have been realized. The results obtained from experiment have been compared with theoretical values. Results show promise.

6.2 Suggestions for Further Research

As this thesis comes to a close, there are a few topics that deserve further investigation. The first topic is synchronous CDMA which can be easily employed in optical systems. Furthermore, we have investigated just two code sequence sets, i.e., Gold and Kasami sequences. There might be a more appropriate sequence set for the nonlinearity suppression task. Our investigation centered on binary sequences and binary signalling schemes. Multi-level sequences are more bandwidth efficient and it is worth to investigate these sequences. We didn't consider Avalanche Photodetector (APD) in our theoritical analysis. APD gain

can enhance the system performance. We did not model laser nonlinearity. Nonlinearity modeling of laser will give us a good insight on the properties of the sequences which are helpful in nonlinearity distortion level suppression.

Appendix A

Gauss Quadrature Rule Approximations

An accurate technique for evaluating probability of error P_e in digital communications systems is based on numerical integration formulas. In this case, it is usual to express P_e by means of integrals, i.e., averages, such as;

$$E[g(z)] = \int_a^b g(x) f_z(x) dx \tag{A.1}$$

where $f_z(\cdot)$ denotes the probability density function of the random variable z. Since evaluation of $E[g(z)]$ is indeed equivalent to the computation of an integral, we can resort to numerical techniques developed to compute approximate values of integrals of the form (A.1). The most widely investigated techniques for approximating a definite integral lead to the formula

$$\int_a^b g(x) f_z(x) dx \cong \sum_{i=1}^{N} w_i g(x_i) \tag{A.2}$$

a linear combination of values of the function $g(\cdot)$. The $x_i, i = 1, 2, ..., N$, are called the nodes of the formula, and the $w_i, i = 1, 2, ..., N$, are called its weights. The set of nodes and weights is usually referred to as a quadrature rule. A systematic introduction to the theory of quadrature rules of the form (A.2) is given in Krylov [40].

The quadrature rule is chosen to render (A.2) as accurate as possible. A first difficulty with this theory arises when one wants to define how to measure the accuracy of a quadrature rule. Since we want the nodes and weights to be independent of $g(\cdot)$, and hence be the same for all possible such functions, the definition of what is meant by "accuracy" must be made independent of the particular choice of $g(\cdot)$. The classical approach here is to select a number of probe functions and constrain the quadrature rule to be exact for these functions. By choosing $g(\cdot)$ to be a polynomial, it is said that the quadrature rule

(A.2) has degree of precision ν if it is exact whenever $g(\cdot)$ is a polynomial of degree $\leq \nu$ [or, equivalently, whenever $g(x) = 1, x, ..., x^{\nu}$] and it is not exact for $g(x) = x^{(\nu+1)}$.

Once a criterion of goodness for quadrature rules has been defined, the next step is to investigate which are the best quadrature rules and how they can be computed. The answer is provided by the following result from numerical analysis, slightly reformulated (see Krylov [40] for more details and a proof):

Given a random variable z with range $[a, b]$ and all of whose moments exist, it is possible to define a sequence of polynomials $P_0(x), P_1(x), ..., deg\ P_i(x) = i$, that are orthonormal with respect to z; that is,

$$E[P_n(z)P_m(z)] = \delta_{mn}, \quad m, n = 0, 1, \ldots \tag{A.3}$$

Denote by $x_1 < x_2 < \cdots < x_N$ the N roots of the polynomial $P_N(x)$ (they are all real, and lie inside $[a, b]$), and by k_n the coefficient of x^n in the polynomial $P_n(x), n = 0, 1, ...$ By defining;

$$w_i = \frac{k_{N+1}}{k_N} \frac{1}{P_{N+1}(x_i)P'_N(x_i)}, \quad i = 1, 2, \ldots, M, \tag{A.4}$$

the set $\{x_i, w_i\}_{i=1}^{N}$ is a quadrature rule with degree of precision $2N - 1$. This is the highest degree of precision that can be attained by any quadrature rule with N weights and abscissas.

The relevant fact here is that the set $\{x_i, w_i\}_{i=1}^{N}$ can be evaluated on the basis of the moments $\mu_1, \mu_2, ..., \mu_{2N-1}$ of z. In other words, no more than the first $2N - 1$ moments of z are necessary to determine explicitly a Gauss quadrature rule with N weights and nodes.*

* It is often claimed that μ_{2N} is also needed to perform this task; see for instance Golub and Welsch [19]. Actually, the role of μ_{2N} is just that of normalizing the polynomial $P_N(\cdot)$, and its values affect neither the nodes nor the weights of the quadrature rule (Gautschi [42]).

To see how to undertake this, we use the fact that a Gauss quadrature rule with N weights and nodes has a degree of precision $2N-1$. Since

$$\mu_k = E[z^k] = \int_a^b x^k f_z(x) dx \tag{A.5}$$

for any $0 \leq k \leq 2N-1$ the Gauss Quadrature rule is exact; that is,

$$\mu_k = \sum_{i=1}^{N} w_i x_i^k, \quad k = 0, 1, \ldots, 2N-1 \tag{A.6}$$

This system of $2N$ nonlinear equations has the weights and nodes as unknowns; by solving it, the Gauss quadrature rule can be found.

In general, it is not convenient to solve directly equations (A.6), except for a very few simple cases. A computationally effective technique to determine Gauss quadrature rules based on the moments of z has been proposed in Golub and Welsch [19]. Now, for the problem at hand, we outline the computation of nodes and weights of Gauss Quadrature rules:

Formulation of Gauss Quadrature Rules From the Moments of z

Denote the first $N_m = 2N_c + 1$ moments of z by the sequence $\mu_n, n = 0, 1, 2, ..., 2N_c$. In the problem at hand the random variables are evenly distributed. Therefore, as previously stated, the odd moments are all zero.

Let $M = [m_{ij}], i, j = 1, 2, ..., N_c + 1$, be the Gram matrix of the system with

$$m_{ij} = \mu_{i+j-2} \tag{A.7}$$

Thus,

$$M = \begin{pmatrix} 1 & 0 & \mu_2 & 0 & . & . & . & \mu N_c \\ 0 & \mu_2 & 0 & . & . & . & . & 0 \\ \mu_2 & 0 & \mu_4 & . & . & . & . & \mu N_c + 2 \\ 0 & . & . & . & . & . & . & . \\ . & . & . & . & . & . & . & . \\ . & . & . & . & . & . & . & . \\ . & . & . & . & . & . & . & . \\ \mu N_c & . & . & . & . & . & . & \mu_2 N_c \end{pmatrix} \tag{A.8}$$

where $\mu = 1$. Also, let $M = R^T R$ be the Cholesky decomposition of M, where T represents the transpose matrix with

$$r_{ii} = \left(m_{ii} \sum_{k=1}^{i-1} r_{ki}^2 \right)^{\frac{1}{2}} \tag{A.9}$$

and

$$r_{ij} = \left(m_{ij} - \sum_{k=1}^{i-1} r_{ki} r_{kj} \right) / r_{ii} \quad i < j \tag{A.10}$$

Because all the odd moments are zero, it follows that $r_{ij} = 0$ when $(i + j)$ is odd. We now have an upper triangular matrix $R = [r_{ij}], i, j = 1, 2, ..., N_c + 1$. The matrix is used to calculate a set of numbers $\delta_j, j = 1, 2, ... N_c$, where

$$\delta_j = \frac{r_{j+1j+1}}{r_{jj}} \tag{A.11}$$

Now we construct a tridiagonal matrix J as follows:

$$J = \begin{pmatrix} 0 & \delta_1 & 0 & . & . & . & 0 \\ \delta_1 & 0 & \delta_2 & . & . & . & 0 \\ 0 & \delta_2 & 0 & . & . & . & 0 \\ . & . & . & . & . & . & . \\ . & . & . & . & . & . & . \\ . & . & . & . & . & . & . \\ . & . & . & . & . & . & . \\ . & . & . & . & . & . & \delta N_c - 1 \\ . & . & . & . & . & \delta N_c - 1 & 0 \end{pmatrix} \tag{A.12}$$

where J is an $N_c \times N_c$ matrix.

By finding the eigenvalues and eigenvectors of the matrix J, it is possible to arrive at the weights and nodes of the quadrature rule. Let the eigenvalue equation be

$$J\tilde{q}_j = \lambda_j \tilde{q}_j \tag{A.13}$$

Then the quadrature rule for the sequence (w_j, z_i) in eq. (4.26) is given by the set of numbers $\{q_{1j}^2, \lambda_j\}$, $j = 1, 2, \ldots N_c$, where q_{1j}^2 is the square of the first element of the eigenvector $\tilde{q}_j$, and λ_j is an eigenvalue in eq. (A.13). Hence, if the first $2N_c + 1$ moments are calculated, then the resulting quadrature rule will contain N_c weights and nodes.

Appendix B

Calculation of the Total Power of Interference due to Laser Nonlinearity

In this appendix, we calculate the power of the interference term arising due to laser nonlinearity in eq.(4.21) which is $\sum_{l=1}^{L} n_l w_l^2 (\frac{2}{9N} E_b)$.

Common parameters given for a laser are Peak Second-Order distortion (PSO) and Composite Triple Beat (CTB) for 2 channels and a large number of channels, i.e., 40 channels. As we have explained in section 2.3, as long as the total driving power is kept the same, C/IMD virtually is not a function of the number of channels.

The total power of interference signals caused by laser-nonlinearity is almost equal to the power of second and third-order IMPs and harmonics. Third-order intermodulation distortion products result in the CTB, defined as the ratio of the carrier to the total third-order interference at the carrier frequency. The PSO is defined as the ratio of magnitude of the unmodulated carrier to the maximum product count within the interval times the magnitude of each second-order IMP. Hence,

$$\sum_{l=1}^{L} n_l w_l^2 (\frac{2}{9N} E_b)$$

which is the interference nonlinearity term for the worst channel is equal to:

$$[2 \cdot 10^{(PSO/10)} + 3 \cdot 10^{(CTB/10)}] E_b \cdot \frac{2}{9N}$$

where PSO and CTB are expressed in dB.

We also point out that given the number of products contributing to the PSO and CTB, one can calculate the maximum allowed magnitude of each type of product. Lasers then can be screened based on the results of a simple 2-tone linearity test [46].

References

[1] M. Kavehrad and P.J. McLane, "Spread Spectrum for Indoor Digital Radio," IEEE Communications Magazine, Vol. 25, No. 5, pp. 32-40, June 1987.

[2] M. Kavehrad and B. Ramamurthi, "Direct-Sequence Spread Spectrum with DPSK Modulation and Diversity for Indoor Wireless Communications," IEEE Transactions on Communications, Vol. COM-35, No. 2, pp. 224-236, Feb. 1987.

[3] D. Brady and S. Verdú, "A Semiclassical Analysis of Optical Code Division Multiple Access," IEEE Transactions on Communications, Vol. 39, No. 1, pp. 85-93, Jan. 1991.

[4] M. Kavehrad, "Multiple FM/FDM Carriers Through Nonlinear Amplifiers," IEEE Transactions on Communications, Vol. COM-29, No. 5, pp. 751-756, May 1981.

[5] A.A.M. Saleh, "Fundamental Limit on Number of Channels in Subcarrier-Multiplexed Lightwave CATV System," Electronics Letters, Vol. 25, No. 12, pp. 776-777, June 1989.

[6] M. Kavehrad and P.J. McLane, "Performance of Low-Complexity Channel Coding and Diversity for Spread Spectrum in Indoor, Wireless Communications," AT&T Technical Journal, Vol. 64, No. 8, pp. 1927-1965, October 1985.

[7] R. Gross and R. Olshansky, "Third-Order Intemodulation Distortion in Coherent Subcarrier-Multiplexed Systems," IEEE Photonics Technology Letters, Vol. 1, No. 4, pp. 91-93, April 1989.

[8] T.E. Darcie and G.E. Bodeep, "Lightwave Multi-Channel Analog AM Video Distribution Systems," Proceedings of GLOBCOM, pp. 1004-1007, 1989.

[9] R. Olshansky, V. Lanzisera and P. Hill, "Simulations Transmission of 100 Mbit/s at Baseband and 60 FM Video Channels for a Wideband Optical Communication Net-

work," Electronics Letters, Vol. 24, No. 19, pp. 1234-1235, Sept. 1988.

[10] T.E. Dercic, R.S. Tucker and G.J. Sullivan, "Intermodulation and Harmonic Distortion in InGaAsP Lasers," Electronics Letters, Vol. 21, No. 16, pp. 665-666, August 1985.

[11] D. Laforgia, A. Luvison and V. Zingarelli, "Bit Error Rate Evaluation for Spread-Spectrum Multiple-Access Systems," IEEE Transactions on Communications, Vol. COM-32, No. 6, pp. 660-669, June 1984.

[12] M. Kavehrad, "Performance of Nondiversity Receivers for Spread Spectrum in Indoor Wireless Communications," AT&T Technical Journal, Vol. 64, No.6, pp. 1181-1210, July-August 1985.

[13] P.S. Henry, "High-Capacity Lightwave Local Area Networks," IEEE Communications Magazine, pp. 20-26, October 1989.

[14] O.C. Kwong, P.R. Prucnal and P.A. Perrier, "Synchronous Versus Asynchronous CDMA for Fiber-Optic LANs Using Optical Signal Processing," Proceedings of GLOBCOM., pp. 1012-1016, 1989.

[15] F. Khaleghi and M. Kavehrad, "A Subcarrier Multiplexed CDM Fiber Local Area Network," Proceedings of Queen's Communications Conference, May 1992.

[16] G. Vannucci, "Combining Frequency-Division and Code-Division Multiplexing in a High-Capacity Optical Network," IEEE Network, pp. 21-30, March 1989.

[17] M.B. Pursley and D.V. Sarwate, "Performance Evaluation for Phase-Coded Spread-Spectrum Multiple Access Communication-Part II: Code Sequence Analysis," IEEE Trans. on Comm. Vol. 68, pp. 598-619, May 1980.

[18] D.V. Sarwate and M.B. Pursley, "Cross-Correlation Properties of Pseudorandom and Related Sequences," Proc. IEEE, Vol. 68, pp. 598-619, May 1980.

[19] G.H. Golub and J.H. Welsch, "Calculation of Gauss Quadrature Rules," Math. Comput., Vol. 26, pp. 221-230, April 1969.

[20] J.E. Mazo, "Some Theoretical Observations on Spread-Spectrum Communications," The Bell System Technical Journal, Vol. 58, No. 9, pp. 2013-2023, Nov. 1979.

[21] T.H. Wood, G.E. Bodeep, Thomas E. Darcie, Gregory Raybon and Peter P. Bohn, " Broadband Upgrade of a Single-Fiber Fiber-in-the-Loop System Using Three-Levels of Multiplexing," Proceedings of OFC, pp. 375-378, Feb. 1992.

[22] R.J.S. Bates and Y.H. Kwark, "Five-Channel 1 Bb/s Aggregate Throughput Subcarrier Multiple-Access Network for Computer Applications," Proceedings of OFC, pp. 216, Feb. 1991.

[23] M. Kavehrad and P.J. McLane, "Performance of Direct Sequence Spread Spectrum for Indoor Wireless Digital Communications," Proceedings of GLOBCOM, New Orleans, LA, Dec. 1985.

[24] M. Kavehrad, F. Khaleghi and G. Bodeep, "An Experiment on a CDM Subcarrier Multiplexed Optical Fiber Local Area Network," Proceedings of Queen's Communications Conference, May 1992.

[25] F. Khaleghi and M. Kavehrad, "A Subcarrier Multiplexed CDM Optical Local Area Network, Theory & Experiment," Proceedings of Canadian Conference, Toronto, Sept. 1992.

[26] W.I. Way, "Subcarrier Multiplexed Lightwave System Design Considerations for Subscriber Loop Applications," Journal of Lightwave Technology, Vol. 7, No. 11, pp. 1806-1818, Nov. 1989.

[27] M.B. Pursley, "Performance Evaluation for Phase-Coded Spread-Spectrum Multiple-Access Communication- Part I: System Analysis," IEEE Trans. on Commu., Vol. COM-

25, No. 8, pp. 795-799, Aug. 1977.

[28] M.B. Pursley and D.V. Sarwate, "Performance Evaluation for Phase-Coded Spread-Spectrum Multiple-Access Communications - Part II: Code Sequence Analysis," IEEE Trans. on Commu., Vol. CDM-25, No. 8, pp. 800-802, Aug. 1977.

[29] M.B. Pursley and H.F.A. Roefs, "Numerical Evaluation of Correlation Parameters for Optimal Phases of Binary Shift-Register Sequences," IEEE Trans. on Commu., Vol. COM-27, No. 10, pp. 1597-1604, Oct. 1979.

[30] D.V. Sarwate and M.B. Pursley, "Crosscorrelation Properties of Pseudorandom and Related Sequences," Proceedings of the IEEE, Vol. 68, No. 5, pp. 593-617, May 1980.

[31] S.Benedetto, E. Biglieri and V. Castellani, "Digital Transmission Theory," New York: Prentice-Hall, 1987.

[32] R.E. Ziemer and R.L. Peterson,"Digital Communications and Spread Spectrum Systems," Macmillan, New York, 1985.

[33] W.Tomasi,"Electronic Communications Systems," Prentice-Hall, New York, 1988.

[34] R.M. Gagliardi and S.Karp,"Optical Communications," R.E. Krieger, Malabar, Florida, 1988.

[35] J.C. Palais,"Fiber Optic Communications," Second Edition, Prentice Hall, Englewood Cliffs, N.J., 1988.

[36] K. Kummerle, J.O. Limb and F.A. Tobagi,"Advances in Local Area Networks," IEEE Press, New York, 1987.

[37] J.G. Proakis,"Digital Communications," McGraw-Hill, New York, 1983.

[38] N.K. Shankaranarayanan, S.D. Elby and K.Y. Lau,"WDMA/Subcarrier-FDMA Light-

wave Networks: Limitations due to Optical Beat Interference," Journal of Lightwave Technology, Vol. 9, No. 7, pp. 931-943, July 1991.

[39] C.Desem, "Optical Interference in Subcarrier Multiplexed Systems with Multiple Optical Carriers," IEEE Journal on Selected Areas IN Communications, Vol. 8, pp. 1290-1295, Sept. 1990.

[40] V.J. Krylov, "Approximate Calculation of Integrals," Macmillan, New York, 1962.

[41] K.Y. Lau and A. Yariv, "Intermodulation Distortion in a Directly Modulated Semiconductor Injection Laser," Appl. Phys. Lett., Vol. 45, pp. 1034-1036, 1984.

[42] W. Gautschi, "On the Construction of Gaussian Quadrature Rules from Modified Moments," Mathematics of Computation, Vol. 24, pp. 245-260, 1970.

[43] W.I. Way, "Frequency-independent Nonlinear Characteristics of a High-speed Laser Diode," presented at the IEEE Int. Microwave Symp., pap. KK-6, 1988.

[44] R. Olshansky *et al.*, "Subcarrier Multiplexed Lightwave Systems for Broad-band Distribution," Journal of Lightwave Technology, Vol. 7, No. 9, pp. 1329-1342, 1989.

[45] J.C. Daly, "Fiber Optic Intermodulation Distortion," IEEE Transactions on Communications, Vol. Com-30, pp. 1954-1958, 1982.

[46] W. R. Bennet, "Cross-modulation Requirements on Multichannel Amplifiers below Overload," Bell Systems Technology Journal, Vol. 19, pp. 587-610, 1940.

[47] P.A. Weldon, W.W. Peterson and E.J. MacLane, "A Survey of Modern Algebra," New York: Macmillan, 1965.